Naval Research Laboratory
Stennis Space Center, MS 39529-5004

NRL/FR/7431--94-9617

High-Frequency Acoustic Scattering from Sediment Interface Roughness and Volume Inhomogeneities

KEVIN B. BRIGGS

Seafloor Sciences Branch
Marine Geosciences Division

December 5, 1994

REPORT DOCUMENTATION PAGE

Form Approved
OBM No. 0704-0188

1. AGENCY USE ONLY *(Leave blank)*	2. REPORT DATE	3. REPORT TYPE AND DATES COVERED
	December 5, 1994	Final

4. TITLE AND SUBTITLE

High-Frequency Acoustic Scattering from Sediment Interface Roughness and Volume Inhomogeneities

5. FUNDING NUMBERS

Job Order No.	574525804
Program Element No.	0601153N
Project No.	R3103
Task No.	000
Accession No.	DN252025

6. AUTHOR(S)

Kevin B. Briggs

7. PERFORMING ORGANIZATION NAME(S) AND ADDRESS(ES)

Naval Research Laboratory
Oceanography Division
Stennis Space Center, MS 39529-5004

8. PERFORMING ORGANIZATION REPORT NUMBER

NRL/FR/7431--94-9617

9. SPONSORING/MONITORING AGENCY NAME(S) AND ADDRESS(ES)

Naval Research Laboratory
Director of Research
Washington, D.C. 20375-5000

10. SPONSORING/MONITORING AGENCY REPORT NUMBER

11. SUPPLEMENTARY NOTES

12a. DISTRIBUTION/AVAILABILITY STATEMENT

Approved for public release; distribution unlimited.

12b. DISTRIBUTION CODE

13. ABSTRACT *(Maximum 200 words)*

High-frequency acoustic and geoacoustic data from five experiment sites with different sediment types are compared with predictions from the composite roughness model to ascertain the relative contribution of interface roughness and sediment volume scattering. Model fits to backscattering data from silty sediments indicate that volume scattering predominates, but measured bottom roughness was sufficient to explain the backscattering measured from a rippled, sandy sediment.

Fluctuations in sediment porosity and sound velocity probably cause volume scattering, which is described by a free parameter in the composite roughness model comparisons. High-resolution vertical profiles of sediment porosity and compressional wave velocity collected from 14 diverse sites on continental shelves are used to calculate vertical spatial autocorrelation functions, variance of the fluctuations, and the dependence of sediment sound velocity and density on sediment porosity for parameterizing sediment volume inhomogeneity. Correlation lengths calculated from autocorrelation functions show maximum variability in poorly sorted sediments. The variance of porosity and velocity fluctuations, which determines the strength of volume scattering, exhibits wide variation with sediment type and depends on the processes that mix and transport sediments. Comparison of data from a large number of locations on continental shelves suggests that fluctuations in sediment porosity are due to biological and sedimentological processes and that fluctuations in sediment velocity are due to hydrodynamic processes.

14. SUBJECT TERMS

acoustics, sediments, mines

15. NUMBER OF PAGES
154

16. PRICE CODE

17. SECURITY CLASSIFICATION OF REPORT	18. SECURITY CLASSIFICATION OF THIS PAGE	19. SECURITY CLASSIFICATION OF ABSTRACT	20. LIMITATION OF ABSTRACT
Unclassified	Unclassified	Unclassified	Same as report

SUMMARY

Recent field work in the field of high-frequency acoustics has focused attention on the relative contribution of sediment roughness and volume scattering to bottom backscattering from the seafloor. Although the importance of seafloor roughness has been accepted for years, few serious attempts have been made to accurately quantify it for testing acoustic models. Furthermore, failure of acoustic models to accurately predict higher measured levels of backscattering at small grazing angles has been attributed to lack of consideration of sediment volume scattering. Acoustic models are only as accurate as the environmental data used to test or develop them, and what has been lacking in model development has been a comprehensive set of environmental data collected with acoustic modeling in mind. This report contains a doctoral dissertation derived from basic research undertaken by the U.S. Navy to understand the fundamental mechanisms of and to model high-frequency scattering from shallow-water ocean bottoms.

A large body of data on sediment roughness, porosity, and compressional wave velocity and attenuation was collected for a variety of sediment types as a result of the Naval Research Laboratory's (NRL) shallow-water high-frequency program. Since 1982, NRL scientists have collected physical and geoacoustic property data to support high-frequency field experiments done in sandy and muddy sediments. Sediment porosity, grain size, compressional wave velocity, and compressional wave attenuation were measured vertically at regular, closely spaced intervals from numerous diver-collected cores and boxcores to ascertain sediment variability. In five experiments, bottom roughness was measured photogrammetrically to estimate roughness power spectra characteristic of the sediments.

High-frequency acoustic and geoacoustic data from five experiment sites with different sediment types are compared with predictions from the composite roughness model to ascertain the relative contribution of interface roughness and sediment volume scattering. Model fits to backscattering data from silty sediments indicate that volume scattering predominates, but that measured bottom roughness was sufficient to explain the backscattering measured from a rippled, sandy sediment. High-resolution vertical profiles of sediment porosity and compressional wave velocity collected from 14 diverse sites on continental shelves are used to calculate the correlation functions of vertical fluctuations for use in acoustic models. Variability in sediment density (or porosity) and velocity probably creates volume scattering, which is a quantity critical to high-frequency scattering models. The variance of the porosity fluctuations varies with the sediment type, and the values are not well documented in the literature. Comparison of data from a large number of locations on continental shelves demonstrates that fluctuations in sediment porosity are due to biological and sedimentological processes, and that fluctuations in sediment velocity are due to hydrodynamic processes. These unique data support the policy of extensive environmental assessment for high-frequency acoustic scattering measurements to develop accurate predictive models for the Navy's use in mine countermeasures and torpedo guidance and control applications.

ACKNOWLEDGMENTS

I wish to express my sincere thanks to my colleagues, Michael Richardson and Darrell Jackson, for their encouragement and guidance, not only in this body of research but also in my career. Many thanks to Don Percival for providing the statistical algorithms and procedures for analysis of the bottom roughness and porosity/velocity vertical profiles. I am indebted to Darrell Jackson and Steve Stanic for supplying the acoustic backscattering data. Thanks to Paul Hines and Richard Keiffer for the many informative discussions about use of these data in developing acoustic models.

Numerous individuals participated in the field and laboratory work from August 1980 to January 1989. Foremost among my fellow workers who helped collect the data reported here are Ricky Ray, Steve Stanic, and David K. Young. Lee Nastav provided the maps and the schematic. Richard Bennett provided the grain size data for the Russian River site. This work would not have been possible without their help.

Many thanks to the Naval Research Laboratory for providing the funding for the projects reported herein and to Philip Valent for granting me the opportunity to attend the University of Miami. Thanks are also due to Hal Wanless, Tokuo Yamamoto, Fred Tappert, Keir Becker, and Don McNeill for advice and critical comments. Finally, I thank my family and friends for their encouragement.

TABLE OF CONTENTS

PAGE

LIST OF FIGURES

LIST OF FIGURES -4-

LIST OF TABLES

UNIVERSITY OF MIAMI

HIGH-FREQUENCY ACOUSTIC SCATTERING FROM SEDIMENT INTERFACE ROUGHNESS AND VOLUME INHOMOGENEITIES

By

Kevin Bradford Briggs

A DISSERTATION

Submitted to the Faculty
of the University of Miami
in partial fulfillment of the requirements for
the degree of Doctor of Philosophy

Coral Gables, Florida

May, 1994

INTRODUCTION

Despite the numerous bottom scattering measurements reported since the inceptive work of McKinney and Anderson (1964), basic acoustic scattering mechanisms are still not completely understood. An understanding of basic acoustic-bottom interaction is essential to developing predictive models for bottom scattering. Typically, models have been developed to describe bottom scattering in terms of two components: interface scattering from bottom roughness (Kuo, 1964; Clay and Medwin, 1977) and volume scattering from sediment inhomogeneities (Ivakin and Lysanov, 1981; Hines, 1990). Some models combine both of these components (Crowther, 1983; Jackson *et al.*, 1986a). The relative importance of these two components, however, has not been established due to a lack of data from well-characterized sediments.

Sediment type, as expressed by particle size, is only an approximate indicator of the scattering strength (Urick, 1983). Results of experiments conducted by Wong and Chesterman (1968), Bunchuk and Zhitkovskii (1980), Boehme *et al.* (1985), and Jackson *et al.* (1986b) reveal that within each sediment type, scattering strength can vary by as much as 10 to 20 dB. Scattering of acoustic energy from the sediment surface is basically controlled by the impedance difference between the overlying water and the sediments. In those sediments in which the compressional wave velocity (one of the two components of impedance) is greater than the velocity of the

overlying water, scattering from the interface is generally considered to predominate. The backscattering strength is thought to vary according to the impedance mismatch at the interface. The magnitude of the impedance disparity varies with sediment type: finer-grained sediments scattering less energy than coarser-grained sediments (McKinney and Anderson, 1964). Furthermore, a rough interface generates higher values of backscattering strength than a smooth interface with the same impedance values. The microtopography of the seabed is of considerable interest as an input to high-frequency acoustic models (Stanton, 1984; Fox and Hayes, 1985; Briggs, 1989).

Roughness Scattering

Data showing dependence of bottom scattering strength on acoustic frequency (10-300 kHz) and grazing angle has been interpreted by Urick (1983) as evidence of bottom roughness controlling acoustic backscattering. Comparison of bottom backscattering strengths at low grazing angles with contemporaneously measured rms-height roughness values, however, reveals little dependence of scattering strength on bottom relief (Stanic *et al.*, 1988, 1989; Gardner *et al.*, 1991). The rms roughness statistic, calculated as the standard deviation around the mean relative height of bottom relief features, is a weak measure of bottom roughness. More useful parameters are the slope and the strength of the roughness power spectrum, which quantify the spatial frequencies of the seafloor microtopography (Bell, 1975; Fox and Hayes, 1985; Briggs, 1989).

The microtopography of the seabed necessarily can be classified as being either anisotropic or isotropic. Observed anisotropy in small-scale bottom roughness is most commonly expressed as current or wind-wave-induced ripples. Isotropic roughness is less easily generalized and includes the biogenic roughness produced by bioturbation, high-frequency roughness due to lag deposits or rubble, and the relatively featureless bottoms created by great hydrodynamic stress or flattening by mobile epifaunal organisms in high densities.

Sediment Volume Scattering

Penetration of sound into the bottom and its subsequent reradiation as backscattering has been discussed as a significant mechanism in the scattering process at low frequencies and high grazing angles (Urick, 1983). But reflection and scattering from subsurface inhomogeneities is a likely occurrence, regardless of frequency or angle, in finer-grained sediments where the impedance contrast between the overlying water and the high-porosity sediment is slight. In such "soft" sediments, much of the acoustic energy impinging upon the sediment-water interface is refracted into the bottom. Upon penetrating the sediment, the acoustic energy is likely to be strongly scattered from buried inhomogeneities which are equal to or larger than the acoustic wavelength in size (specular reflection) and weakly scattered by inhomogeneities smaller than the acoustic wavelength (diffraction).

Subsurface structures capable of scattering high-frequency sound are typically shell lag layers or burrows, but can be any discontinuity in the sediment fabric. Shell

lag layers can be generated by the migration of sand ripples and subsequent burial of coarse shell hash which has collected in ripple troughs. Also, bioturbation by selective deposit feeders can create buried shell layers. Shell lags are significant sound scatterers for reasons related to density inhomogeneities both intrinsic and extrinsic to the shells. Despite the porous nature of weathered/bored carbonate shells and the similar density of carbonate shells to quartz sand (2.70 vs. 2.65 g/cm^3), the shells are nevertheless denser than the saturated sediments surrounding them. Conversely, the presence of buried shells can reduce bulk density of sediments by creating water-filled voids between the coarse shells. In some cases these voids may be filled with fine sediment derived from settling of suspended sediment load after storms and also regular wave/tidal pumping action. The ability of buried carbonate shells and tests of marine organisms to affect compressional wave transmission through sediments has been demonstrated numerous times (Richardson *et al.*, 1983a, 1986; Briggs *et al.*, 1985, 1986, 1989a, 1989b, 1989c; Stanic *et al.*, 1989).

Migration of sand ripples may create discontinuities in the sediment fabric in the absence of coarse lag deposits by sorting of sediment into planar bottomset laminae and dipping foreset and stoss-side laminae (Reineck and Singh, 1980). Distinctive oscillatory-flow bed configurations are generated by storms and are preserved as hummocky cross-stratification (Harms *et al.*, 1975; Southard *et al.*, 1990). If the internal structure of asymmetrical wave ripples are preserved, the resultant buried features may provide discontinuities which could display enough of a density difference to cause volume scattering.

Animals burrowing in the sediment fabric create low-density voids which may or may not be infilled with sediment. Burrowers with carbonate tests (e.g. urchins, sand dollars, and mollusks) may, in fact, be scatterers themselves. Moreover, the reworking of sediment by burrowers disrupts and eventually destroys structure created by hydrodynamic processes like storms (Richardson *et al.*, 1983a) and may effect temporal changes on scattering from the sediment volume.

Backscattering Experiments and Models

Experimental evidence of the source of bottom backscattering has not been conclusive, however, because not all experimental acoustic data have been accompanied by detailed measurements of the physical parameters pertinent to describing scattering from the sea floor. A recent comparison of backscattering measurements collected from GLORIA data with some core data by Lyons (1991) is an attempt to understand the fundamentals of bottom backscattering. Conclusions drawn from the modeling results are weak, however, due to lack of rigor in numbers of cores collected and absence of bottom roughness measurements. In experiments of Boehme *et al.* (1985) and Boehme and Chotiros (1988), the presence of diverse bedforms and sediment types within the study areas precludes rigorous modeling efforts. It is difficult to characterize scattering mechanisms accurately in study areas that are not statistically uniform or homogeneous.

In this study, high-frequency (20-180 kHz) backscattering data from five shallow-water sites on the continental shelf will be compared with backscattering predictions

from a physical model using extensive geoacoustic data collected contemporaneously with the acoustic experiments as model inputs. The five experimental sites were chosen from many surveyed over the past years based on the availability of acoustic data, comprehensiveness of the environmental characterization, and uniformity of substrate. The composite roughness model of Jackson *et al.* (1986a) is a physical model incorporating the bottom roughness, sediment inhomogeneity, sediment velocity ratio, and sediment density ratio as descriptive parameters. This model was chosen because of (a) the confidence in and repeatability of the measurements required as inputs to the model, (b) the sensitivity of the model to roughness and sediment volume contributions and (c) the applicability of the model to high-frequency scattering. It is this model that will be used in combination with field experiments to investigate the mechanisms of sediment volume scattering. Predictions from this model have been found to compare well with backscattering intensity as a function of frequency and grazing angle measured from various sediment types (Jackson *et al.*, 1986a,b). The current treatment of the contribution of sediment volume scattering to the overall backscattering intensity is a descriptive model in which the sonar equation is used with an assumed volume scattering strength. Because of this assumption, the sediment volume scattering parameter is actually a free parameter and lacks association with measured physical properties of the sediment. For the purposes of this investigation the model is assumed to be valid, yet weak because of its lack of an explicit sediment inhomogeneity parameter.

Lack of an explicit approach to quantifying sediment volume scattering is

addressed by Hines (1990) in his derivation of a theoretical model for predicting acoustic backscatter from the sediment volume. The model of Hines is based on the premise that scattering from the sediment volume is created by fluctuations in sediment density or sound velocity. Characterizing the fluctuations in sediment porosity vertically and horizontally within the sediment fabric and assessing the variance of these fluctuations are essential to this model. The variance of porosity fluctuations is used to address scattering magnitude and an exponential correlation function of these fluctuations is used to determine the frequency and grazing angle dependence of the backscatter.

The correlation length associated with sediment density and acoustic wave velocity fluctuations has been invoked as a physical parameter for volume scattering models by a number of authors (Nolle *et al.*, 1963; Bunchuk and Zhitkovskii, 1980; Ivakin and Lysanov, 1981; Crowther, 1983; Stanic *et al.*, 1988; Hines, 1990). In each case, lack of sufficient physical property data forced the authors into extrapolating meager existing data and making assumptions in order to arrive at a value for correlation length. In the absence of actual physical measurements, Nolle *et al.* (1963) and Hines (1990) assume correlation lengths are related to mean grain size and the acoustic wavelength. Moreover, Hines allows the porosity variance to be a free parameter in his model so as to fit the model to the data.

Fortunately, a large body of data on sediment porosity and compressional wave velocity does exist for a variety of sediment types as a result of the Naval Research Laboratory-Stennis Space Center (NRL-SSC) shallow-water high-frequency program.

Since 1982, NRL scientists have collected physical and geoacoustic property data to support high-frequency field experiments in sandy and muddy sediments. Sediment porosity and compressional wave velocity as well as sediment grain size have been measured vertically at regular, closely spaced intervals from numerous diver-collected cores and boxcores in order to ascertain sediment variability. Values for the correlation function (and, subsequently, correlation length) considered appropriate for sediment volume inhomogeneities in shallow-water environments are determined from these types of data. In addition to the data-model comparisons from five study sites, this investigation will discuss the relationships among bulk properties of the sediment volume (grain size, porosity, and compressional wave velocity) and the potential for volume scattering from sediment inhomogeneities based on measurements collected from 14 different sites.

METHODS

Geological Description of Study Areas

All experiment sites were located on or proximal to continental shelves. Table 1 lists the 14 study areas from which physical and geoacoustic samples were collected, their geographical locations and water depths. The environments were diverse in terms of sediment type and water depth, hence, some sites in Table 1 were subdivided according to sediment type.

Backscattering data were obtained in addition to geoacoustic data at all of the shallow-water sites except Long Island Sound and La Spezia. Only the Quinault Range, Arafura Sea, Russian River, Panama City (I), and the Jacksonville (II) sites are subjected to model-data comparisons in this study, and geological descriptions of these five sites are given in subsequent subsections. Less than complete physical property data or lack of proper controls in backscattering data collection are responsible for exclusion of the remainder of the sites from data-model comparisons. Nevertheless, all available geoacoustic data from all 14 sites will be used to develop mathematical relationships between sediment physical and acoustic properties and volume scattering from various sediment types. Methods applied to stochastic parameterization of sediment inhomogeneity as an input for the volume scattering model of Hines (1990) are described in "Prediction of Sediment Volume Scattering" in the discussion section.

The Long Island Sound locations were a silty clay deposit 6 km south of New

Table 1. Listing of experimental sites, their locations, and water depths.

Experimental Site	Latitude	Longitude	Water Depth (m)
Long Island Sound	41°11'N	73°55'W	16
	41°14'N	73°45'W	10
Mission Bay, CA	32°46'N	117°14'W	18
Montauk Point, NY	41°04'N	71°35'W	35
Quinault Range, WA	47°34'N	124°35'W	49
Charleston, SC	32°25'N	79°49'W	20
La Spezia, ITALY	44°04'N	9°52'E	8-13
	44°05'N	9°55'E	5
Arafura Sea, AUSTRALIA	10°01'S	137°50'E	47
Panama City, FL (I)	29°51'N	85°47'W	34
Panama City, FL (II)	29°41'N	85°41'W	29
Jacksonville, FL (I)	30°38'N	80°57'W	21
Jacksonville, FL (II)	30°36'N	80°53'W	26
St. Andrew Bay, FL	30°10'N	85°43'W	10
	30°08'N	85°43'W	10
Straits of Juan de Fuca, WA	48°18'N	124°54'W	150
	48°13'N	125°09'W	120
	48°24'N	125°34'W	140
	48°26'N	125°25'W	120
	48°07'N	125°16'W	280
Russian River, CA	38°39'N	123°29'W	90

Haven Harbor, Connecticut, designated the NWC station by Rhoads *et al.* (1978) and an area of clayey silt off the Thimble Islands designated the FOAM station by Goldhaber *et al.* (1977). The Mission Bay locations were one mile off Mission Beach, San Diego, California, in a transitional area characterized by fine sand migrating over a coarse sand lag deposit (Richardson *et al.*, 1983b). The Montauk Point, New York, site was located at the southern terminus of a drowned barrier island spit south of Block Island (McMaster and Garrison, 1967). The Charleston, South Carolina, site was located 34 km from the Charleston Harbor jetties in an area characterized by a major transition in sediment types and dynamics and proximal to abundant Pleistocene rock outcrops (Briggs *et al.*, 1986). The La Spezia locations were a protected area of silt clay in the eastern part of the Gulf of La Spezia and an area of hard-packed, very fine sand off Venere Azzurra beach near La Spezia, Italy (Richardson, 1986). The Panama City (II) site is located 32 km east of Cape San Blas, Florida in a rippled, coarse sand deposit originating from a drowned relict beach. The Jacksonville (I) site is located 50 km northeast of Mayport, Florida in a moderately sorted, medium sand on the top of a broad topographic swell that is an expression of buried and probably eroded feature of coastal sediments (Briggs *et al.*, 1989c). The St. Andrew Bay, Florida, locations were a lagoonal mud within the bay and a migrating fine sand in the ship channel (Briggs, 1991). Five locations were investigated in the approached to the Strait of Juan de Fuca: two locations in a prism of Holocene silty fine sand and medium sand in the Juan de Fuca Trough, a location in the Nitinat Trough filled with glacial drift consisting of silty sand, a location in the

Nitinat Trough in a prism of Holocene silty clay and a location in the Juan de Fuca Canyon in a glacial outwash of clayey silt (Herzer and Bornhold, 1982).

Each of the following five experiment sites represents a specific environment that exhibits different features for sediment roughness and volume scattering potential. The Quinault Range, Washington, is a sandy site with well defined oscillatory ripple bedforms; the Arafura Sea, Australia, is a muddy site with a high concentration of coarse shell hash embedded in the sediment matrix; the Russian River site, California, is a muddy site with storm-generated bedforms; the Panama City (I) site is a sandy site with a relatively smooth, isotropic bottom; and the Jacksonville (II) site is a sandy site with a smooth, isotropic bottom with a high concentration of coarse shell hash on the surface of the sediment.

Quinault Range

The Quinault Range site is located 17 km west of the Washington coast in 49 m water depth in the Quinault Tracking Range, a torpedo testing range used by the U. S. Navy (Fig. 1). The site is located within a siliciclastic sand facies deposited from the Columbia River, the mouth of which is located 148 km to the south (Kulm *et al.*, 1975). Surficial sediments are sands that have less than 5 % silt- and clay-sized particles (Krell, 1980). Although most of the sand is supplied by the Columbia River, the nearby Queets and Hoh Rivers contribute some sand. A significant portion of the sand is derived from weathering of basalt from the Olympic Mountains and, consequent to the volcanic origin of the mountain range, the sands are enriched with

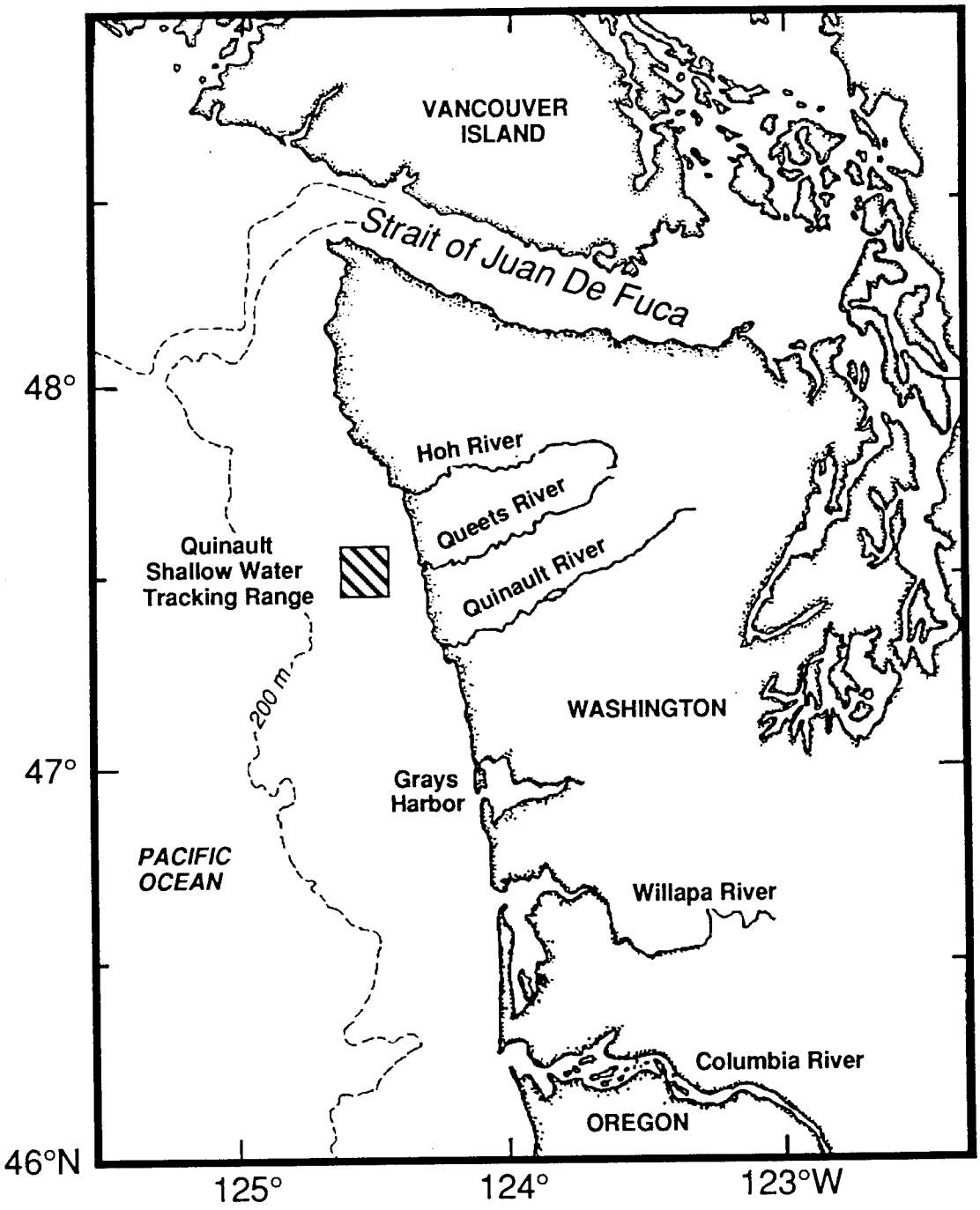

Figure 1. Map of the Washington coast showing the study site in the Quinault Range.

dark, ultramafic rock fragments giving them a 2-4.5% greater bulk density than pure quartz sands (Stewart, 1980). Northward flowing bottom currents (1 to 2 km day^{-1}) and storm events are responsible for distributing Columbia River sediments on the Washington continental shelf with storm events winnowing out the fine sediment and depositing them in deeper waters (Barnes *et al.*, 1972). Sediments in the Quinault Range are in dynamic equilibrium with present hydrographic conditions. Long-period ocean swell, usually generated from a persistent winter low pressure system in the Gulf of Alaska are responsible for producing symmetrical ripples at the water depth of the experiment site. Locally generated wind waves modify the sand ripples to some extent, even at a water depth of 49 m (Komar *et al.*, 1972).

The sea floor at the Quinault Range site is characterized by a shallow-water sand benthic biological community (Lie and Kisker, 1970). Dominant macrobenthic animals are the cumacean *Diastylopsis dawsoni*; the amphipods *Ampelisca macrocephala* and *Paraphoxus obtusidens*; the bivalves *Tellina salmonea*, *Macoma expansa* and *Siliqua patula*; and the polychaetes *Owenia fusiformis*, *Chaetozone setosa* and *Nephthys* sp. Due to the low biomass, small size and lack of dominant mobile surface deposit feeders within this benthic community, only minimal disturbance of oscillatory ripples is likely.

Arafura Sea

The Arafura Sea site is located 255 km north-northwest of Cape Arnhem, Australia in 47 m water depth (Fig. 2). The sediments are generally clayey sands and

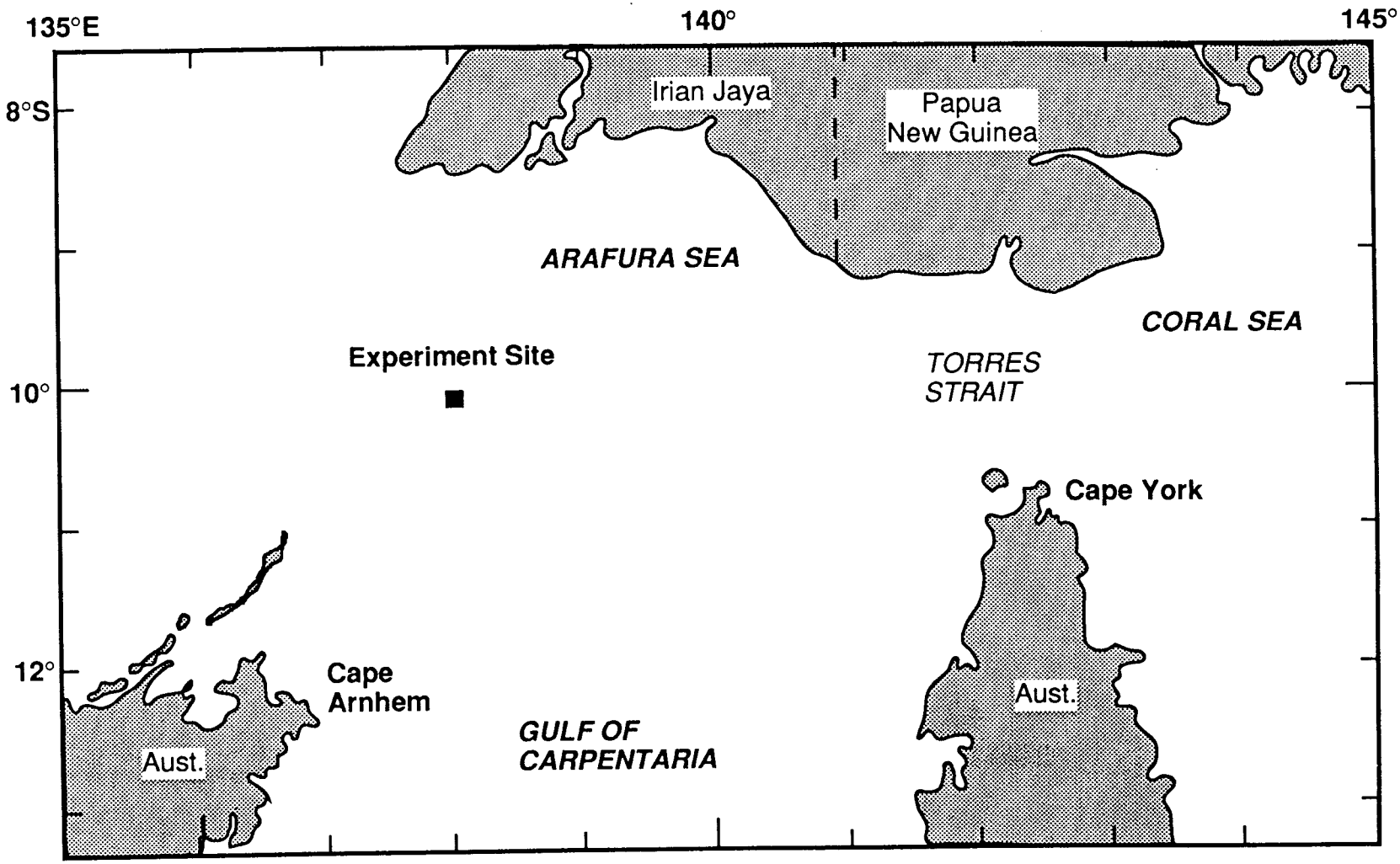

Figure 2. Map of the northern Australia and southern New Guinea coasts showing the study site in the Arafura Sea.

sand-silt-clays characterized by coarse calcareous material derived from relict shallow-water mollusks and coralline algae deposited during Pleistocene low sea-level periods (Jongsma, 1974). The Arafura Sea is a shallow inland sea between Australia and the island of New Guinea which is underlain by a sequence of sedimentary rocks over continental crust. The sea floor is of low relief, sedimentary input is relatively low, and the surface sediments have been considerably reworked over time by waves and currents. X-radiographs made from sediment slabs show no recognizable bedding and visible structure within the top 20 cm is the result of bioturbation (Briggs *et al.*, 1989a). The topography and sediments of the Arafura Sea have a mixed terrestrial/ marine source resulting from multiple subaerial exposures during the Pleistocene (Jongsma, 1974). The site is located on the Wessel Rise, placing it on a local topographic and deep-seated structural high elevation (Phipps, 1967). Hence, the site is an area of attenuated Holocene sediment thicknesses. The relict surface sediments are the top of a Plio-Pleistocene sequence probably between 10 and 75 m thick (Jongsma, 1974). Side-scan sonar images of the experiment site show the seafloor to be homogeneous, virtually featureless and of low backscattering intensity, although pockmarks of less than 10 m in diameter do occur sporadically (Briggs *et al.*, 1989a).

Russian River

The Russian River site is located 33 km northwest of the mouth of the Russian River and 180 km northwest of San Francisco at the mid-shelf STRESS (Sediment

TRansport Events on Shelves and Slopes) experiment site in 90 m water depth (Fig. 3). The topography and sediments of the northern California coast are strongly influenced by plate-boundary tectonics and Holocene sedimentation. The San Andreas fault system creates underwater escarpments and outcrops that are blanketed with 5 m or less of fine-grained sands and silts on the inner shelf (Cacchione *et al.*, 1983). Holocene sediments up to 15 m thick in deltaic and coastal deposits thin seaward to about 1 m thickness at the 110-m isobath. Beneath these onlapping Holocene sediments is a prominent erosional unconformity indicating their deposition following erosion by sea level transgression (Field *et al.*, 1992). Predominantly siliciclastic sediment is supplied to the shelf chiefly from the Russian and Gualala Rivers (Cacchione *et al.*, 1983). River-derived silt is transported to the northwest by storm-generated waves and currents (Drake and Cacchione, 1985). Frequent, intense winter storms create short-lived bedforms at the 90-m shelf site (Gross *et al.*, 1992). High rates of bioturbation by surface and subsurface deposit feeders (brittle stars and heart urchins, respectively) modify storm-generated seafloor topography by smoothing current ripples and generating mounds, trails and excavations (Cacchione *et al.*, 1983).

Panama City (I)

The Panama City (I) site is located 35 km south of the jetties at Panama City, Florida in 34 m water depth (Fig. 4). Fine quartz sand with about 10 % carbonate shell fragments covers this area which is representative of inner-shelf sand facies of

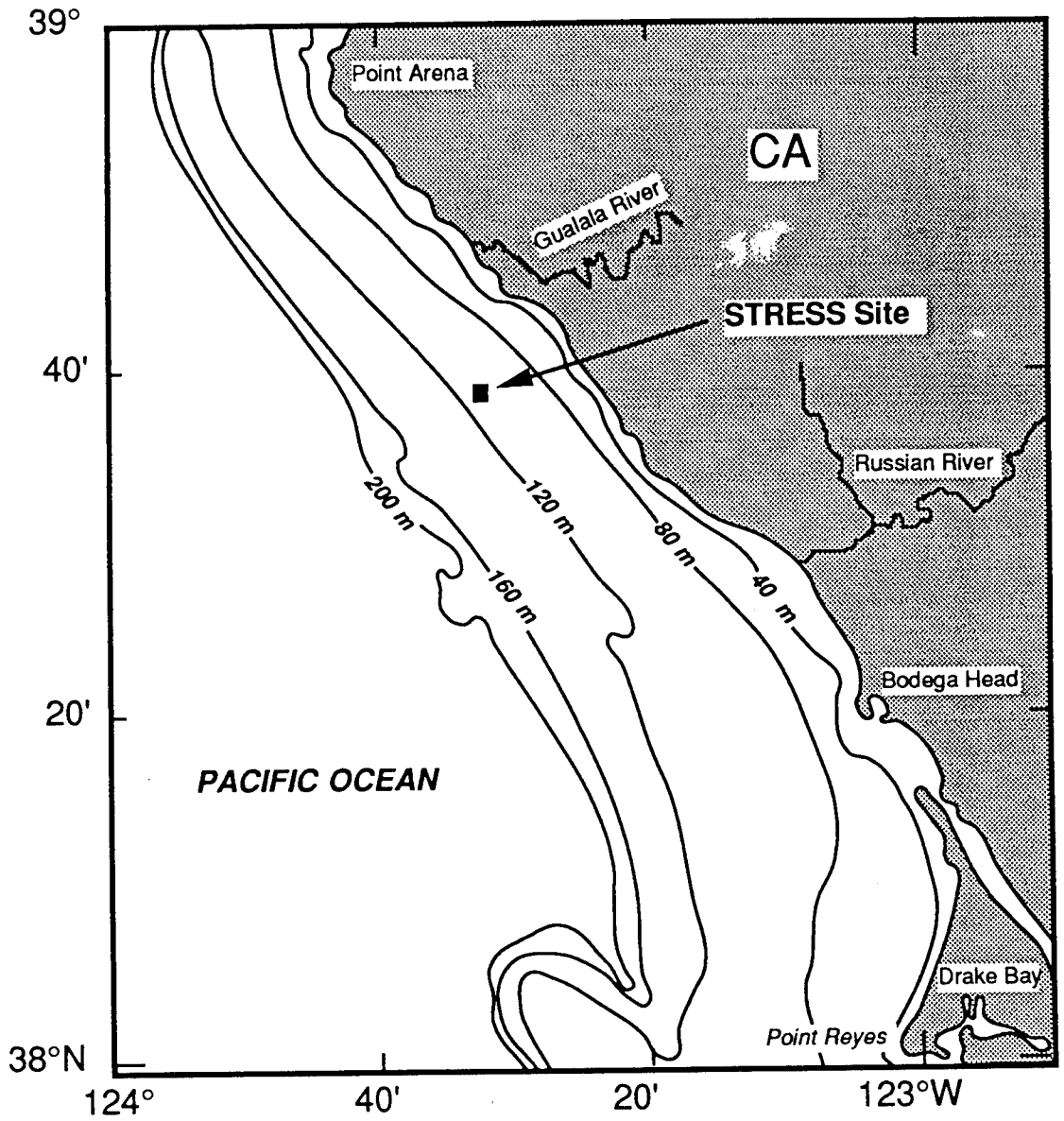

Figure 3. Map of the California coast showing the study site off the Russian River.

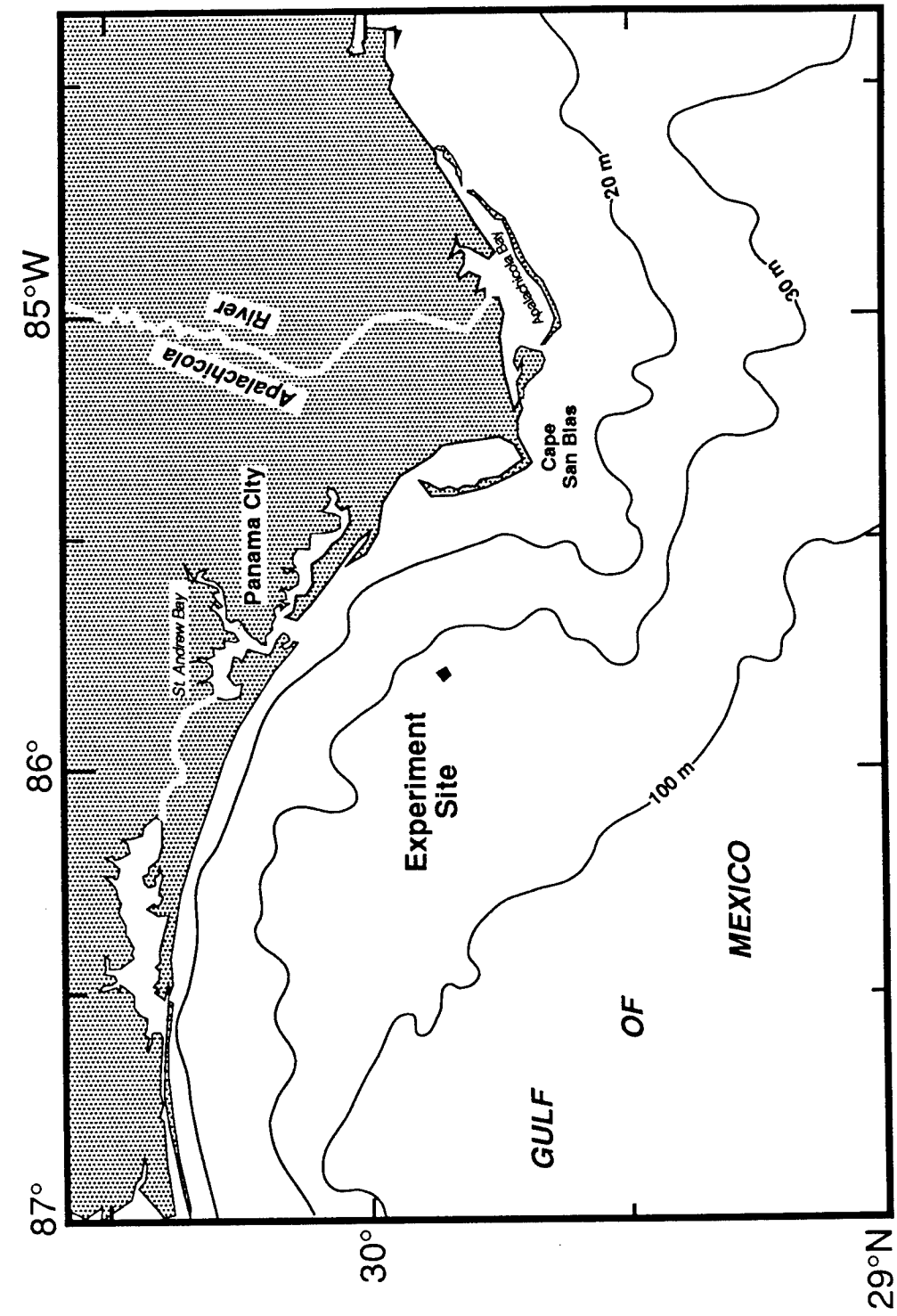

Figure 4. Map of the northwestern Florida coast showing the study site off Panama City.

the northeastern Gulf of Mexico (Doyle and Sparks, 1980). This deposit is known as the Cape San Blas Sand Facies and comprises the eastern portion of the Mississippi-Alabama-Florida (MAFLA) sand sheet. The sand sheet is typically 2 to 10 m thick and covers an erosional surface cut into partially consolidated, frequently late Miocene sediments (Pyle *et al.*, 1977). Fine-grained sediments contributed by the Apalachicola River to the east accumulate in the estuaries or behind barrier islands and rarely are advected to this part of the shelf. The sands composing the shelf are reworked relict sediments (Schnable and Goodell, 1968); no significant coarse-grained clastic sediment in the area is being supplied by the Apalachicola River. A series of ridges or sand shoals prograding south-southwest from Cape San Blas serves to separate the carbonate-rich facies to the east-southeast from the quartz-rich facies of the experiment site to the west (Doyle and Sparks, 1980).

The morphology of the area is dominated by the subdued, north-south trending ridges which characterize the shelf. The ridges are slightly asymmetrical with the steep sides facing east, wavelengths of about 200 to 1000 m and amplitudes of 1 to 3 m. The ridges and scattered large-scale bedforms originate from storm-generated currents (Neurauter, 1979). Bathymetry and side-scan sonar surveys of the area reveal the experiment site, which is located in a relatively large expanse between ridges, to be essentially flat and of uniform sediment characteristics.

Jacksonville (II)

The Jacksonville (II) site is located 50 km northeast of Mayport, Florida in a

coarse, sandy shell hash within a broad, shallow depression in 26 m water depth (Fig. 5). The experiment site is within the regional linear-sand-ridge morphology characteristic of the inner- and mid-shelf sea floor of the Atlantic continental shelf from Long Island to Florida (Duane *et al.*, 1972). The axial trend of the apparently discontinuous ridges is northeast-southwest, with wavelengths of 1 to 2 km and amplitudes of 2 to 4 m. This local relief is superimposed on a larger feature of broad northwest-southeast trending swells that are prominent to the west and north of the site (Briggs *et al.*, 1989b). These larger features are 6 to 10 m in height with a 4 to 5 km spacing. The swells are a local, persistent morphological feature resulting from an expression of buried and possibly eroded strata of coastal or nearshore sediments. According to Duane *et al.* (1972), the linear ridges are a dynamic morphological feature created as a response to long-term net tidal- and larger-scale currents transporting sediments over the shelf. Recent evidence from high-resolution seismic and vibracore records, however, reveal the mid-shelf ridges to be the eroded remnants of barrier inlets which are reworked into ridge morphology in the process of sea level transgression (Garcia de Figueiredo, 1984). Alternating bands of coarse shell hash and shelly sand cause faint lineations within the highly reflective sea floor imaged with side-scan sonar (Briggs *et al.*, 1989b). This pattern is also evident to divers as alternating dark and light bands, with the dark areas corresponding to coarser sediment. The shells and shell fragments causing the banded appearance of the sea floor are merely a veneer over medium or sand and exhibit no relief.

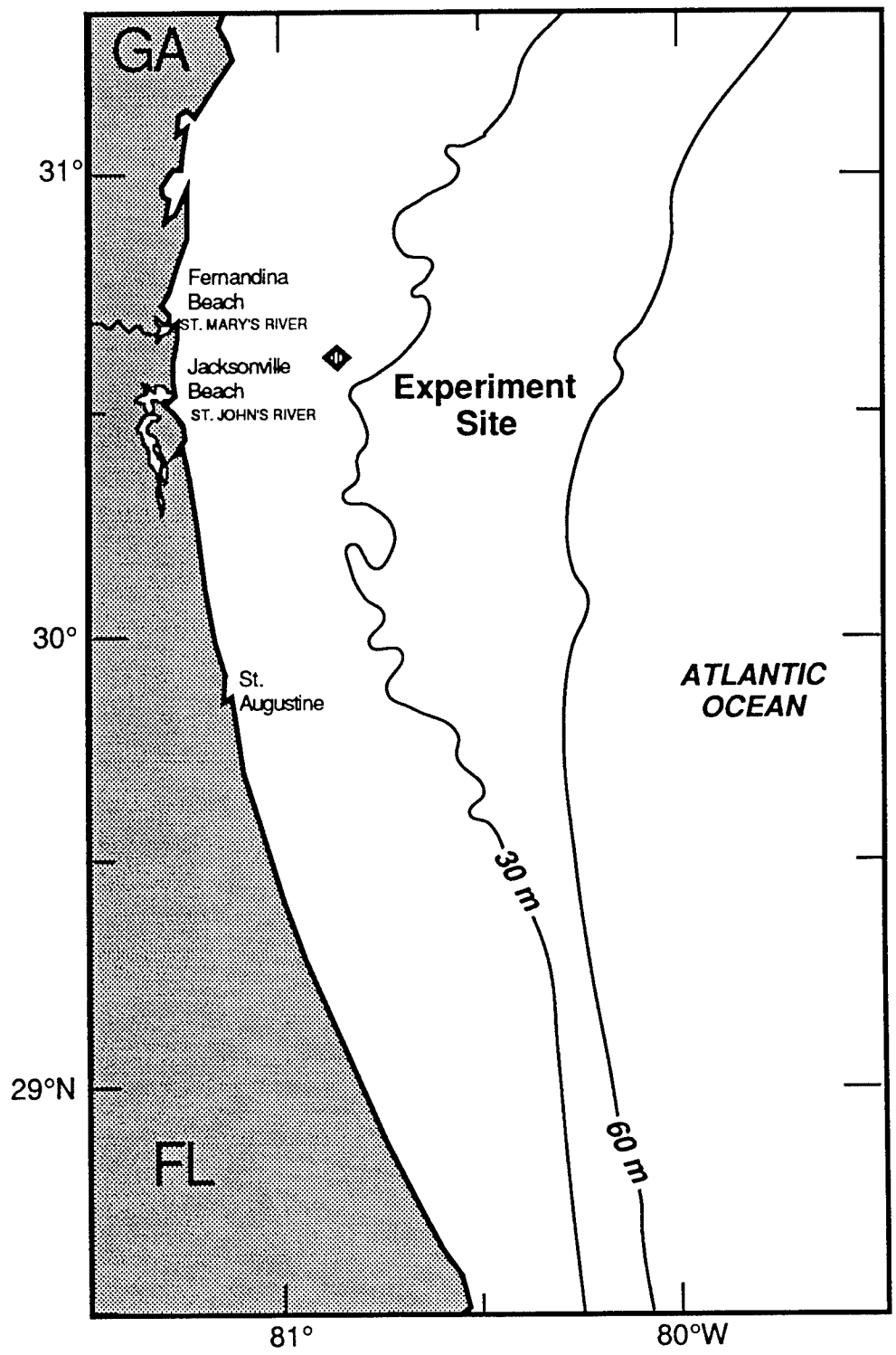

Figure 5. Map of the northeastern Florida coast showing the study site off Jacksonville.

Core Collection and Analysis

Cores on which geoacoustic and physical property measurements were made were 6.1-cm diameter polycarbonate plastic cylindrical core liner material cut to 45-cm lengths. Each core was bevelled at one end to facilitate the manual penetration into the sediment. Cores were capped at both ends immediately upon collection (to retain the water overlying the sediment) and kept in an upright position during transport aboard ship and over land to the laboratory for analysis. Collection, measurement, and handling procedures were designed to minimize sampling disturbance and to maintain an intact sediment-water interface within the core samples. Cores penetrated 9 to 39 cm into the sediment, depending on the sediment texture. Of the 14 experimental sites, five sites were sampled from boxcores (Montauk Point, Quinault Range, Arafura Sea, Straits of Juan de Fuca, and Russian River), one site was sampled by probes in diver-collected box cores (Long Island Sound), and the rest were hand-cored directly by divers (Briggs *et al.*, 1986; 1989a,b,c; Richardson *et al.*, 1983a,b,c; 1986).

Measurements of compressional wave velocity and attenuation were made within 24 to 36 hours of collection, once the cores had equilibrated with laboratory temperature. Temperature and salinity of the overlying water were measured with a YSI Model 43TD temperature probe and an AO Goldberg temperature-compensated salinity refractometer.

Sediment compressional wave velocity and attenuation were measured at 1-cm intervals using a pulse technique through the sediment cores and a distilled water

reference core with an Underwater Systems model USI-103 transducer-receiver head (Fig. 6). A Tektronix PG501 pulse generator was used to trigger a Tektronix FG504 function generator and a Hewlett Packard 1743A dual-time interval oscilloscope. The function and pulse generators drove the USI-103 transducer with a 400-kHz, 20 volt peak-to-peak sine wave triggered for 25 μs duration every 2 ms. The received signal was filtered by a Krohn-Hite band-pass filters (1 to 1000 kHz low cut-off and high cut-off frequencies) set in the maximally flat butterworth position prior to making time delay and received voltage measurements. Time delay measurements were made as the fourth sine-wave peak intersected with the volts-per-division baseline. Received voltage measurements were made using the maximum height of the fourth sine wave peak. The fourth peak was chosen in order to obviate the difficulties occasionally encountered in discerning the leading edge of the signal in cases where sound velocity is measured in sediments exhibiting high attenuation of the signal due to scattering.

Differences in time delay between distilled water and sediment cores were used to calculate sediment compressional wave velocity. The sound velocity through the sediment C_s (m sec^{-1}) is calculated from:

$$C_s = \frac{C_w}{1 - \frac{\Delta t C_w}{d}},$$

where C_w (m sec^{-1}) is the measured sound velocity through distilled water, Δt (sec) is the measured time arrival through sediment and d is the inside diameter of the

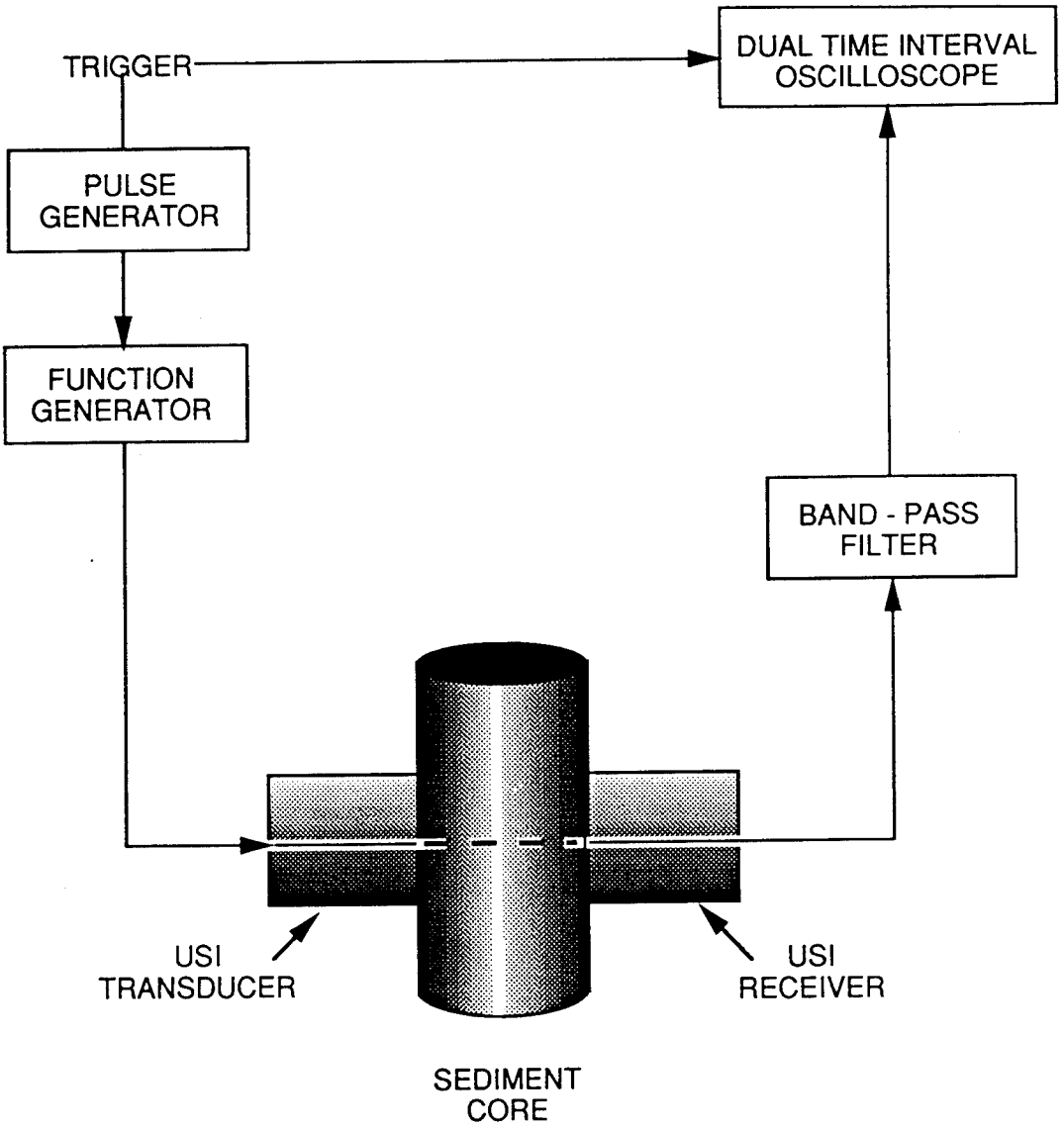

Figure 6. Schematic of the USI-103 velocimeter apparatus used to measure compressional wave velocity and attenuation.

core (0.061 m). All reported sound velocities are corrected to a common temperature, salinity and pressure (23°C, 35‰, 1 atm) after Hamilton (1971). Sediment sound velocity was also expressed as the ratio of measured sediment velocity to measured velocity of the overlying water in the core (same temperature, salinity, and depth). The sediment compressional wave velocity ratio is one of four input parameters for the composite roughness model and is displayed in the Results section by area in Figs. 7, 9, 11, 14 and 16.

Sediment compressional wave attenuation was calculated as 20 log of the ratio of received voltage through distilled water to received voltage through sediment. Attenuation is the amount of acoustic energy loss due to dissipative effects such as heat loss from frictional forces as well as loss due to scattering of energy. Values of attenuation were expressed in units of dB $m^{-1}kHz^{-1}$ and are identical to the constant, k, where

$$\alpha = kf^n$$

and α is the attenuation of compressional waves in sediment in dB m^{-1}, f is the transmitted signal frequency in kHz, and n is the exponent of frequency (Hamilton, 1972). Hamilton assumes the exponent to be 1 throughout the range of frequencies employed, although Stoll (1974) prefers to describe the exponent as varying from 2 at lower frequencies to 0.5 at higher frequencies. Attenuation is calculated in this study using Hamilton's assumption of linear frequency dispersion.

The probes used to measure sound velocity in box cores collected from Long Island Sound were a system of piezoceramic transducer/receivers operated at a

frequency of 70 kHz (Richardson *et al.*, 1983a). In this system, the sine wave was triggered for 10 μs duration every 2 ms. The electric energy was transferred into mechanical energy using a piezoceramic thin sheet transducer cut from G1195 series thin sheet manufactured by Gulton Industries. The transducer was epoxied at one end into a 15-mm long, 10-mm wide window machined into a 2.4-mm thick phenolic sheet potted with Scotch Cast 8. The mechanical energy was transferred to electrical energy by piezoceramic receivers built as identically as possible to the transmitter. The signals were amplified by Burr-Brown 3622K differential amplifiers (20 dB gain). All other electronic measurement tools were identical to those described previously for the USI-103 apparatus.

Samples were extruded from sediment cores upon completion of acoustic measurements and sectioned at 2-cm intervals (1-cm intervals in cores from Long Island Sound) to determine sediment porosity and grain size distribution. Cohesive sediments were extruded above the end of the core liner with a plunger and sliced off with a spatula; sands were sampled by scooping out the top 2 cm of sediment within the core liner without exposing the sediment above the core liner. Immediately after sectioning, the sediment samples were placed in preweighed aluminum pans, weighed, dried at 105°C for 24 hours, cooled in a desiccator and reweighed. Percent water was calculated by dividing the weight of evaporated water (difference between wet and dried sediment weights) by the weight of the dried solids and multiplying by 100. In most cases, average grain density was determined with a Beckman Model 930 air comparison pycnometer on selected samples. An average

value for grain density was assumed to be 2.65 g cm^{-3} when the pycnometer was not used. Porosity values were determined from tables relating porosity to water content and grain density (Lambert and Bennett, 1972). Reported values of porosity were not corrected for pore water salinity. Salt-free porosity values may be calculated by multiplying reported values by 1.012.

Sediment grain size was determined from disaggregated samples by dry sieving with a sieve shaker for sand-sized particles and on separate undried samples by use of a Micromeritics Model 5000 Sedigraph for silt- and clay-sized particles when samples were collected from muddy environments. Prior to size fractionation, sediment samples were soaked overnight in 200 ml of dispersant solution (2.5 g of sodium hexametaphosphate per liter of distilled water), then disaggregated by sonicating the sample with an ultrasonic disruptor for 12 minutes while stirring with a magnetic stirrer. The disaggregated sample was wet-sieved with dispersant through a 62-μm screen to separate the sand-sized fraction from the silt- and clay-sized fraction. The finer fraction was collected in a 1000-ml graduated cylinder, and enough dispersant was added to fill the graduated cylinder to 1000 ml. The coarser fraction was rinsed off the screen into a beaker with distilled water and then dried.

The dried, coarser fraction was fractionated into either whole phi or quarter-phi intervals with a sieve shaker and each fraction was individually weighed to determine the sand-sized particle distribution. Grain size is expressed as phi units (ϕ), or the negative of the base-two logarithm of the particle diameter in millimeters. The silt- and clay-sized fraction was thoroughly agitated by vigorous stirring and aeration. A

20-ml aliquot sample representative of the total distribution of particles in suspension was pipetted from the graduated cylinder and into a preweighed beaker, dried in an oven and weighed. Fine particle fractionation for sediments with 5% or less estimated silt and clay by weight was accomplished by taking a 20-ml aliquot at the appropriate time and depth within the graduated cylinder prescribed by Folk (1965) for the silt-clay break (8 phi). Subtraction of the 8-phi weight from the total weight yielded the silt weight. The silt weight was separated into eight equal half-phi intervals and the clay weight was separated into six equal whole-phi intervals. For samples with significant (>5% by weight) fine particle fractions, the fines were allowed to settle for five days before 20-ml aliquot samples were pipetted from the appropriate depths in the cylinder and into preweighed beakers, dried and weighed to estimate the weight of clay-sized particles in the 10 to 11, 11 to 12 and 12 to 14 phi intervals. At the conclusion of six days of settling, all particles 10 phi and coarser were near the bottom of the graduated cylinder. At this time the supernatant was slowly siphoned into another graduated cylinder, leaving the settled particles and about 200 ml of dispersant and sample. The supernatant volume was recorded. A 20-ml aliquot sample was pipetted from the supernatant after agitation, dried and weighed to estimate the weight of the remaining particles finer than 10 phi. Finally, the sample remaining in the graduated cylinder was sonicated and stirred for 12 minutes in a beaker prior to size determination with the Micromeritics Sedigraph. The Sedigraph determines the concentration of silt- and clay-sized particles in liquid suspension at various depths in a sample cell by means of a finely collimated,

horizontal x-ray beam. The concentration was presented in the form of a cumulative "percent-finer-than" distribution trace in relation to the Stokesian diameter of the particles.

Grain size distributions were analyzed and plotted as weight percent histograms and cumulative weight percent for all phi sizes through 14 phi. The fraction finer than 12 phi was equally divided between the 12 to 13 phi and 13 to 14 phi intervals to reduce skewing effects of lumping all fines into one bin. The mean grain size and sorting coefficient were calculated according to the graphic formula of Folk and Ward (1957). Sediments were divided into size classes of gravel, sand, silt and clay using the Wentworth scale.

Collection of cores was accomplished with the goal of ascertaining the variability of surficial geoacoustic properties over a wide area selected as an experiment site. Hence, the locations for core collection were chosen randomly and without intent to ascertain spatial correlation of the parameters in the horizontal dimension.

Photogrammetry

Stereo photographs of the sediment surface at the Quinault Range, Arafura Sea and Russian River sites were made with two parallel Photosea 70D 70-mm underwater cameras operating in tandem with two Photosea 1500D 150 Joule underwater strobes on a balanced steel frame. The distance between the 70-mm water-corrected lenses of the two cameras (camera base distance) was either 22 cm in parallel configuration or 40 cm in convergent configuration resulting in

approximately 50% image overlap in the stereo pairs. A glass reseau plate mounted in the film magazines superimposed a precise arrangement of fiducial marks on the images. The fiducial marks were used in the photogrammetric analysis later in the laboratory. Cameras and strobes were simultaneously actuated by a bottom contact switch connected to a weighted compass vane. Stereo photographs were taken at distances of 91, 122 and 183 cm from the bottom by changing the length of wire connecting the bottom contact switch to the compass vane. A series of paired photographs were taken for each focal setting by alternately raising and lowering the camera package (bottom-bounce method) while drifting across the experiment site. Several frames were trimmed off the film rolls and developed in the field to determine optimum photographic distance from the bottom (usually a function of water clarity) and to insure proper operation of the cameras.

Stereo photographs of the sediment surface at the Panama City and Jacksonville sites were made with a Photosea 2000 35-mm underwater stereo camera and a 100-Joule Photosea 1000 underwater strobe mounted in a molded fiberglas diver module. The diver module was mounted in a rigid 2.54-cm nominal diameter PVC frame to maintain constant focal distance and orientation with respect the bottom. Two Nikon 28-mm water-corrected lenses were separated by 61 mm in the Photosea stereo camera system, yielding a 57.2 x 65.9-cm overlap area at the 91-cm focal distance from the camera to the bottom. Orientation of the photographs was determined by photographing a diver's compass on the sea bottom as the first photograph of a photographic transect.

All stereo photographs were recorded on 10-m strips of Kodak Ektachrome 64 film. The stereo photographs were processed as continuous rolls and examined for clarity and exhibition of representative features of the experiment site. Measurement of bottom roughness was accomplished with the photogrammetric analysis of stereo photographs by one of two methods. Either contours of bottom microtopography were produced by Aerial Cartographic Technology of Cranston, Rhode Island, at 2-mm intervals using a Kern-2AT stereoplotter (Quinault Range), or roughness height values were digitized at regularly spaced intervals using a Benima (Hasselblad) AB photogrammetric stereocomparator (Arafura Sea, Russian River, Panama City, Jacksonville). Contoured data were used to produce orthogonally oriented transects of roughness heights nearly identical to those generated directly with the stereocomparator. Photogrammetric software provided by Benima corrected the measurements for distortion caused by refraction in sea water and lens aberrations. Use of the stereocomparator allows high frequency sampling of bottom roughness with accuracy of nearly 0.1 mm. The relative orientation calculation in the photogrammetric software performed a *de facto* least-squares detrending operation on the digitized height data. Transects were generally oriented according to the azimuthal directions of the acoustic transmitters used in collecting backscattering data. At the Russian River site where ripples dominated the bottom topography, half of the transects were oriented perpendicularly to the strike of the ripple crests and the other half of the transects were oriented orthogonally to the crest-to-crest transects.

Variability in terms of spatial frequency was assessed with the power spectrum. The power spectral density function was calculated for each set of 64, 128 or 256 points using manipulations suggested by Don Percival of Applied Physics Laboratory-University of Washington for application to bottom roughness analysis. Equally spaced raw data were prewhitened by taking differences of adjacent data points. Possible leakage was eliminated by subtracting the sample mean from the prewhitened data. The resultant data were tapered with a 20 percent cosine bell taper to suppress side lobes in the spectral domain. After a fast Fourier transform was used to compute the periodogram, the power spectrum was corrected for prewhitening by dividing each value by $4 \sin^2 \pi f_j \Delta$, where f_j is defined by $j/N\Delta$, j = 0, 1, 2, ... $N/2$, and Δ is the digitizing interval. Periodograms were filtered by ensemble averaging spectra from the same orientation or from all orientations if the roughness was isotropic. Regressions of (log) power spectral values against (log) spatial frequency values for each orientation were calculated to yield regression slopes. The slopes represent the power law behavior of all the spectra from a particular orientation superimposed on one another. Averaging of spectra in this way avoids biasing in the low-frequency portion of the spectra, where fewer data points are available to indicate the central tendency of the entire spectrum.

Backscattering Measurements

Backscattering strength was measured at the Quinault Range and Arafura Sea sites using a towed platform described in Jackson *et al.* (1986b). The acoustic

transducer platform used three different planar arrays to cover the frequency range from 15 to 45 kHz. The arrays were divided into upper and lower halves, and one half was used for transmission in order to widen the vertical beamwidth. A wide range of grazing angles were covered by making the transmitting and receiving beams 30° to 40° wide in the vertical plane. Azimuthal resolution was assured by keeping the horizontal bean widths between 15° and 20°. Beamwidth is defined as the full interval between 3-dB points. Acoustic pulses were transmitted with pulse lengths of 0.3 to 2 ms and source levels on the order of 205 dB *re*:1 μPa at 1 m.

Backscattering strength was measured at the Russian River site using a circularly scanning sonar operating at a fixed acoustic frequency of 40 kHz and covering an area within a circle of radius 75 m (Jackson and Briggs, 1992). The planar-array sonar rotated on a bottom-deployed tripod at an altitude of 5.2 m from the bottom. A fixed beam depression angle of 15° and a vertical beamwidth of 27° provided a range of grazing angles from 4° to 30°. Horizontal beamwidth was 6.5°. The sonar platform made ten scans per day, with each scan consisting of 69 separate transmissions made at 5° angular intervals and 5 s time intervals (one scan covered 345° in less than 6 min). Acoustic pulses were transmitted as a linear FM sweep with a pulse length of 2 ms and a sweep width of 2 kHz.

Collection and processing of acoustic data from the Quinault Range, Arafura Sea and Russian River sites were conducted by Darrell Jackson of the Applied Physics Laboratory, University of Washington. Split-beam processing was used with the towed platform to determine the angle of arrival of backscattered acoustic energy to

ensure that sea-surface reverberation did not contaminate the data (Jackson *et al.*, 1986b). In addition, data with a signal-to-noise ratio of 10 dB or less were rejected. Data from separate passes made with the towed platform at different sonar beam depression angles were combined to present a range of grazing angles from 5° to 90°.

Measurements are reported in terms of backscatter strength as a function of grazing angle (Urick, 1983). Backscatter strength is defined as 10 log $\sigma(\theta)$, where $\sigma(\theta)$ is the backscattering cross section per unit of surface area per unit solid angle, and θ is the grazing angle. Because $\sigma(\theta)$ is a ratio of cross section to area, it is dimensionless, and is given by:

$$\sigma(\theta) = r^2 10^{0.2\alpha r} I_s / I_0 A ,$$

where I_s is the backscattered intensity (including the receiver beam deviation loss) averaged over an ensemble of pings, I_0 is the incident intensity (including receiver beam loss), α is the attenuation coefficient of the water in dB m^{-1}, r is the slant range and A is the ensonified area. Because the ensonification area is not uniform, the quantity $I_0 A$ is defined as follows:

$$I_0 A = \frac{I_1 c \tau}{2r} \int_0^{2\pi} b(\theta, \psi) d\psi ,$$

where 10 log I_1 is the source level, c is the sound velocity in water, τ is the pulse length, and 10 log $b(\theta, \psi)$ is the round-trip beam loss in dB as a function of grazing angle θ and azimuthal angle ψ. The spherical coordinate system (with a vertical polar axis) is not aligned with the transducer beam axis, therefore the integral is a

function of both the grazing angle and the beam axis depression angle.

For the towed sonar platform, the backscattered intensity I_s was computed by averaging the squared envelope of the received signal over a time window on the order of the pulse length and over an ensemble of 20 to 30 successive pings. Noise intensity (measured with the transmitter turned off) was subtracted from the measured backscatter intensity. For the scanning sonar tripod, backscattering intensity was calculated as before, but averaged from 69 successive pings from one scan. Averages over portions of a scan were employed to examine anisotropy in backscattering strength. Contamination from sea-surface reverberation was eliminated by rejecting data at ranges comparable to or greater than the distance from the transducer to the sea surface (85 m). The scanning sonar recorded the noise level prior to each ping.

Backscattering strength was measured from the Panama City (I) and Jacksonville (II) sites using a transmitting system and receiving array mounted on a twin-hull - catamaran tower. The tower was towed to a predetermined location and deployed on the ocean bottom with the aid of divers (Stanic *et al.*, 1988). The transmitting system used a pair of broadband parametric sources to cover the frequency range from 15 to 180 kHz. The sources were located at an altitude of 7.6 m from the sea floor. Grazing angles from 5° to 30° and azimuthal angles were examined through the use of a triaxial positioner. Beam widths were less than 3° due to the use of parametric sources. Because the beam patterns of the sources were circularly symmetrical, the effective ensonified area was a projection of a circular area on the

bottom with a diameter equal to the interval between 3-dB points. Acoustic pulses were transmitted with a pulse lengths of 5 ms and source levels between 187 and 214 dB *re*:1μPa at 1 m. Backscattering measurements at the Panama City (I) site were collected with a two-dimensional spatial array of 12 hydrophones. Measurements at the Jacksonville (II) site were collected with a similar array consisting of 16 hydrophones. The hydrophones were EDO model 6660 omnidirectional type with broadband receiving capabilities up to 250 kHz. Two elliptical filters per hydrophone were used to eliminate high-range primary frequencies generated by the parametric sources.

Collection and processing of acoustic data from the Panama City (I) and Jacksonville (II) sites were conducted by Steve Stanic of NRL-SSC, Mississippi. A number of successive pings were ensemble averaged and backscattering strength was calculated similar to the procedure for the Quinault Range, Arafura Sea and Russian River experiments.

Sound velocity profiles of the water column were generated from conductivity and temperature measurements and used to estimate the possible effects of raybending on the acoustic paths. Data were rejected if calculated raybending effects were not negligible.

RESULTS

Mean values for sediment compressional wave velocity ratio, porosity and mean grain size for all experiment sites and sediment type are listed in Table 2. The geoacoustic, physical property and bottom roughness data from the five experiment sites for which data-model comparisons are generated are given below. Acoustic backscattering data from the five experiment sites are presented in the "Data-Model Comparisons" section of the Discussion.

Quinault Range

A large number of samples within and just outside of the experiment site demonstrated homogeneity with respect to geoacoustic properties. That is, a *t*-test of means ($\alpha < 0.05$) proved the data for sediment sound velocity, attenuation, porosity and mean grain size did not differ significantly from one location to another (Richardson *et al.*, 1986). The surficial sediments were sampled to a depth of 23 cm with a total of 29 subcores. The vertical distribution of sediment porosity, mean grain size, velocity ratio, and attenuation are displayed in Fig. 7. The parameters of porosity, velocity ratio and attenuation were required to provide inputs directly (velocity ratio) and indirectly (porosity and attenuation) for the composite roughness model of Jackson *et al.* (1986a). The slight increase in porosity with depth in the cores corresponded to an increase in the percent silt and clay. The highest values of porosity and percentages of silt and clay were found in the 12 to 18 cm depth

Table 2. Mean values for sediment compressional wave velocity (V_p) ratio, compressional wave attenuation (dB m^{-1} kHz^{-1}), porosity and mean grain size (ϕ) for each sediment type and experimental site.

Experimental Site	Sediment Type	V_p Ratio	Atten. (k)	Porosity (%)	ϕ
Long Island Sound					
NWC	silty clay	0.977	—	78.2	8.4
FOAM	clayey silt	0.986	—	74.2	7.3
Mission Bay, CA	fine sand	1.097	0.47	—	3.6
	coarse sand	1.148	0.29	—	1.0
Montauk Point, NY	fine sand	1.139	0.22	37.1	2.0
Quinault Range, WA	fine sand	1.112	0.43	41.6	2.9
Charleston, SC	med. sand	1.123	0.73	39.4	1.7
La Spezia, ITALY	silty clay	0.982	0.23	66.4	9.0
	v.fine sand	1.096	0.38	44.8	4.2
Arafura Sea, AUSTRAL.	clayey sand	0.988	0.84	70.5	5.2
Panama City, FL (I)	fine sand	1.133	0.59	39.9	2.6
Panama City, FL (II)	coarse sand	1.111	1.04	40.8	0.9
Jacksonville, FL (I)	med. sand	1.146	0.53	37.2	1.3
Jacksonville, FL (II)	shelly sand	1.113	1.42	40.0	0.8
St. Andrew Bay, FL	clay	0.993	0.10	87.4	10.9
	fine sand	1.139	0.24	39.0	2.2
Straits of	silty f. sand	1.056	0.59	54.6	4.0*
Juan de Fuca, WA	med. sand	1.153	0.41	38.5	1.9
	silty sand	1.103	0.63	45.5	5.0*
	silty clay	0.985	0.27	82.1	8.0*
	clayey silt	0.994	0.49	73.2	7.0*
Russian River, CA	clayey silt	1.009	0.56	63.4	6.4

* estimated from texture

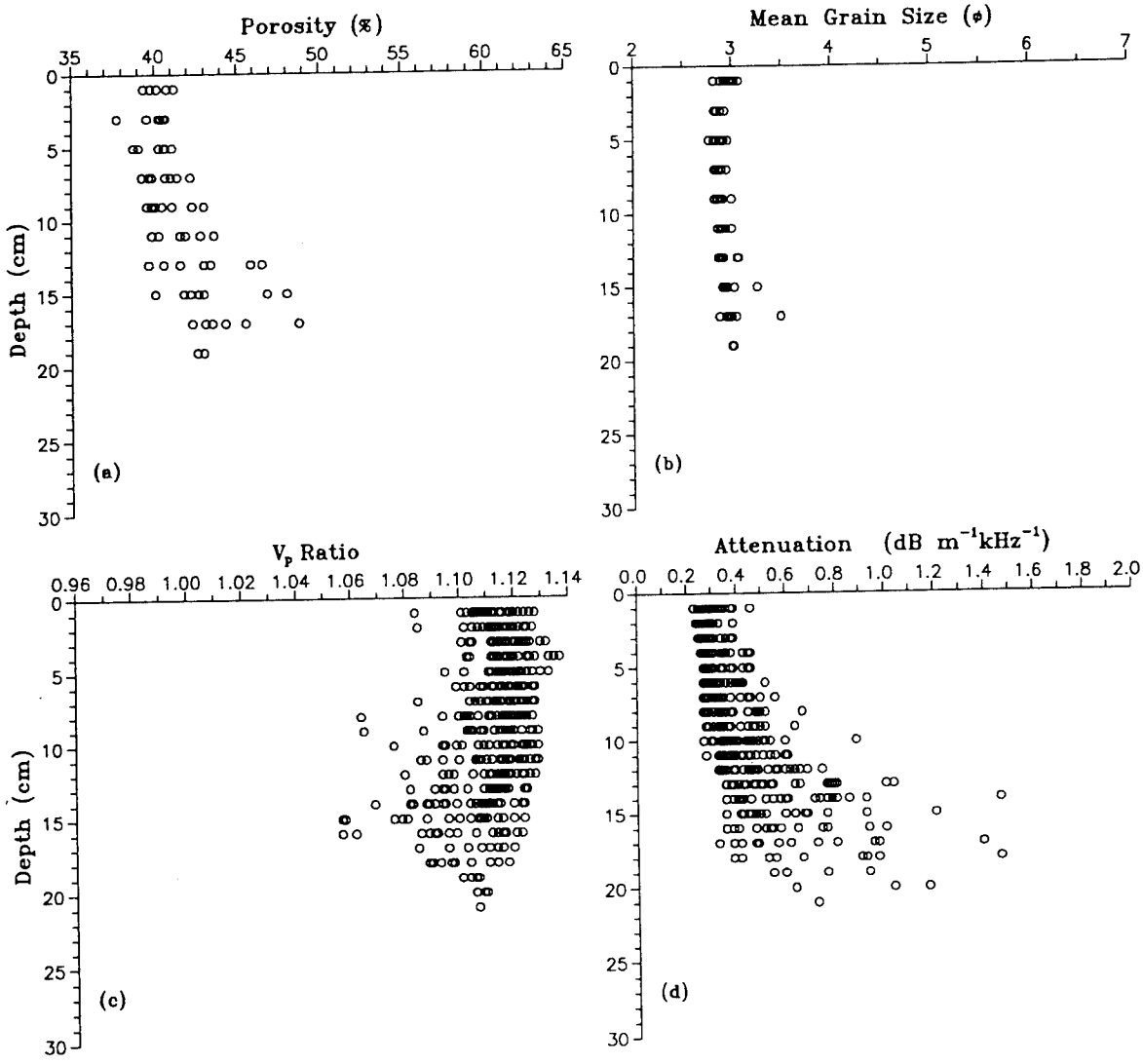

Figure 7. Profiles of geoacoustic properties for the Quinault Range site: (a) porosity, (b) mean grain size, (c) sound velocity ratio, (d) attenuation.

interval. Sediments were moderately to moderately well sorted, near-symmetrical to fine-skewed, fine to very-fine sands. Little downcore variation was evident in grain size until the 12 to 18 cm depth interval, where a layer of coarse shells and a greater percentage of silt and clay began. Compressional wave velocity ratio decreased and attenuation increased with increasing depth. Variability of values of velocity ratio and attenuation was greatest below 12 cm depth in the cores. The vertical gradients and high lateral variability in velocity and attenuation are probably due to the layer of coarse shell and fines. The polymodal grain size distribution represents a buried palimpsest lag deposit common on the surface of continental shelves at depths subject to bottom wave surge (Swift *et al.*, 1971).

The most significant feature in bottom photographs taken at the Quinault site was the presence of sand ripples. The morphology of the ripples was not particularly steep or sharp-crested; the ripples were probably features persisting from the last major winter storm which occurred in the months preceding the experiment. The strike of most ripples ran north-northwest to south-southeast and the mean ripple length was nearly 12 cm. Three 31.5-cm-long roughness profiles along the strike and three 31.5-cm-long roughness profiles across the strike (crest to crest) were digitized from each of 11 stereo photographs such that the orientations lined up with the ship's azimuthal headings during measurement of acoustic backscatter strength. Sixty-four digitized points were made at 0.5-cm intervals.

Periodograms estimating the roughness power spectra for the two orientations of roughness profiles are presented in Fig. 8. Each periodogram represents an

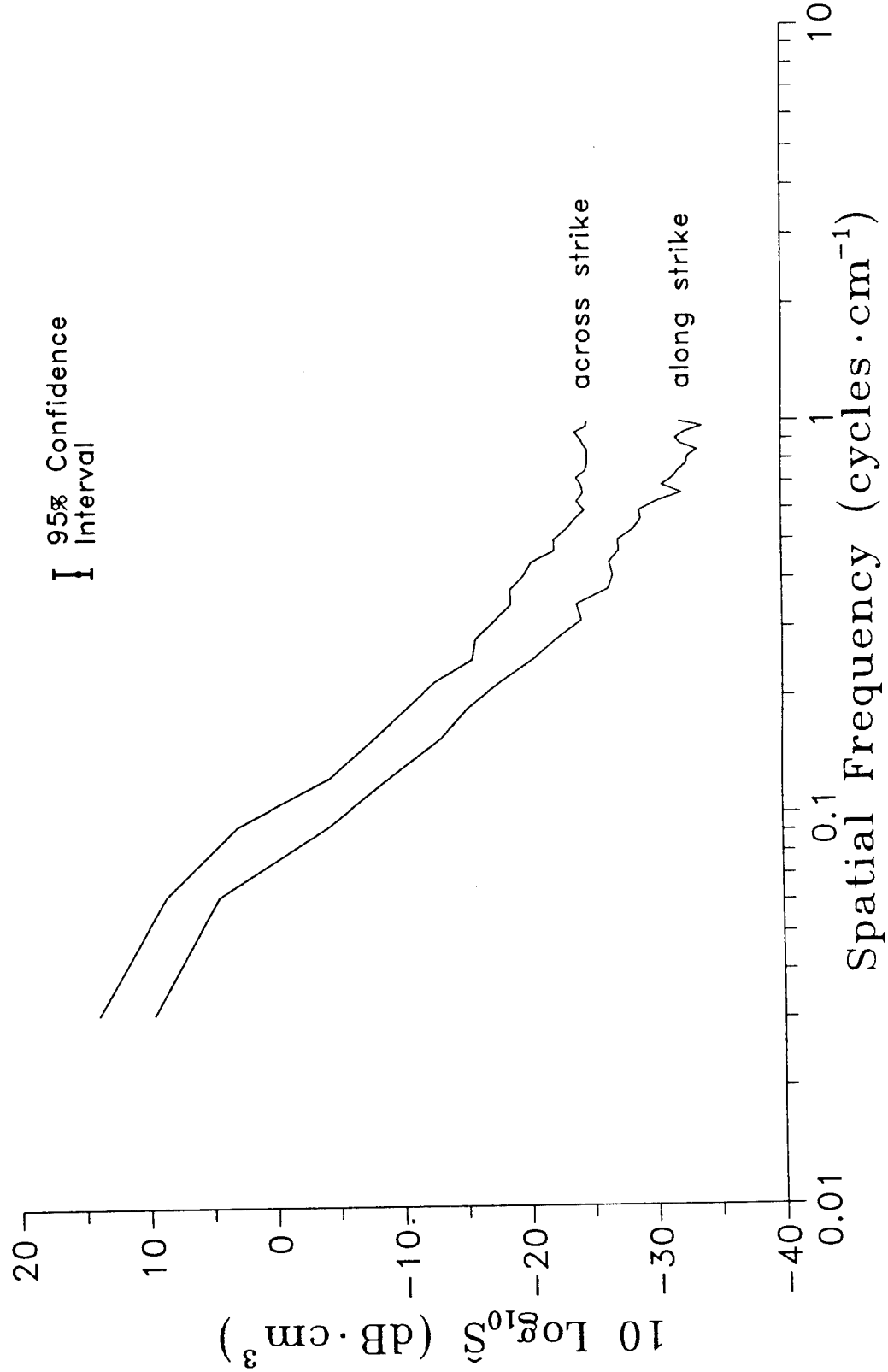

Figure 8. Roughness power spectra for the Quinault Range site in crest-to-crest (across strike) and along strike orientations.

averaging of 33 spectral function ordinates (corresponding to 33 roughness profiles) for each orientation. Observed sand ripple wavelengths of 12 cm were difficult to resolve in the across-strike spectrum in Fig. 8 due to the short pathlength (31.5 cm) employed at this site. Roughness spectra derived from profiles oriented along the strike of the ripples were slightly steeper (-2.92) than spectra from profiles oriented across the strike (-2.67). Table 3 displays the slope and intercept for roughness spectra for all five experiment sites. Occurrence of relatively greater variance in the highest spatial frequencies in across-strike spectra prevented a "roll off" consistent with the lower spatial frequencies and resulted in a less steep slope for the across-strike spectrum. A statistical test for the equality of regression slopes (Sokal and Rohlf, 1969), however, showed that no significant difference exists at the 0.05 level between slopes of spectra from the Quinault site.

Despite the lack of difference in spectral slope, there was a significant difference in variance between along-strike and across-strike spectra at all measured spatial frequencies. Computation of 95 % confidence intervals for each periodogram value was made from tabulated chi-square values at 0.975 and 0.025 levels, with 66 (*i.e.*, 2 × 33) degrees of freedom divided by an adjustment factor of 1.116 to account for the effects of tapering the data (Bloomfield, 1976). The upper confidence limit was calculated as 1.487 × $S(f)$; the lower limit was calculated as 0.719 × $S(f)$. The confidence interval is applicable to each point of the periodograms because, in this case, band width is equal to the frequency interval (3.125×10^{-2} cm^{-1}).

Table 3. Average values of roughness spectral parameters.

Site	Slope	Intercept (cm^3)
Quinault (Along Strike)	-2.92	0.00028
Quinault (Across Strike)	-2.67	0.00033
Arafura Sea	-2.18	0.00069
Russian River (Along Strike)		
Pre-storm	-2.65	0.000072
Post-storm	-2.73	0.000057
Russian River (Across Strike)		
Pre-storm	-2.38	0.000130
Post-storm	-2.56	0.000127
Panama City (I)		
20 m from tower	-1.97	0.00200
50 m from tower	-1.81	0.00283
Jacksonville (II)	-1.47	0.00534

Arafura Sea

Vertical distribution of sediment porosity, mean grain size, velocity ratio, and attenuation for the 12 cores (three from each box core) collected at the Arafura Sea site are presented in Fig. 9. Considerable variability exists in these geoacoustic properties with the exception of the sediment velocity ratio.

Values of sediment porosity ranged from 62.1 to 83.7 % and were distributed around a mean value of 69.7 % in the eight cores from which porosity was measured from the experiment site. Sediments at the top 4 cm of the cores had a higher water content than deeper layers and exhibited much greater variability in porosity. Sediment porosity values were calculated from an estimated average grain density of 2.68 g cm^{-3}, based on the great abundance of carbonate shell hash in the silt-clay matrix.

The grain size distribution showed the sediments at this site to be clayey sands and sand-silt-clays. Hence, mean grain size is a misleading parameter because of bimodal size distribution. Sediments at the site were essentially sand- and gravel-sized particles (averaging 55% of sample weight) embedded in a silty clay matrix. X-radiography of cores revealed the sediments to vary in terms of being grain- or matrix-supported. Variation in mean grain size within the site was due to differences in proportions of coarser components. The coarse material consists of sand- and gravel-sized mollusk shells, shell fragments, and carbonate rocks. An indication of the abundance of coarse material was that the weight percentages of gravel-sized

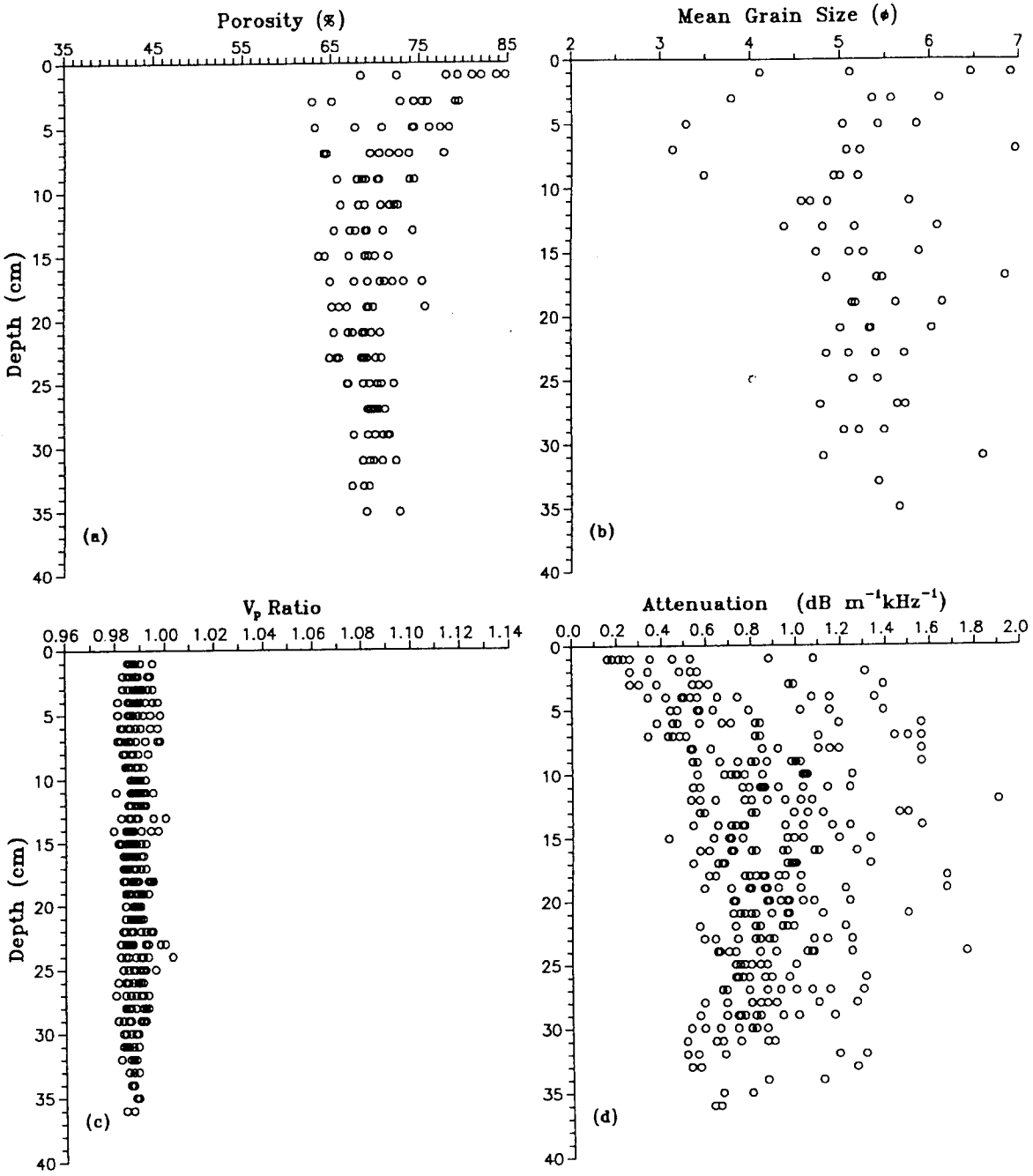

Figure 9. Profiles of geoacoustic properties for the Arafura Sea site: (a) porosity, (b) mean grain size, (c) sound velocity ratio, (d) attenuation.

particles in the four cores analyzed for grain size distribution averaged 11 %.

Values of sediment compressional wave attenuation averaged 0.84 dB m^{-1} kHz^{-1} and exhibited a coefficient of variation of 34.36 %. It is Rayleigh scattering of the 400 kHz-frequency acoustic energy by the shells and shell fragments rather than intrinsic absorption by the medium which is probably responsible for the great variability in the values of acoustic attenuation (Hamilton, 1972; Richardson, 1986). The majority of the velocity ratio values were distributed around the mean value of 0.986 to a maximum depth in the sediment of 38 cm. The relative constancy of the velocity ratio is indicative of the homogeneous silty clay matrix supporting the carbonate inhomogeneities. In contrast, the inhomogeneities which are embedded in the matrix create variability in compressional wave attenuation, grain size and, to a lesser extent, porosity.

Impressions from video and stereo photographic observations of the experiment site were that the sea floor was isotropically flat, but punctuated by numerous small mounds and burrows. The mounds were generated by burrowing infauna and were loosely aggregated, fine-grained features of high porosity, but were probably poor scatterers of high-frequency sound despite attaining heights of up to 10 cm.

The sea floor of the experiment site was biologically active as seen from video images. There were numerous sessile, soft-bodied organisms on the sediment surface. Most were probably macrophytic green and red algae; some soft corals (gorgonaceans and pennatulaceans), stalked sponges, stoloniferous bryozoa, and anemones (actiniarians and ceriantharians) were visible. The significance to sound

scattering of the presence of these benthic flora and fauna is more likely to be the material to which these organisms are attached rather than the size or shape of the soft-bodied organisms themselves. Algae, bryozoa, and soft corals in particular need a hard substrate to attach holdfasts: gravel-size carbonate shells and rocks near the sediment surface meet this criterion.

Orientations of roughness profiles were aligned with the ship's azimuthal directions as at the Quinault site. Periodograms estimating the roughness power spectra for three 35.56-cm profiles in the two orthogonal orientations from 12 stereo photographs were calculated and compared statistically. Each periodogram was calculated from 128 digitized points at 0.28-cm intervals. Confidence intervals were calculated as described previously and all values of the periodograms were within the 95 % intervals regardless of orientation. Power spectra showed few differences from among various photographs, and these differences were most pronounced at the low-frequency end of the spectra where there were fewer data to average. No significant differences between slopes of north-south and east-west profiles were found when the equality of regression slopes was tested by the analysis of covariance (ANCOVA), confirming the bottom roughness at the Arafura Sea site to be isotropic with respect to spatial periodicity at the physical scale measured. The averaged periodogram for the 72 spectra is displayed in Fig. 10 and the slope and intercept of the averaged spectra is displayed in Table 3. The average values reported in the table correspond to the periodogram that has been averaged over the 12 photographs rather than an arithmetic average of the 12 slope and intercept values.

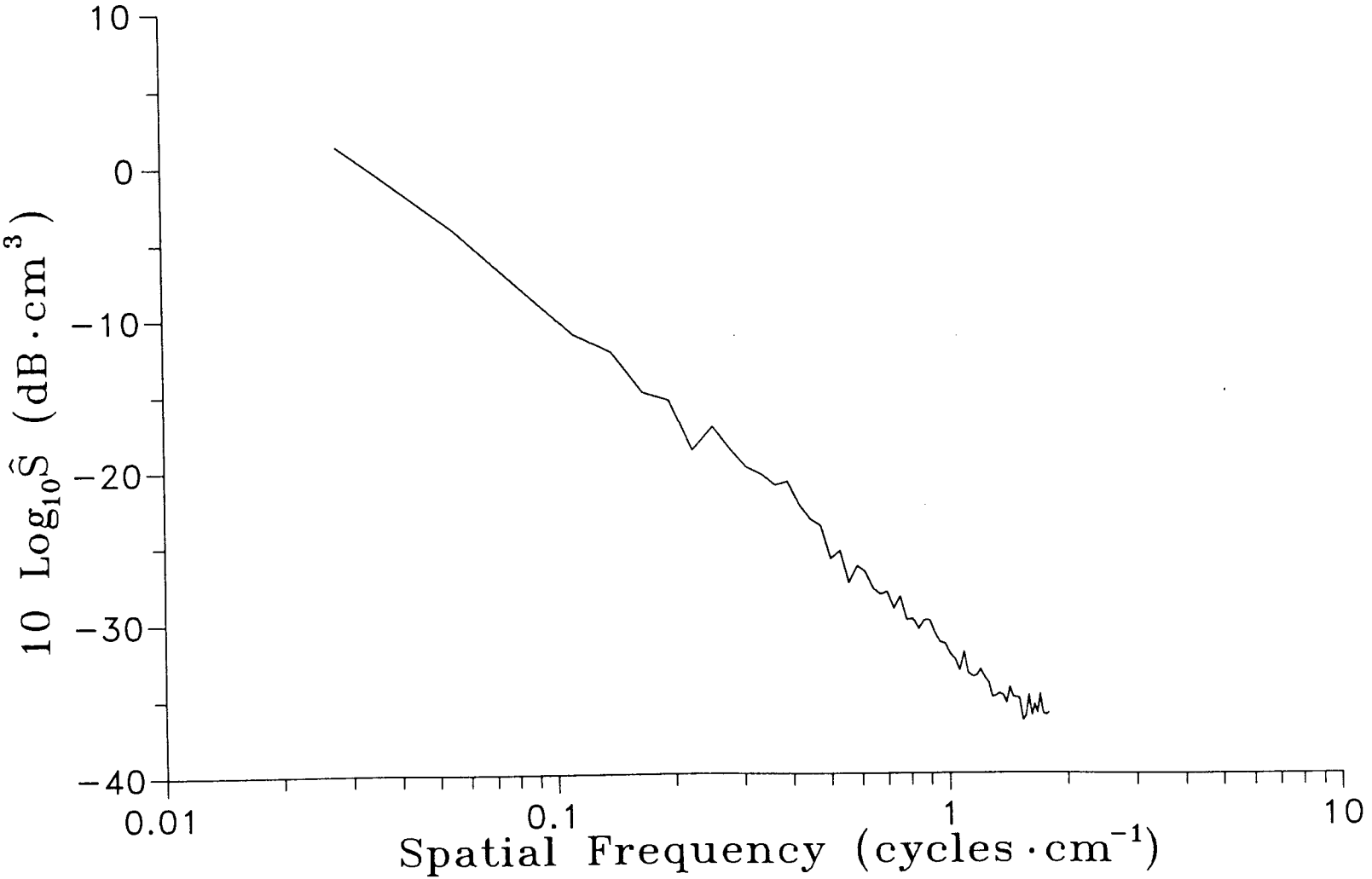

Figure 10. Roughness power spectrum for the Arafura Sea site.

In order to examine the behavior of bottom roughness at larger scales, an additional 14 pairs of stereo photographs taken at the 122-cm focal distance were selected from 56 possible pairs for analysis based on image clarity and presence of representative features. From these 14 pairs, 15 roughness profiles of 71.4 cm length were analyzed regardless of orientation (because of lack of anisotropy measured in the 12 previous stereo photographs). In order to preserve the spectral resolution obtained in the spectra derived from shorter pathlengths, the digitizing interval was maintained at 0.28 cm. The roughness periodogram generated from the 256 digitized points from the 71.4-cm paths was averaged over all 15 ordinates and appeared similar to the periodogram generated from the 35.56-cm paths. The values for slope and intercept of the 71.4-cm spectra were -2.25 and 4.7×10^{-4} cm^3, respectively. These values are within the range of variability of the values from the shorter paths for this site and the spectrum is virtually identical to Fig. 10.

Russian River

A total of 12 subcores were collected from six box cores; half were collected in early December and the other half were collected in late January. Two additional cores were collected in late February for grain size analysis. In the interim between sampling events several winter storms occurred, as evidenced by bottom photographs and current meter and transmissometer data provided by collaborators on the STRESS experiment. The vertical distribution of sediment porosity, mean grain size, velocity ratio, and attenuation are displayed in Fig. 11. Pre-storm and post-storm

data were combined in Fig. 11 due to considerable overlap of the data.

Sediment porosity decreased steeply only in the first 8 cm, and an increasing gradient occurred in the sediment velocity ratio and attenuation. The higher water content and consequent lower velocity ratio and attenuation of the top 8 cm of sediment was probably due to this layer being an active zone of bioturbation by burrowing infauna (Richardson and Young, 1980). Below this reworked zone, some variability was due to random inhomogeneities created by deeper-burrowing, though sparser, infauna. Data outlying the cluster of points in each vertical profile plotted in Fig. 11 represented sampling of voids or infilled burrows within the sediment matrix. Outlying grain-size data was extremely fine-skewed and likely represented infilling of burrows, voids, or excavations with finer sediments which were in suspension.

The dominant fauna identified from photographs were heart (spatangoid) urchins and brittle stars. Densities of urchins at the sediment-water interface were witnessed to be as great as 25 individuals m^{-2}; brittle stars exposed on the sediment surface reached densities of up to 22 individuals m^{-2}. Urchin densities on the sediment surface as high as only 8 individuals m^{-2} were reported for this site by Nichols *et al.* (1989). Spatangoid urchins exhibit behavioral responses to light, in that they generally remain buried during daylight hours and emerge from the sediment at night (Chesher, 1969). Two sets of photographs made at night indicated average densities of heart urchins to be 8.7 and 2.8 individuals m^{-2}, respectively. Daytime photographs indicated an average of only 1.6 urchins m^{-2}. Nighttime densities of brittle stars

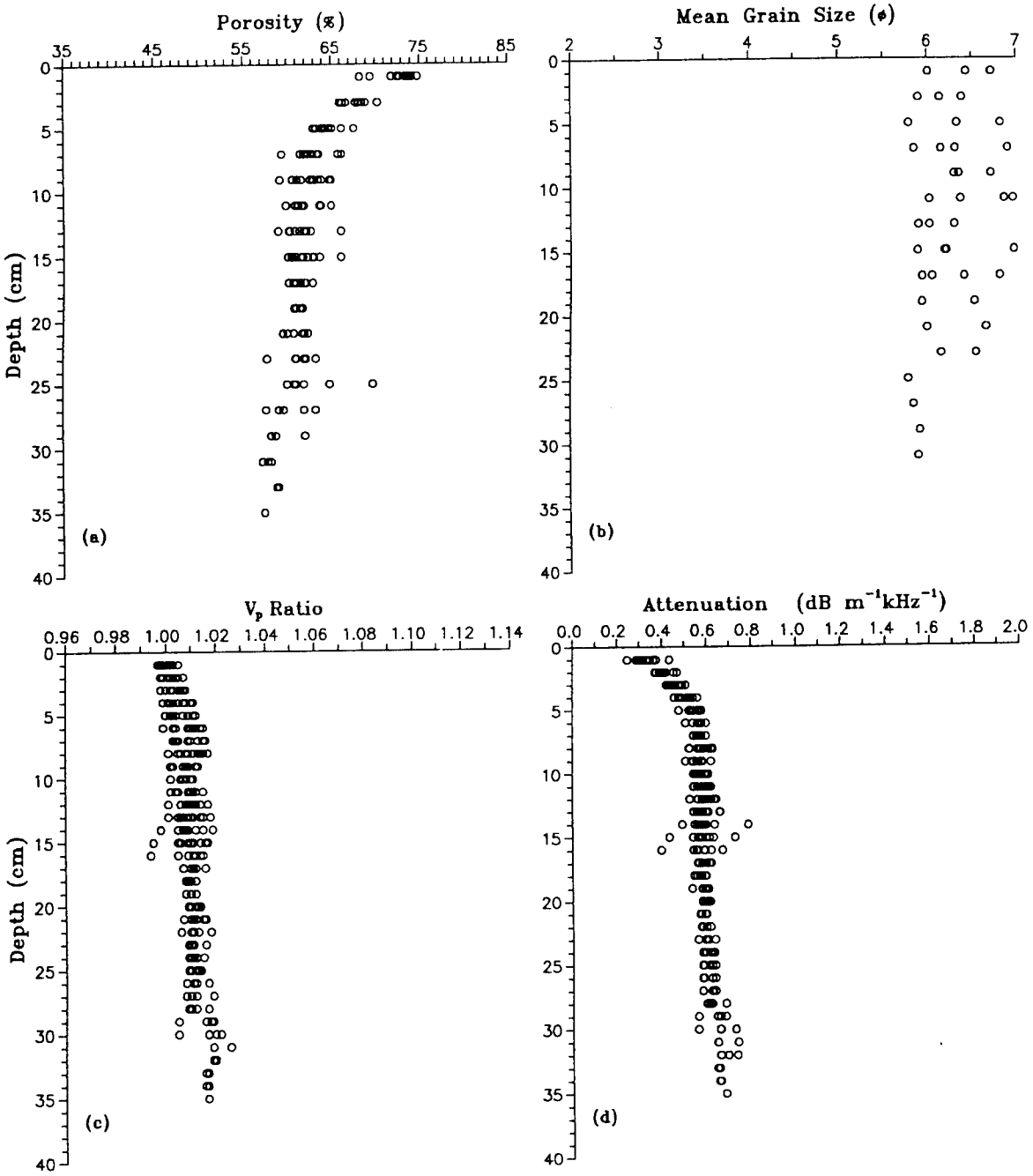

Figure 11. Profiles of geoacoustic properties for the Russian River site: (a) porosity, (b) mean grain size, (c) sound velocity ratio, (d) attenuation.

averaged 1.0 and 8.9 individuals m^{-2}, and daytime densities averaged 3.3 individuals m^{-2}. None of these differences, however, can be considered statistically significant because of the wide variability in the counts from photographs. Moreover, brittle stars probably played a lesser role in creating fluctuations in scattering strength due to a smaller effective surface area compared to that of the heart urchins.

Spatial variability exhibited in the bottom photographs was due to the tendency of the fauna to form herds (Chesher, 1969). Chesher (1969) showed differential rates of movement for spatangoid urchins of 3 to 6 cm/hr during daylight hours and 7 to 8 cm/hr at night. Acoustic scattering may occur from the fauna or from their effect on the sediment. Howard *et al.* (1974) showed evidence of how movement of the urchins disturbs the upper layers of sediment by creating voids and increasing sediment porosity. Consequently, diurnally fluctuating foraging by herds of urchins may affect the sediment velocity and density ratios. The effect of foraging was evident in Fig. 11, where a steep gradient of porosity extended to about 6 cm depth into the sediment. Although Howard *et al.* (1974) indicated that heart urchins off the coast of Georgia burrowed to a maximum depth of 14 cm, this may be the effective depth of foraging of the buried urchins at this site.

Photographs of the sediment-water interface before the storm events indicated a low relief, uniform bottom with scattered pits and mounds generated by infauna. The roughness of the interface may be classified as isotropic due to the random nature of the bioturbation of the sediments. Photographs taken following the storms indicated well defined ripples with the strike trending north-northeast to south-

southwest (21° to 201°) and ripple heights averaging 1.9 cm. Based on measured current speed, wave orbital velocity and wave period during major storm events in the interim, ripple height and length were predicted to be much greater (Gross *et al.*, 1992). Therefore, the bottom roughness indicated by these photogrammetric data was the result of a more recent, yet less intense storm (R. Wheatcroft, *pers. communication*). Three roughness profiles along the strike and three roughness profiles across the strike were made from each of 9 stereo photographs. Pre-storm roughness profiles from 5 stereo photographs were oriented according to the post-storm ripple orientation as determined by the compass vane in the post-storm photographs.

No significant difference was found between the slopes of the two different orientations of pre-storm roughness spectra displayed in Fig. 12. An analysis of covariance (ANCOVA) for testing the equality of slopes of regressions of spectral values on spatial frequency was used to calculate an F statistic as utilized previously for the Quinault Range and Arafura Sea roughness data (Sokal and Rohlf, 1969). Periodograms estimating the post-storm roughness spectra for the two orientations of roughness profiles are displayed in Fig. 13. Slopes of post-storm roughness spectra exhibited a statistical difference in the ANCOVA test ($\alpha < 0.01$) between the two orientations. Storm-generated ripples were responsible for a statistical difference ($\alpha < 0.01$) between the slopes of spectra representing pre-storm and post-storm roughness in the across-strike orientation. The difference between the pre- and post-storm spectra is evident in the lower frequency portion of the spectra.

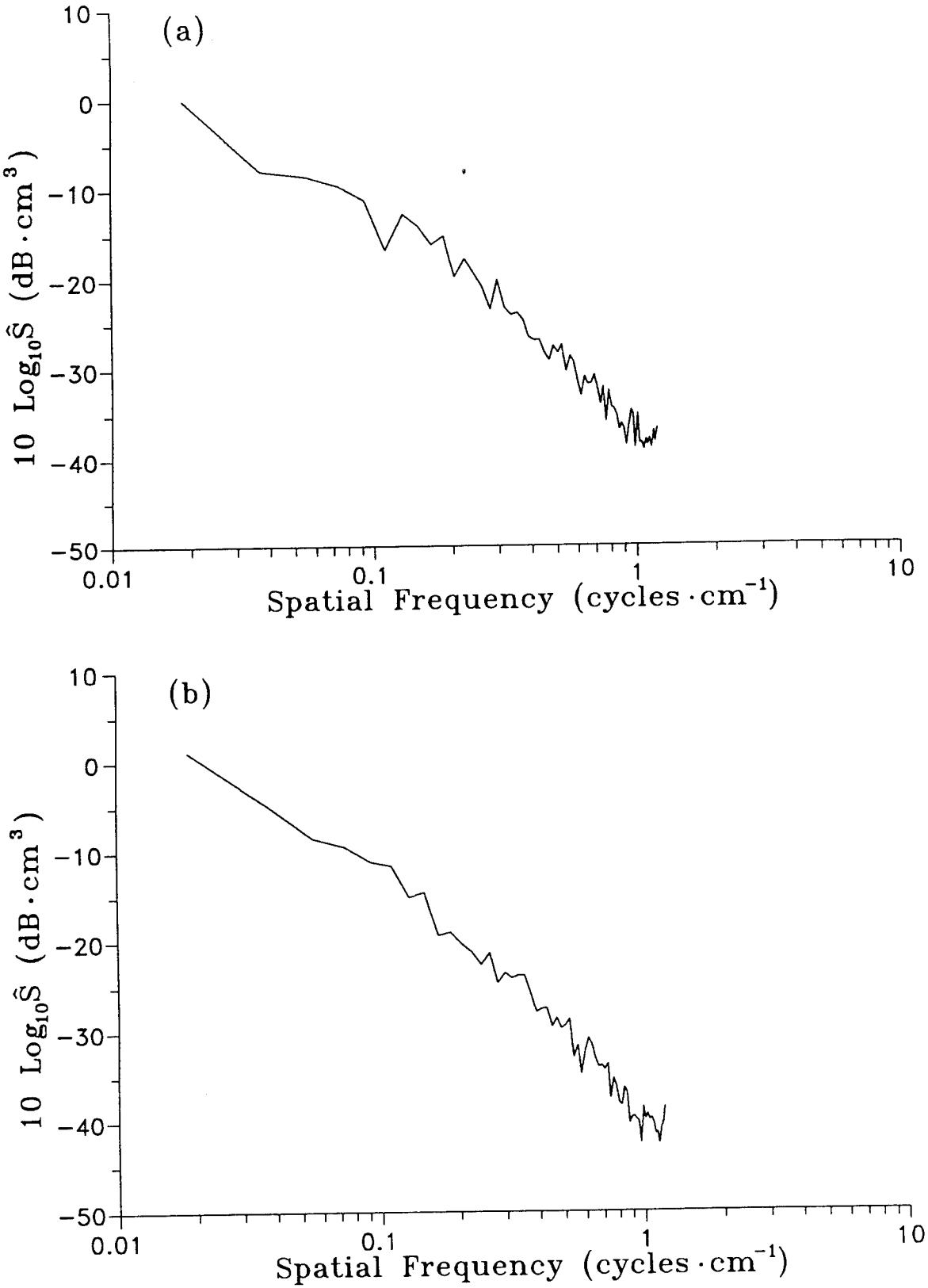

Figure 12. Pre-storm roughness power spectra for the Russian River site: (a) crest-to-crest (across strike) and (b) along strike orientations.

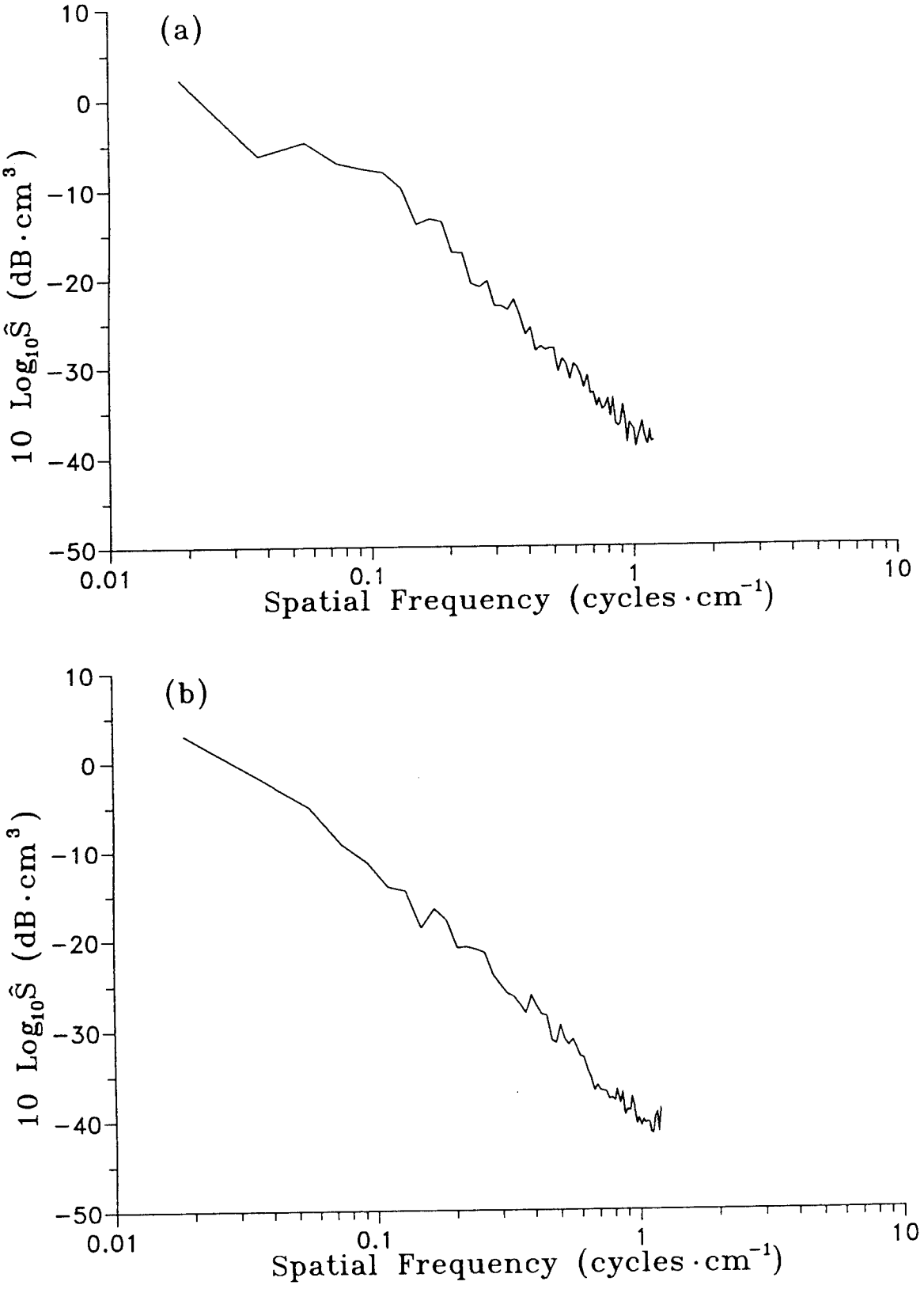

Figure 13. Post-storm roughness power spectra for the Russian River site: (a) crest-to-crest (across strike) and (b) along strike orientations.

Panama City (I)

Observations by divers and side-scan-sonar records indicated the experiment site to be uniform, of low relief and isotropic in terms of sediments and interface characteristics. The vertical distribution of sediment geoacoustic properties for the 15 cores collected at the experiment site are displayed in Fig. 14. Values of sediment compressional wave velocity ratio, attenuation, porosity and mean grain size exhibited relatively low variability when compared with the other experiment sites.

Values of sediment porosity averaged 39.0 % and ranged from 34.6 to 42.5 %. There was a slight decrease in porosity with increasing depth in the sediment. Sediment porosity and bulk density (average: 2.016 g cm^{-3}) were calculated assuming an average grain density of 2.65 g cm^{-3}.

Sediments at the experiment site were moderately sorted to poorly sorted fine sands. There was very little variation in mean grain size with increasing depth in the sediment, although coarse-skewed distributions occurred at 5 and 19 cm depth due to the presence of some gravel-sized shell fragments.

Values of compressional wave velocity ratio averaged 1.113, with a coefficient of variation of 0.87 %. This variation was small compared with that of velocity ratios from sandy sites like Quinault Range (CV = 1.19 %). The only discernible trend in sediment sound velocity ratio was a slight increase down to 4-cm sediment depth, then a constant value below 4-cm sediment depth.

Values of sediment compressional wave attenuation averaged 0.58 dB m^{-1} kHz^{-1} and ranged from 0.42 to 0.98 dB m^{-1} kHz^{-1}. Variability of the attenuation values at

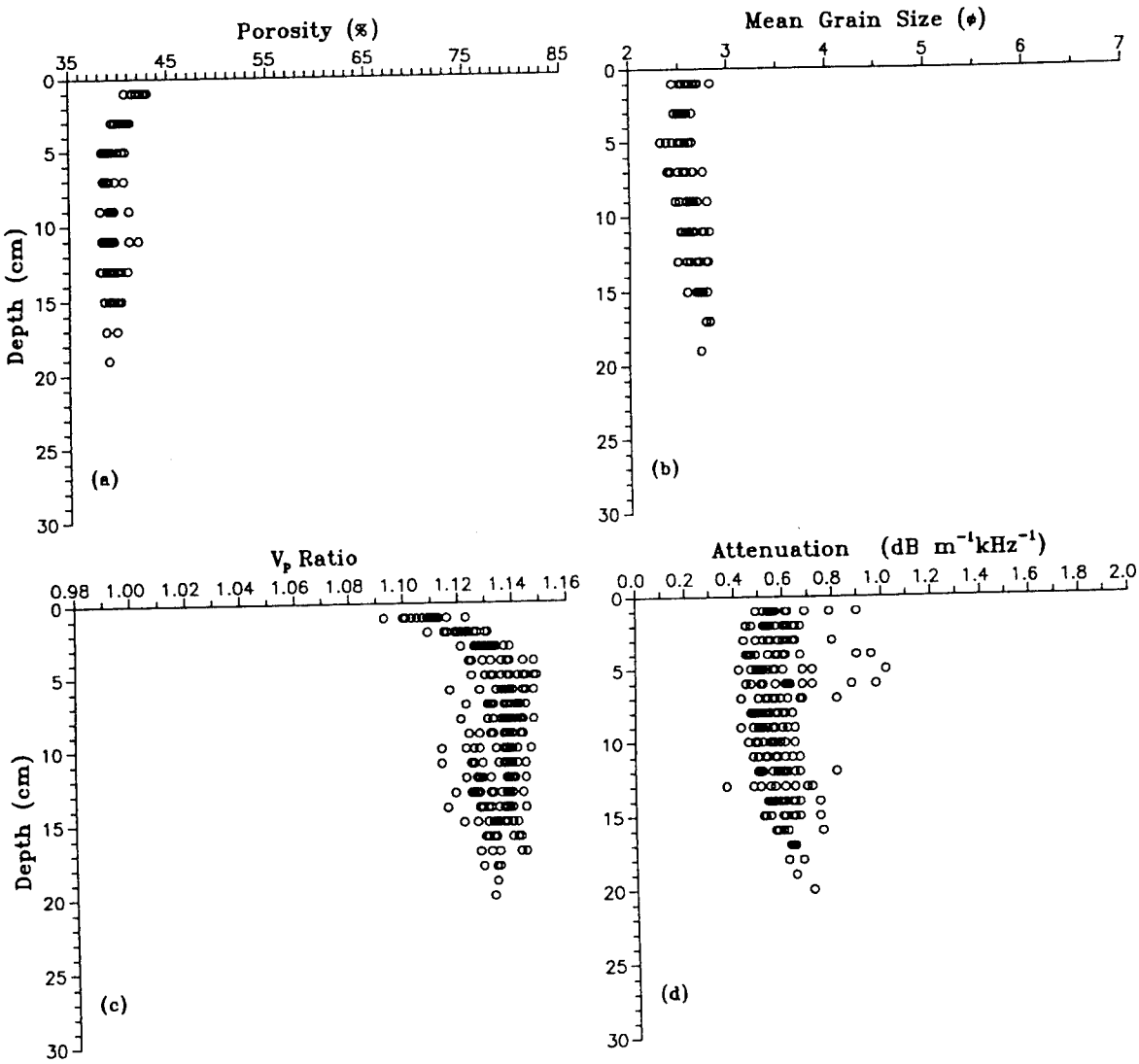

Figure 14. Profiles of geoacoustic properties for the Panama City site: (a) porosity, (b) mean grain size, (c) sound velocity ratio, (d) attenuation.

various depths in the sediment, though relatively low, was caused by the presence of buried mollusk-shell fragments. Attenuation of the acoustic energy by Rayleigh scattering from gravel-sized shell hash was less at this experiment site than at the Quinault Range or Arafura Sea sites.

Bottom roughness was determined from two photographic transects aligned with the 270°W azimuthal direction of the acoustic measurements. The transects were located 20 m and 50 m from the base of the tower. From 55 stereo-pair photographs, 25 were chosen for photogrammetric analysis. Relative sediment height was determined for 128 equally spaced (0.42 cm) points along six digitized roughness profiles in each stereo pair. Three profiles (53.34 cm long) were oriented parallel with the azimuthal direction of the acoustic measurements (270°W) and three profiles were oriented orthogonal to that azimuth (0°N). Optical distortion was apparent in 74 of the 150 roughness profiles and these data were eliminated from further analysis.

Features responsible for variations in relative sediment height at the Panama City (I) site were randomly distributed mounds and pits created by the activity of benthic invertebrates and demersal fishes. Because of the origin of the microtopographical relief, roughness anisotropy was not expected to occur. Periodogram estimates of power spectra were calculated from the two photographic transects (Fig. 15). The slopes and intercepts (Table 3) from the power spectra were calculated by regressing (log) power spectrum value on (log) spatial frequency. An analysis of covariance for testing the equality of regression slopes revealed no significant differences ($\alpha < 0.01$)

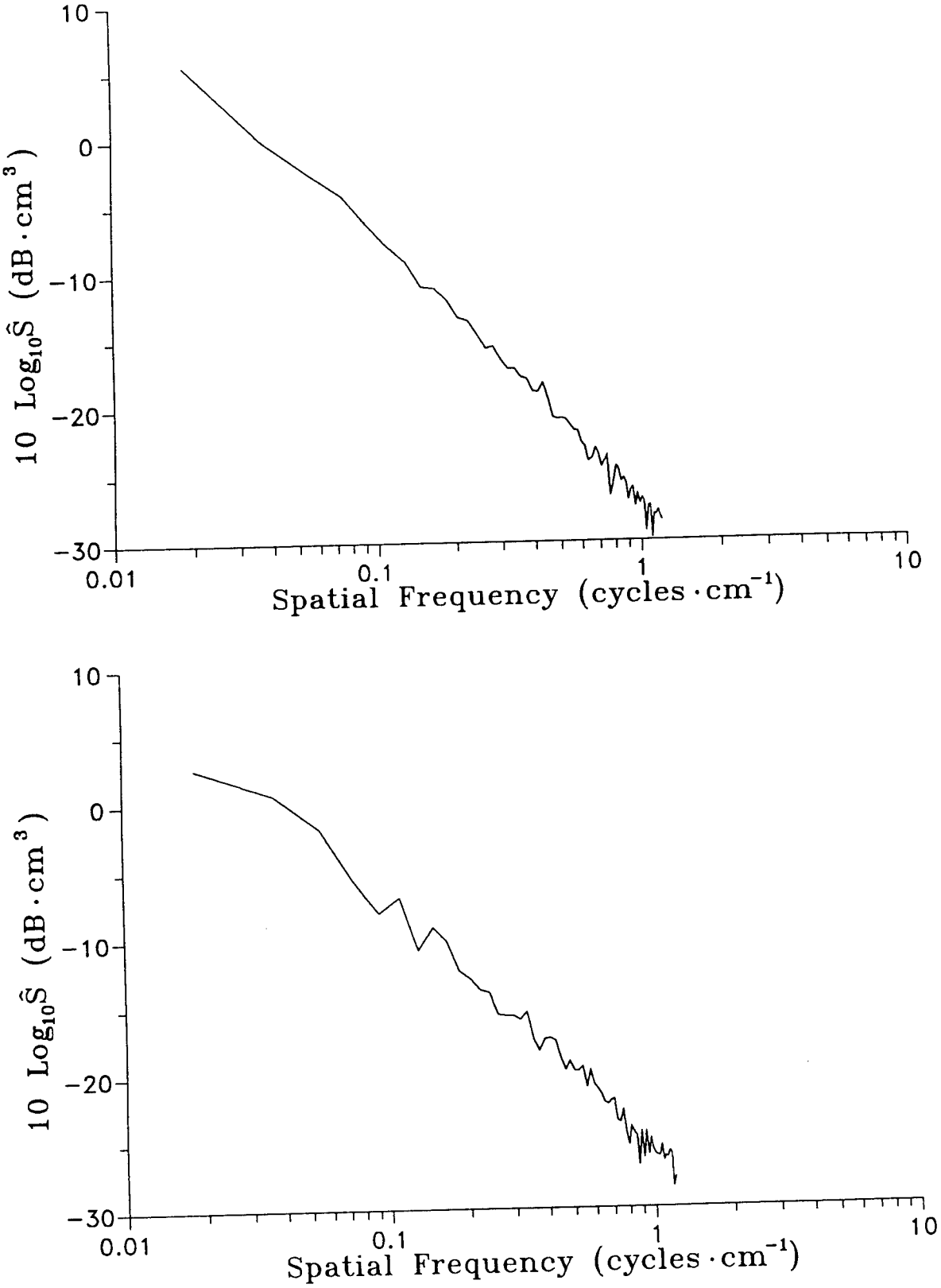

Figure 15. Roughness power spectra for the Panama City site: (a) 20 m from tower and (b) 50 m from tower.

between power-spectrum slopes for different azimuthal directions at either transect. There is a difference, however, between power-spectrum slopes corresponding to the two transects. Roughness profiles located 20 m from the base of the acoustic tower generated power-spectrum slopes that were steeper than those generated from profiles located 50 m from the tower (Table 3). The steeper spectra exhibit both more roughness power in the low-frequency domain and less roughness power in the high-frequency domain than the spectra generated from profiles farther from the tower.

Jacksonville (II)

Side scan sonar and bathymetry records revealed alternating bands of coarse shell hash and shelly sand, but no significant relief. The coarse sediment may have offered enough resistance to sediment transport by currents to result in an extremely flat bottom essentially devoid of bedforms. The vertical distribution of sediment geoacoustic properties for the 15 cores collected at the experiment site are displayed in Fig. 16.

Values of sediment porosity averaged 39.0 % and ranged from 32.0 to 46.1 %. The vertical distribution of porosity values decreased slightly with increasing sediment depth. Below 16 cm sediment depth, porosity values increased slightly as the percentage of fines increased. Measured values of average grain density were high (mean: 2.69 g cm^{-3}) due to high concentration of calcium carbonate mollusk shell fragments.

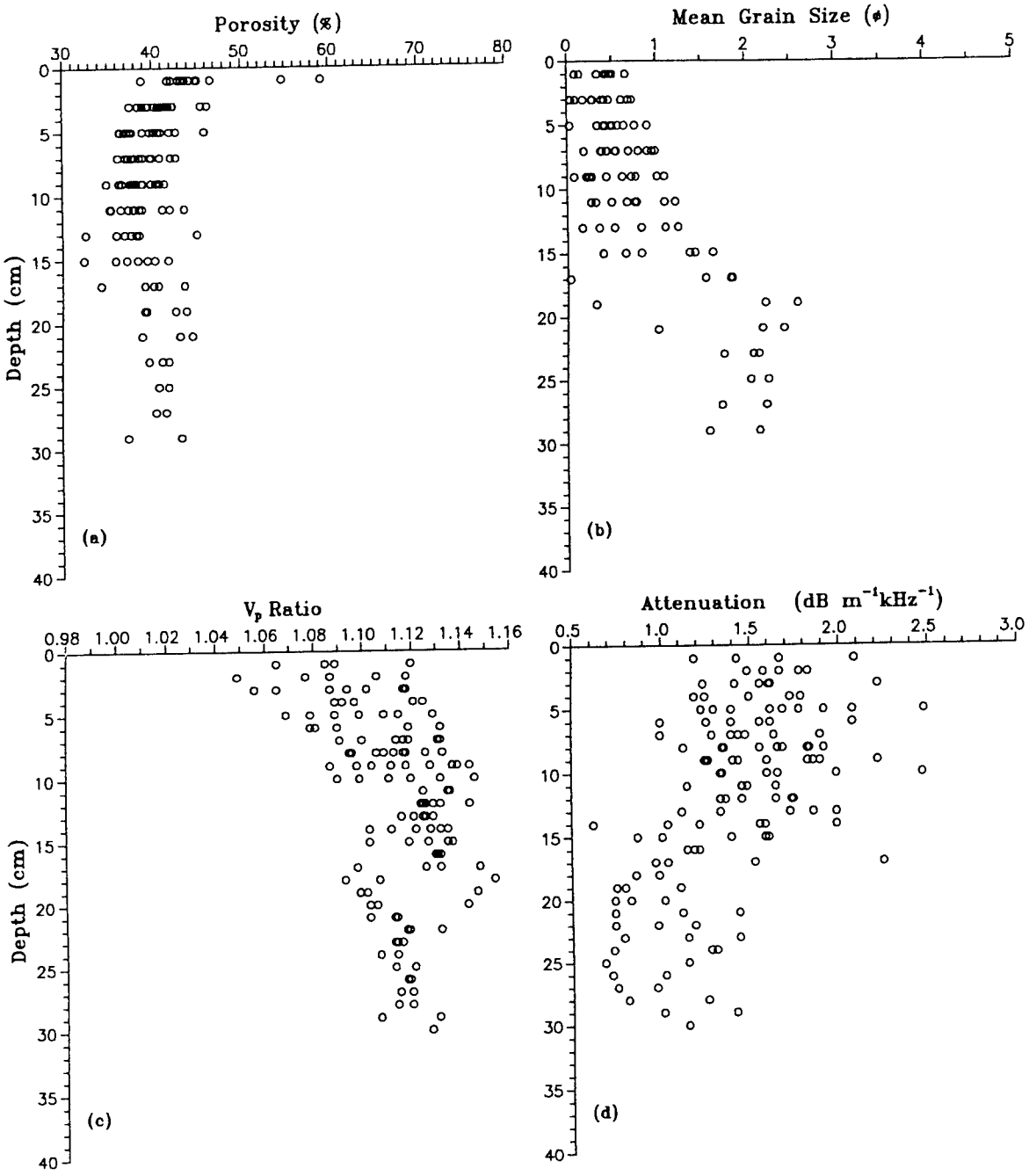

Figure 16. Profiles of geoacoustic properties for the Jacksonville site: (a) porosity, (b) mean grain size, (c) sound velocity ratio, (d) attenuation.

The mean grain size of sediment samples from 12 cores was 0.84 phi (0.557 mm) which corresponds to a coarse sand. However, grain size distributions indicated the mean to be coarse-skewed from a medium sand mode by high concentrations of shell fragments in the size fractions from coarse sand (1.0 ϕ) to pebble gravel (-4.0 ϕ). The top 18 cm of sediment was characterized by coarser material (0.61 ϕ, or 0.655 mm) and overlaid a finer sediment (1.85 ϕ, or 0.277 mm) of less than 5% gravel by weight (Fig. 16). The high concentrations of shells in the surficial sediment was obvious from observations and sediment surface samples from divers. Denser concentrations of shell hash distributed in parallel, alternating bands were oriented north-south. These bands averaged 42 cm in width and had an average periodicity of 78 cm (midpoint to midpoint). Despite a lack of significant elevation difference between the darker, concentrated shell bands and the lighter, sparse shell bands, differences in grain size characteristics did exist in the top 2 cm of sediment. Gravel fraction percentages of the darker bands averaged 57.5 %, whereas gravel fraction percentages of the lighter bands averaged only 17.8%. In addition to the larger proportion of gravel, larger fragments and greater number of whole shells were found in the darker bands.

Compressional wave velocity ratio values averaged 1.113 and exhibited a coefficient of variation of 1.76 %. A wide range of velocity ratio values at the sediment surface contributed to the high variability of this parameter. Variations in sound velocity in the top 3-cm section of the cores may have resulted from difficulties in measuring coherent acoustic signals in very coarse sediments. Scattering of the

400-kHz signal by shells larger than an acoustic wavelength (4 mm) and receiving multipath signals through various large pore spaces effected by the shells could have produced velocity data lower than expected for coarse sands. Failure to detect coherent high-frequency signals is common in coarse sediments (Briggs *et al.*, 1986; Richardson, 1986; Richardson *et al.*, 1986) and is related to the difficulty in finding the leading edge of the received signal as a consequence of scattering of the acoustic energy. Measurement of the wrong peak would result in greater time delays (and slower calculated velocities).

Sediment compressional wave attenuation values averaged 1.46 dB m^{-1} kHz^{-1} and exhibited a coefficient of variation of 32.77 %. Magnitude and variability of attenuation measurements were highest in the top 18 cm of sediment (Fig. 16). Such high values of attenuation were due to Rayleigh scattering of acoustic energy by varying amounts of mollusk shells and shell fragments. It is apparent that values of attenuation reported here do not represent only intrinsic attenuation.

Bottom roughness measurements were made from photographic transects oriented at 150°SE and 240°SW to coincide with the azimuthal directions of the acoustic transmitter used in the experiment. Stereo photographs from two dives were analyzed; one station was located 15 m southeast of the acoustic tower and the other station was located 30 m southeast of the tower. The sea floor at the experiment site was generally devoid of significant topographical features except for occasional regular urchins (*Lytechinus callipeplus*) which occur in over 5 % of the photographs. These urchins became conspicuous to investigators due to their behavior of attaching

large bivalve shells over their aboral surface with their pedicellariae.

Twenty-four (12 in each azimuthal direction) representative stereo photographic pairs were selected from the total of 113 bottom stereo photographs to statistically characterize a range (12° to 28°) of grazing angles in both azimuthal directions. Relative sediment height measurements were made by digitizing 128 equally spaced (0.42 cm) points along three digitized roughness profiles in each stereo pair. Restricting the digitized area to the three profiles oriented parallel to the photographic transect prevented optical distortion from occurring in any of the 53.34-cm-long profiles. Periodogram estimates of power spectra were calculated from the two photographic transects. The ANCOVA for testing the equality of slopes of the power spectra reveals no significant differences ($\alpha < 0.01$) between power spectra slopes for different azimuthal directions at either station. Regression slopes of 18 aggregated periodograms (six stereo pair photographs for each of two stations and orientations; three profiles per stereo pair photograph) rather than regression slopes of the average periodograms were tested by ANCOVA. That is, 1152 data pairs were regressed instead of the 64 data pairs resulting from an average periodogram. The slope of the power spectrum averaged from all periodogram ordinates (4608 data pairs) was -1.47 (Fig. 17). Values of power spectrum slope and intercept are displayed in Table 3. Values of slopes at this site were 0.5 to 1.0 slope units (cm^3) less steep than measured roughness power spectra from other shallow water sites. Less steep power spectra slopes at this site were indicative of a greater proportion of roughness power concentrated in the higher spatial frequencies.

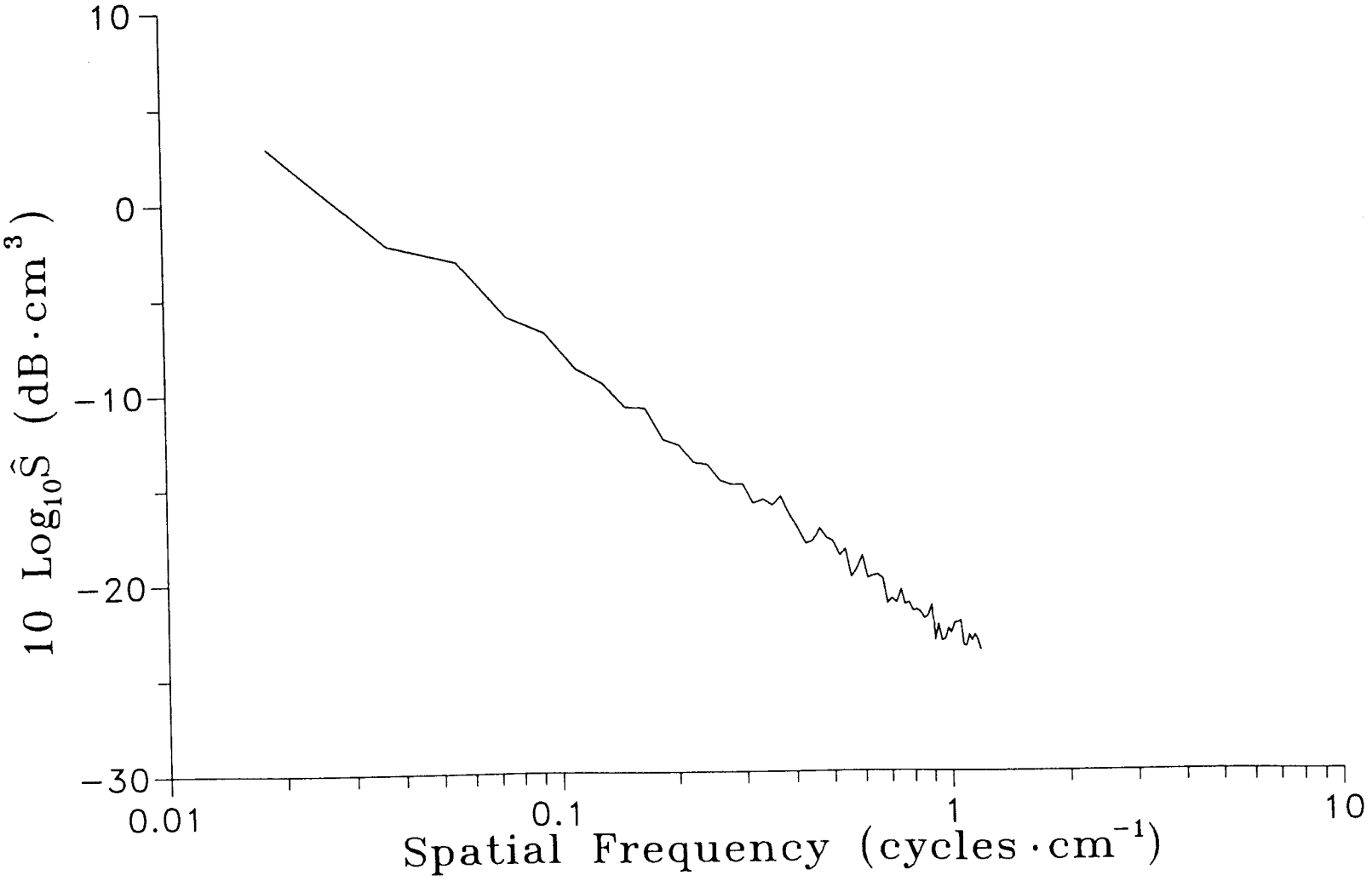

Figure 17. Roughness power spectrum for the Jacksonville site.

DISCUSSION

Data-Model Comparisons

In this section, backscattering data from the five experiment sites will be compared with the composite roughness backscatter model using the geoacoustic and roughness data as inputs. Through these comparisons of model predictions with field measurements, the mechanisms responsible for scattering may be elucidated. The model is described by Jackson *et al.* (1986a) and modified as discussed in Jackson and Briggs (1992). The model as well as the input parameters are described briefly in Appendix A, with the emphasis on the recent modifications.

The input parameters (v, ρ, V_p, δ, σ_2, γ and w_2) given in Table 4 are obtained from surficial values (0-2 cm sediment depth) of the geoacoustic parameters presented in Figs. 7, 9, 11, 14 and 16. Surficial values of sound velocity ratio, density ratio and attenuation are preferred (especially in sands) over values obtained by averaging over the entire core due to the limited depth of penetration into the sediment by high-frequency acoustic energy. Surficial values of these three parameters for the Jacksonville (II) site are obtained from data collected as deep as 4 cm due to measurement difficulties resulting from determining sediment properties (especially porosity) from the gravel-sized shell hash. The greater number of reliable data from the deeper interval provides more representative average values. Values of the volume scattering parameter (σ_2) in Table 4 are obtained by fitting the model to the data. Through manipulation of the value for σ_2, the contribution of sediment

Table 4. Input parameters used in data-model comparisons: compressional wave velocity of overlying water (v), density ratio (ρ), compressional wave velocity ratio (V_p), loss parameter (δ), volume scattering parameter (σ_2), spectral exponent (γ), and spectral strength (w_2). Spectral parameters indicate along strike ($\parallel$) and across strike ($\perp$) orientation of roughness measurements.

Site	v	ρ	V_p	δ	σ_2	$\gamma_\parallel$	$\gamma_\perp$	$w_{2\parallel}$	$w_{2\perp}$
Quinault Range	1.113	1.95	1487	0.0091	0.001	3.92	3.67	0.00598	0.00422
Arafura Sea	0.988	1.36	1539	0.00557	0.005	3.18	3.18	0.00318	0.00318
Russian River									
Pre-storm	1.002	1.42	1488	0.0101	0.002	3.65	3.38	0.000846	0.000912
Post-storm	1.002	1.42	1488	0.0101	0.002	3.73	3.56	0.000826	0.001296
Panama City (I)									
20 m from tower	1.109	1.92	1533	0.0189	0.001	2.97	2.97	0.00590	0.00590
50 m from tower	1.109	1.92	1533	0.0189	0.001	2.81	2.81	0.00590	0.00590
Jacksonville (II)	1.090	1.93	1542	0.0563	0.004	2.47	2.47	0.00522	0.00522

volume scattering to total backscatter strength is elucidated.

Backscattering data from the Quinault Range are displayed in terms of scattering strength as a function of grazing angle in Fig. 18. The data displayed in the figure were obtained across the strike of the sand ripples. Although one would expect scattering from the faces of the ripples to result in higher scattering strengths for the across-strike direction than resulted from the along-strike direction, scattering strengths measured in orthogonal directions were essentially equal when considering experimental error. Backscattering strength as a function of grazing angle measured for the different towing directions appears in Fig. 11 of Jackson and Briggs (1992). The data displayed in Fig. 18 were collected at 25 kHz and 35 kHz. Data collected at other frequencies indicated the same isotropy in scattering strength.

Figure 18 compares backscattering data collected at frequencies of 25 and 35 kHz from the Quinault Range with predictions from the composite roughness model using the inputs from Table 4. The value chosen for the volume scattering parameter increases the predicted strength to the measured data, but only effectively in the range of grazing angles from 25° to 60°. Outside this angular range the volume scattering cross section is comparably smaller than the surface roughness scattering cross section, resulting in little or no contribution of sediment volume scattering to the predicted backscattering strength. Fluctuation of the volume scattering (σ_2) parameter from 0.0003 to 0.003 generates predictions that fall within the 3 dB error of the backscattering measurements. The fine-sand sediment at the Quinault Range is probably a transitional case in terms of the model in that surface roughness and

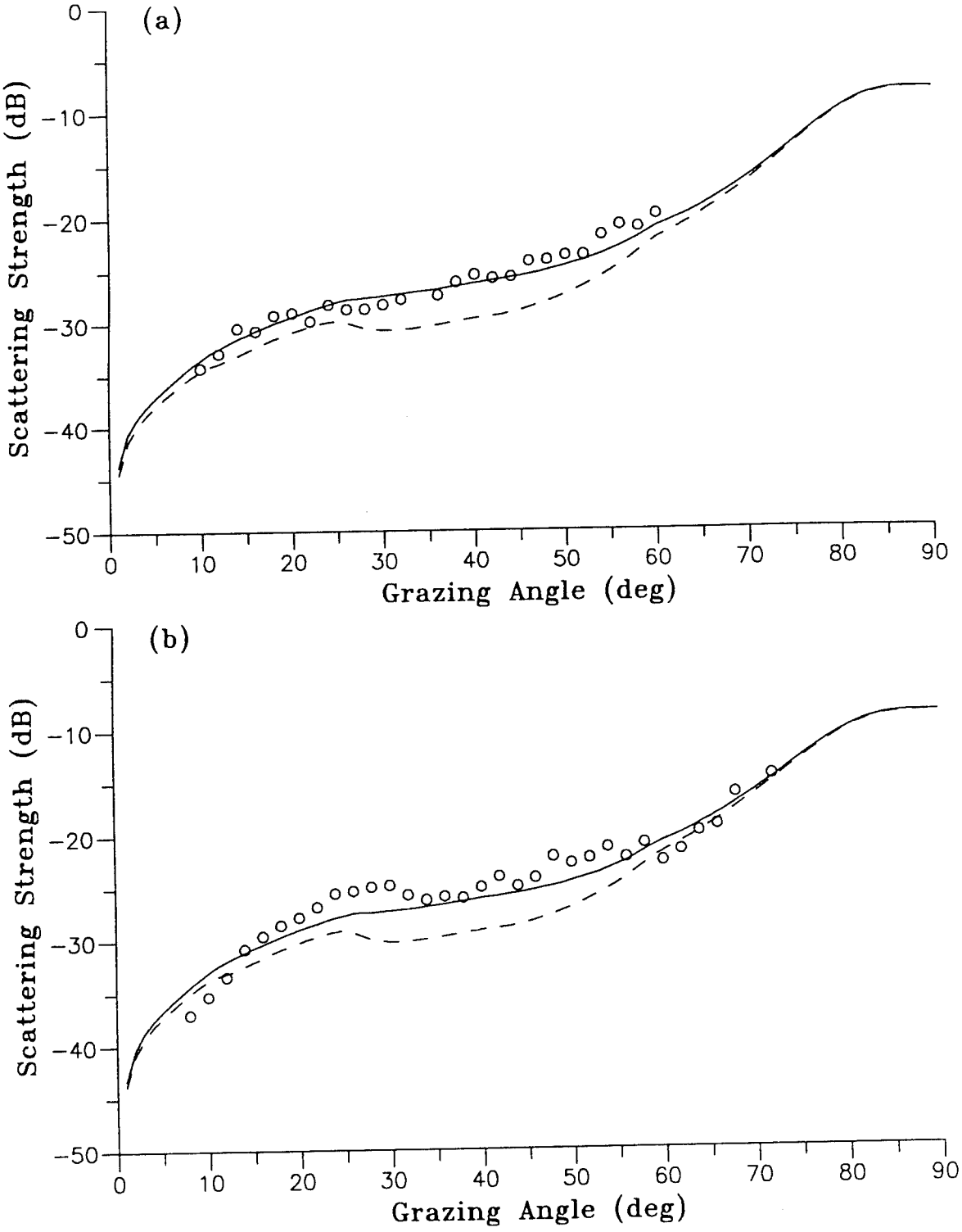

Figure 18. Comparisons of backscattering strength model predictions with backscattering strength measurements at the Quinault Range site. The dashed curves show the model prediction for roughness scattering only and the solid curves show sediment volume and roughness scattering: (a) 25 kHz, (b) 35 kHz.

sediment volume scattering contributions are approximately equal. At grazing angles less than critical (26°) and greater than 70°, surface roughness dominates sediment volume scattering.

The spectral exponents in Table 4 used to generate the model predictions are very near the value of 4, especially the along-strike value of γ = 3.92. A spectral exponent of 4 results in an infinite value for rms slope in the model, and γ = 3.92 generates an impracticably large rms bottom slope of 33° (Jackson and Briggs, 1992). The large slope is a result of a faulty extrapolation of the power behavior of the roughness power spectrum into a lower spatial frequency domain than the stereo photographic data allow. Such an extrapolation implies that the bottom roughness is characterized by steep-sided ripples with slopes of 33° and wavelengths longer than the 31.5-cm profiles digitized from the stereo photographs. The model predicts elevated scattering-strength values due to artificial increases in the grazing angle created by the steep slopes. The spectral exponent value for the across-strike direction (γ = 3.67) yields an rms slope of 12°, which is the value chosen for the model predictions. Fixing the rms slope value, the model shows negligible anisotropy for along- and across-strike directions and agrees with the collected backscattering data. The fact that estimates of the slope of the roughness power spectra are not significantly different would seem to corroborate the lack of anisotropy over the physical scales measured. The variances of the two spectra, however, are different (Fig. 8). In other applications of the model no exaggerated rms slope values are obtained as long as $\gamma < 3.7$.

Although visual impressions from photographs of the experiment site are that of a strongly directional ripple field with prominent crests and troughs, acoustic measurements, modelling and roughness-power-spectrum analysis reveal that the apparent anisotropy is actually very subtle from a physical-mathematical aspect. This result is in agreement with results published by Jackson *et al.* (1986b) and Boehme and Chotiros (1988). Data of Boehme and Chotiros (1988), however, do show directional anomalies in the statistical behavior of the backscattered-signal envelope.

Figure 19 displays the backscattering data from the Arafura Sea in terms of scattering strength as a function of grazing angle. Levels of scattering strength were comparable to those at the Quinault Range site despite the muddy sediments of the Arafura Sea. The entire experiment site was remarkably homogeneous and exhibited no backscattering anisotropy. Data were rather constant with a standard deviation of only 1 dB. Scattering strength (at 20° grazing angle) was also constant over a range of frequencies from 15 to 45 kHz.

In contrast to the Quinault Range site, the Arafura Sea site is characterized by relatively little contribution to backscattering by surface roughness scattering. Figure 19 shows the large disparity between the roughness scattering portion predicted by the model and the measured data. Hence, the model prediction matches the data well when a relatively large value for sediment volume scattering parameter (σ_2 = 0.005) is chosen. Reasonable fits between the model and the data are achieved using values of σ_2 in the range from 0.004 to 0.006. The Arafura Sea sediments contain large percentages of gravel-sized shell hash within the finer particle matrix, and it is

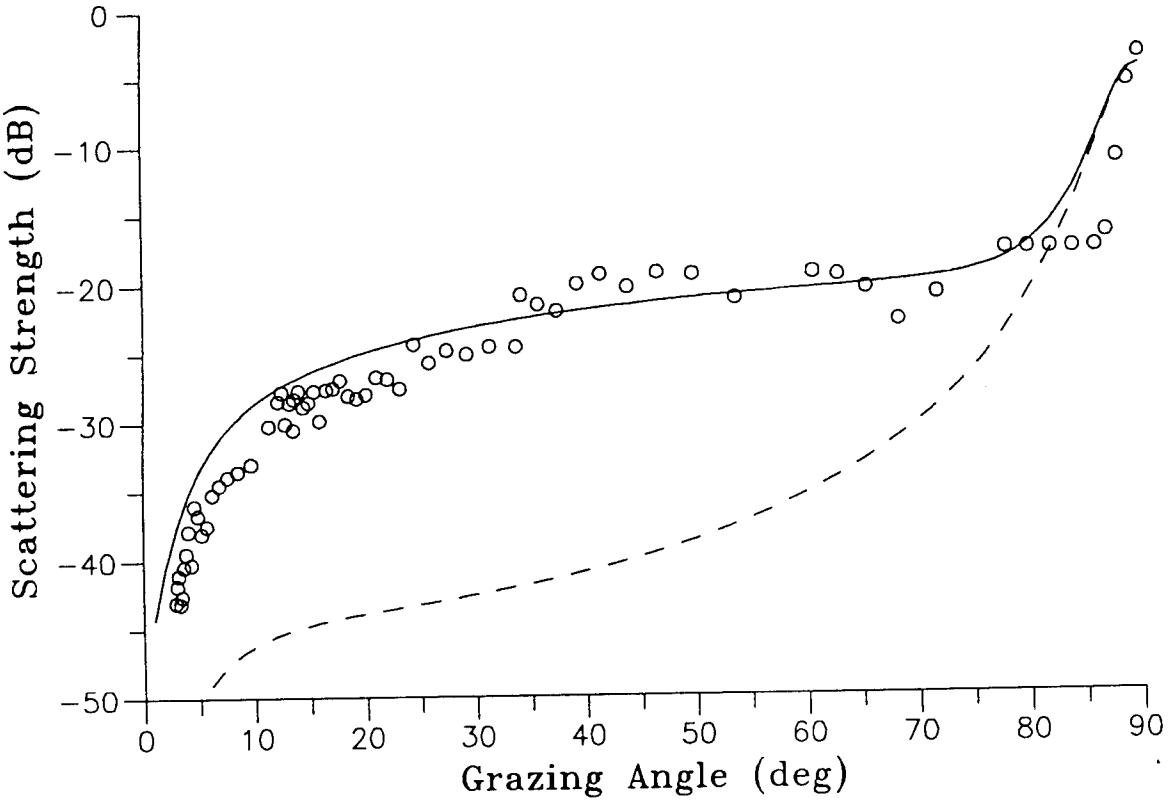

Figure 19. Comparisons of backscattering strength model predictions with backscattering measurements at the Arafura Sea site. The dashed curves show the model prediction for roughness scattering only and the solid curves show sediment volume and roughness scattering. The frequency is 20 kHz.

these shells and shell fragments that are implicated as volume scatterers (Briggs *et al.*, 1989a).

Backscattering data collected from the Arafura Sea exhibit little dependence on acoustic frequency (Jackson and Briggs, 1992). Sandy silt sediments from the North Sea show this same lack of frequency dependence in backscatter strength (Jackson *et al.*, 1986b). The frequency independence of backscattering in sediments allowing significant penetration of acoustic energy (those sediments referred to as "soft", such as muds) may offer an insight into the cause of sediment volume scattering. If σ_2 is independent of frequency, and if the absorption coefficient α increases linearly with frequency (Hamilton, 1972), then the sediment volume scattering cross section σ_V must increase linearly with frequency (at least within the frequency range 10-100 kHz). The volume scattering cross section can be related to power spectra of sediment property (*i.e.*, density, porosity, sound velocity, or compressibility) fluctuations through perturbation theory. According to theory, the spectra S_i are related to the spatial wave number k_a such that

$$S_i \propto \frac{1}{k_a^3},$$

if the sediment volume scattering cross section is to maintain its linear relationship with frequency. The spectrum S_i is significant to the problem of volume scattering in that it represents a self-similar fractal random process. In other words, the inhomogeneities within the sediment will have the same physical structure regardless of the resolution with which the inhomogeneities are measured. Over the observed

frequency range of 15 to 45 kHz, acoustic wavelengths varied from 10.3 to 3.4 cm. Consequently, the inhomogeneities that are responsible for volume scattering in Arafura Sea sediments should be within this scale of wavelengths and be uniformly distributed with respect to volume (or cross-sectional area). Results of meristic analysis of the shell hash sieved from cores from the Arafura Sea indicate no particles are large enough individually to cause frequency-independent scattering, nor are the particles distributed equally according to volume (Briggs *et al.*, 1989a). Thus, the scatterers of interest are either (a) larger inhomogeneities within the finer sediment matrix such as burrows, (b) the shell-hash particles acting collectively as a larger, composite inhomogeneity, or both (a) and (b). If these mechanisms of sediment volume scattering are valid, then sediment-property measurements such as grain-size analysis that disrupt the existing fabric are useless in characterizing the responsible inhomogeneities.

Figures 20 and 21 display the backscattering data from the Russian River site in terms of scattering strength as a function of grazing angle. Data from scans were chosen for averaging from those collected 1 h after midnight to minimize possible scattering by pelagic organisms. The backscattering data from the Russian River site are averaged over all azimuths and over the entire 49-day deployment and compared with model predictions in Fig. 20. The azimuthal dependence of scattering strength was examined by averaging ten scans each 24 h period, for two periods (Fig. 21). Within each scan, the averages contained nine pings from an azimuth of 201°SSW (along strike), 111°ESE (across strike), and 291°WNW (across strike). The pre-

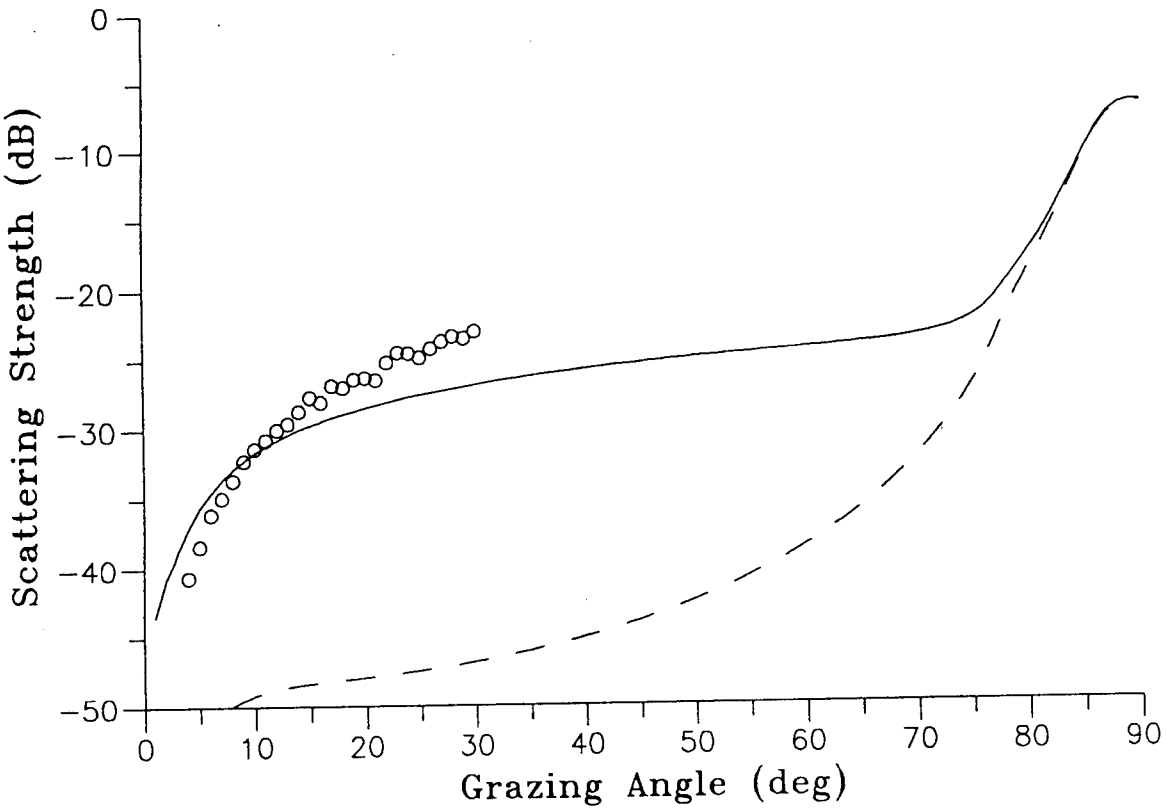

Figure 20. Comparisons of backscattering strength model predictions with backscattering strength measurements at the Russian River site. The dashed curves show the model prediction for roughness scattering only and the solid curves show sediment volume and roughness scattering. The frequency is 40 kHz and the model parameters are those for pre-storm, along-strike conditions.

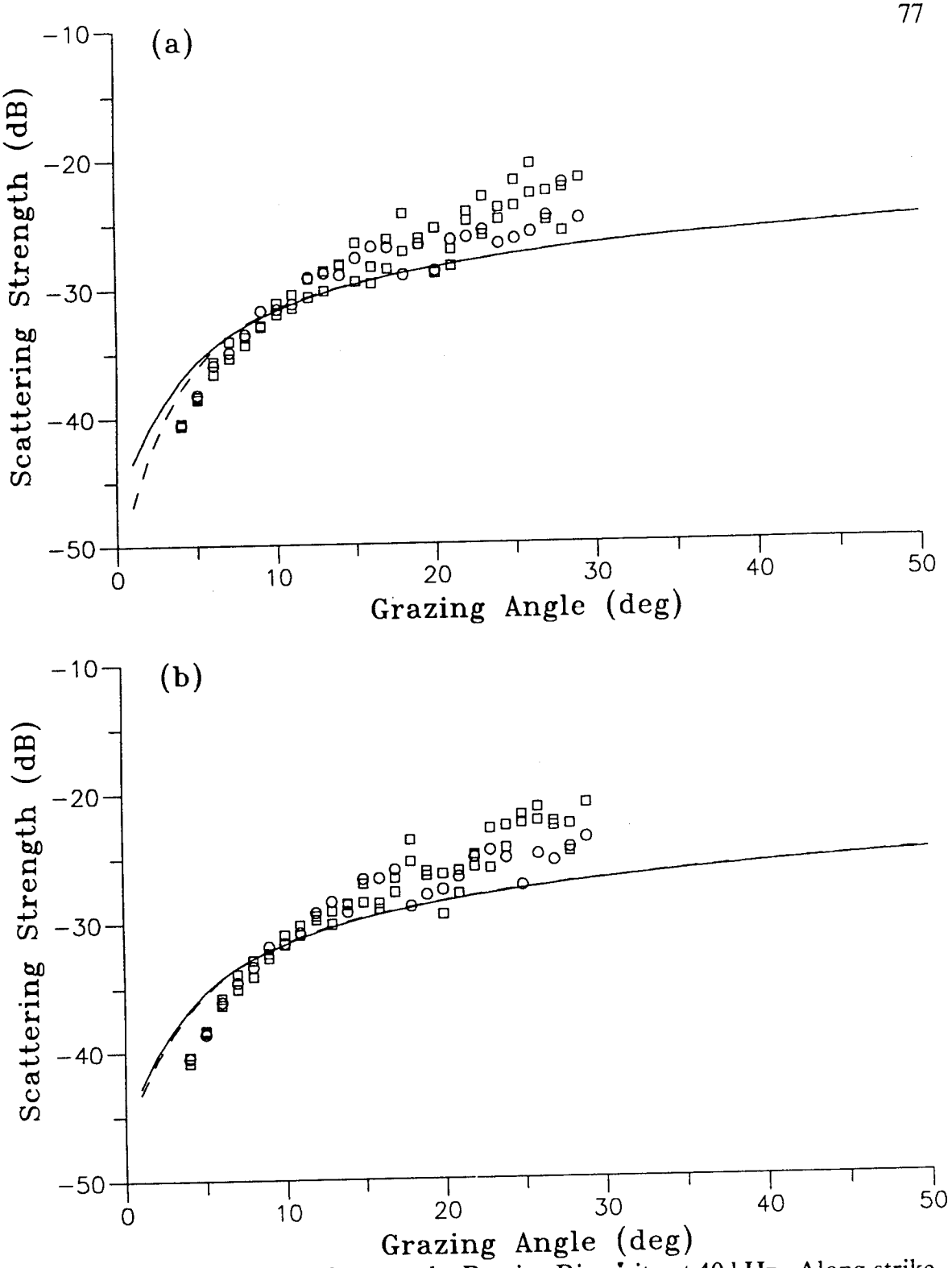

Figure 21. Azimuthal dependence at the Russian River site at 40 kHz. Along-strike model curves are shown as solid lines and corresponding along-strike data are shown as circles (201° azimuth). Across-strike model curves are shown as dashed lines and corresponding across-strike data are shown as squares (111° and 291°): (a) pre-storm, (b) post-storm.

storm data were collected in the period from 3-13 December 1988 and spanned the period during which the pre-storm geoacoustic measurements were made. The post-storm data were collected in the period from 12-21 January 1989, which was a little more than a week before the geoacoustic measurements were made (26-27 January). Variability in the data displayed in Fig. 21 was higher than in the other backscatter plots due to averaging over smaller data sets.

No anisotropy in backscattering was evident in data collected from grazing angles less than 20°. At angles steeper than 20°, average scattering strength was higher for data collected in across-strike directions (2 dB) than for the along-strike direction. Notably, this pattern of higher scattering strength in across-strike directions was evident in both pre-storm and post-storm measurements. It is not altogether clear whether this 2-dB average difference was caused by anisotropy in scattering or lack of uniformity in the substrate. The 20 to 30° angular interval corresponded to 9 to 14 m across the sea floor. Due to the small area over which data was collected and averaged, the difference in scattering strengths from the orientations could be caused by spatial heterogeneity of the surface sediment properties. Spatial variability in scattering strength on a similar scale was reported for medium sands from Charleston (Boehme and Chotiros, 1988).

As one might expect from a muddy, acoustically penetrable sediment, the predicted roughness scattering portion of the model underestimates the measured data by a large margin. The model prediction fits the measured data in Fig. 20 using $\sigma_2 = 0.002$. The backscattering strength appears to increase more rapidly with

increasing grazing angle in the data than in the model prediction. The steeper angular dependence of the data may be caused by a vertical gradient in σ_2. Although the model assumes that σ_2 is homogeneous and isotropic in three dimensions, a positive depth gradient in σ_2 could be responsible for scattering strength increasing more rapidly with increasing grazing angle than predicted by the model. The scattering strength increases more rapidly because steeper grazing angles allow penetration of acoustic energy to depths where σ_2 is larger. Indeed, relatively steep gradients do occur in values of porosity, sound velocity ratio and attenuation in the top 8 cm of sediment (Fig. 11).

Figure 21 shows practically insignificant azimuthal dependence of the measured data and the model predictions at the Russian River site both before and after the period of winter storms. There is a slight azimuthal dependence in the data at grazing angles greater than 20°, but the model can not account for this trend due to the assumption of isotropic sediment volume scattering. Although there is a significant difference between roughness power spectra for the post-storm period, the model predicts only a small anisotropy that is apparent only at grazing angles less than 5°.

Figure 22 displays the backscattering data collected at a frequency of 60 kHz from the Panama City (I) site in terms of scattering strength as a function of grazing angle. Estimates of scattering strength were made using data from the hydrophone positioned at the center of the array. Measured backscatter levels at small grazing angles are similar to those measured at the fine sand at the Quinault Range, but

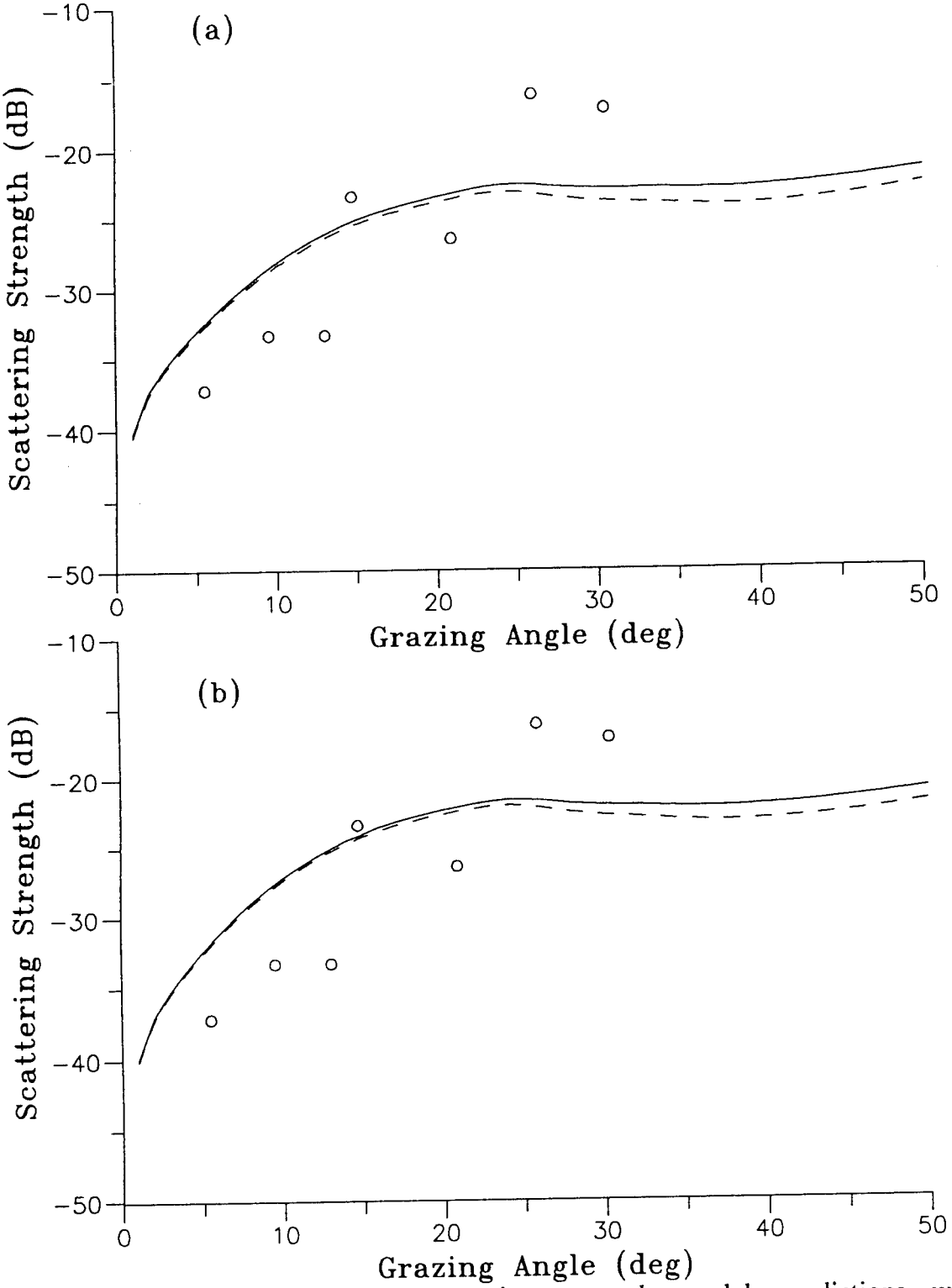

Figure 22. Comparisons of backscattering strength model predictions with backscattering measurements at the Panama City (I) site. The dashed curves show the model prediction for roughness scattering alone and the solid curves show sediment volume and roughness scattering. The frequency is 60 kHz: (a) 20 m from tower, (b) 50 m from tower.

continue to increase to levels greater than the Quinault data at grazing angles greater than 21°. Variability in scattering strength measurements was such that no anisotropy in backscattering was evident in data collected at all acoustic frequencies (20, 40, 60, 90, 110, 150 and 180 kHz). Error in estimating scattering strength was small based on ping-to-ping statistical variability, on the order of 1-2 dB (Stanic *et al.*, 1988). Signal fluctuations due to water column inhomogeneities or schooling fish probably dwarfed any errors in scattering strength estimates. In fact, the magnitude of the error in estimating the scattering strength was small in comparison to the magnitude of the variations in signal strength attributed to variability in physical properties of the sea floor.

A low value for the σ_2 parameter (0.001) of the composite roughness model fits the measured data because of the low potential for sediment volume scattering at this site. That is, not much contribution to scattering from the sediment volume is expected from a sand bottom. Figures 22a and 22b illustrate the model's response to two different bottom roughness regimes at the experiment site. A slightly steeper slope of the roughness spectra (-1.97) in the area 20 m from the acoustic tower decreases the level of the model prediction in Fig. 22a about 1 dB from the prediction in Fig. 22b. In both areas, however, scattering strength is overestimated by the model at small grazing angles and underestimated by the model at angles larger than 25°. The scattering strength derived from the sediment volume contributes up to 1 dB more scattering strength at larger grazing angles.

The roughness regime near the tower corresponds to grazing angles in the vicinity

of 21°; the roughness regime 50 m from the tower corresponds to grazing angles in the vicinity of 9°. The fit of the model curve and the backscatter data does not appear to be improved in the vicinity of the corresponding grazing angles. Hence, differences in bottom roughness in these two areas have little effect on prediction of backscattering levels, but define a range of variability for the roughness parameters.

Figure 23 displays the backscattering data collected at frequencies of 20 and 40 kHz from the Jacksonville (II) site in terms of scattering strength as a function of grazing angle. Levels of measured scattering strength are high, even at grazing angles less than 15°. Despite the apparent lack of uniformity in the distribution of coarse shell hash on the sediment surface, no azimuthal dependence in the scattering strength measurements was found. Scattering strength estimates at the Jacksonville (II) site were greater than those estimates from the other experimental sites (*e.g.*, 3-5 dB greater than from Quinault Range fine sands and 8-10 dB greater than from Panama City fine sands). Variability in the measurements of scattering strength was high. The coefficient of variation for individual pings was generally over 40 % (Stanic *et al.*, 1989). Variation in the measurements may have been caused by small-scale fluctuations in the sound velocity profile due to internal waves, tidal currents or wind-wave action.

Backscattering strength is underestimated by the model using conventional values of σ_2 for sands because low slope values for roughness spectra result in low roughness scattering predictions. In Fig. 23b, the prediction is increased to the level of the measured data by adjusting $\sigma_2 = 0.004$. Using the same value for σ_2 at 20

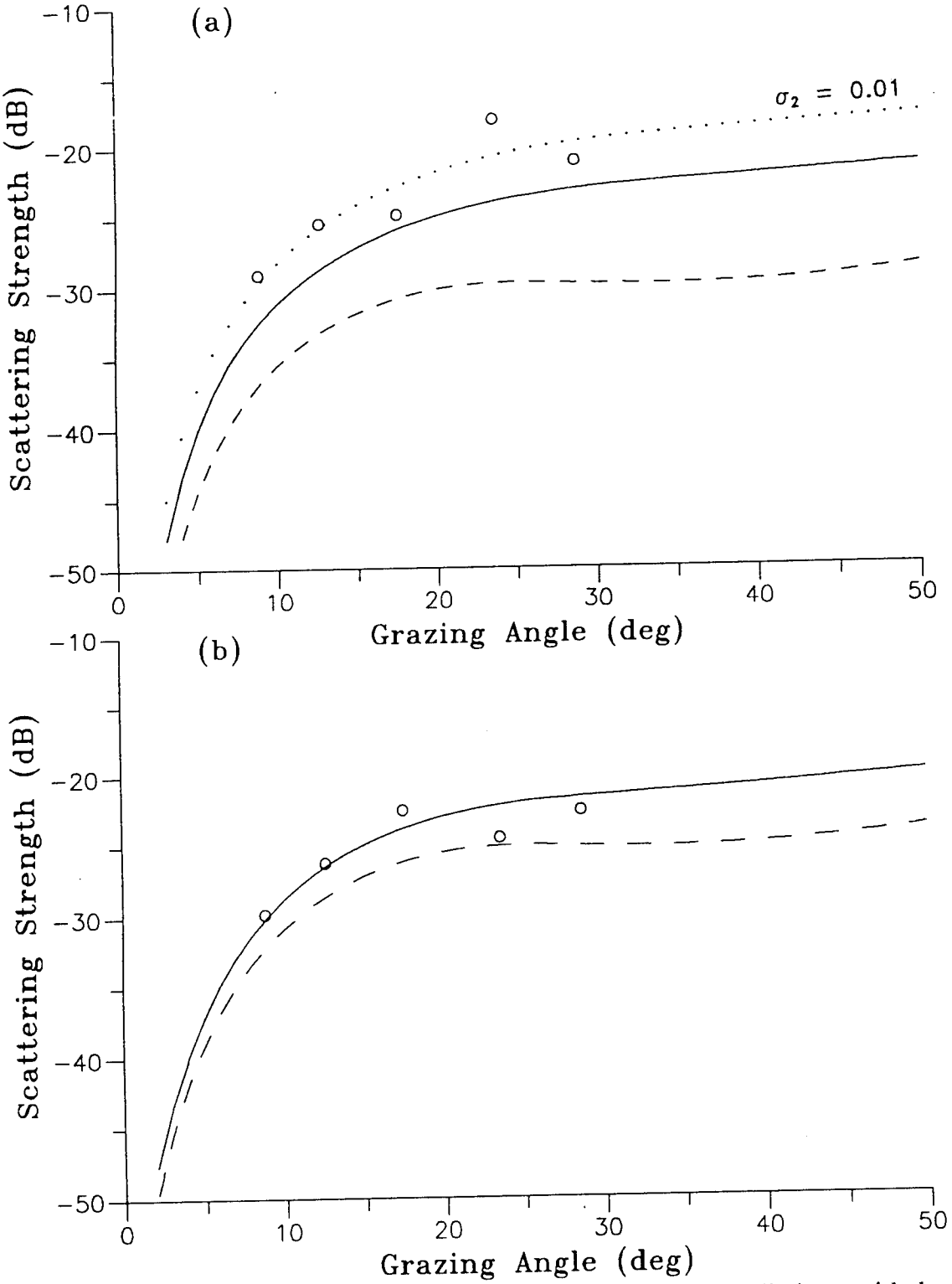

Figure 23. Comparisons of backscattering strength model predictions with backscattering strength measurements at the Jacksonville (II) site. Dashed curves show the model prediction for roughness scattering only and solid curves show sediment volume and roughness scattering: (a) 20 kHz, (b) 40 kHz. (Dotted curve includes volume and roughness scattering).

kHz, the model consistently underestimates the measured scattering strengths (Fig. 23a). In fact, the measured data at 20 kHz are fitted best using σ_2 = 0.01 (dotted curve in Fig. 23a). Values of σ_2 this large are reported by Stewart and Chotiros (1992), but no evidence supports significant volume scattering from these sediments. Assuming for the sake of argument that values of α are high (584 dB m^{-1} at 400 kHz) due to intrinsic attenuation, values of the scattering cross section (σ_v) would have to be very large to attain a value of σ_2 as large as 0.01. Even if the value of α is considered to be inflated because of scattering of the 400-kHz acoustic energy by the shell fragments, values of σ_V would have to be uncharacteristically large (for coarse sand) to accommodate large values of σ_2. A more likely explanation is the failure of the roughness component of the model to predict the proper scattering level for this type of sediment. In Fig. 23, the volume scattering component is being used to artificially increase the level of the predicted backscattering strength. This action is probably not a legitimate use of the model. The composite roughness model assumes single scattering only, and if multiple scattering is occurring the model is not appropriate.

Prediction of Sediment Volume Scattering

The inputs to the composite roughness model are directly related to measured geoacoustic properties except for the sediment volume scattering parameter. A different model is required to include the mechanism of sediment volume scattering and to make predictions based on existing core measurements. The volume

scattering model of Hines (1990) is a theoretical model involving the penetration, scattering and retransmission of spherical waves through a planar interface. The model assumes scattering is generated by fluctuations in porosity within the sediment volume. Parameters determining the intensity of scattering and the frequency and grazing angle dependence of scattering are the mean-square value and the correlation function of the porosity fluctuations, respectively. Also needed to generate numerical estimates from the model are expressions for the dependence of sediment sound velocity and density on porosity. Although predictions from the Hines model agree with backscatter data in the literature, actual sediment physical and geoacoustic data have not been used to ascertain the correlation function and variance (mean-square value) of the porosity fluctuations. Hence, to date, the model of Hines as well as the composite roughness model of Jackson *et al.* (1986a) have not been tested without fitting the model predictions to measured data using a free parameter. In order to test the assumptions of the volume scattering model of Hines, geoacoustic data collected by NRL can used to evaluate three parameters integral to the models: the dependence of sediment bulk density and sound velocity on sediment porosity, correlation functions of sediment porosity and velocity fluctuations, and variances of sediment porosity and velocity fluctuations.

Dependence of bulk density and sediment sound velocity on porosity

Estimates of the dependence of sediment bulk density and sound velocity on sediment porosity ($\partial\rho/\partial\beta$ and $\partial V/\partial\beta$, respectively) are made by fitting linear curves

to empirical relationships. Empirical relationships between sediment bulk density and porosity or between sediment sound velocity and porosity are often established by petroleum and defense researchers in order to interpret seismic and acoustic data. Obtaining estimates of $\partial\rho/\partial\beta$ and $\partial V/\partial\beta$ by fitting linear curves to empirical relationships such as those compiled by Hamilton and Bachman (1982) and Bachman (1985), as is done by Hines, should be regarded with some skepticism. A linear relationship between sediment density (ρ_s) and porosity (β) does exist for a given fluid density (ρ_w) and grain density (ρ_g):

$$\rho_s = \rho_w\beta + \rho_g(1-\beta)$$

Because the density of seawater changes little throughout the environments under investigation and grain density is a fairly conservative property in most of the environments on the continental shelf, we may differentiate with respect to porosity after multiplying and combining terms to find the dependence of density on porosity:

$$\frac{\partial\rho}{\partial\beta} = (\rho_w - \rho_g)$$

For a seawater density of 1025 kg/m^3 and a average grain density of 2650 kg/m^3 based on quartz grains with insignificant organic matter associated with the solid component of the sediment, the value for $\partial\rho/\partial\beta$ is -1625 kg/m^3. High amounts of low density organic matter in the lagoonal clay in St. Andrew Bay, Florida depress the value for average grain density values to 2350 kg/m^3 and result in the lower value for $\partial\rho/\partial\beta$ in this study of -1327 kg/m^3. Steeper values (slopes) of the dependence of sediment density on porosity would result from sediments consisting

of particles denser than quartz, such as carbonate and heavy minerals. The estimated value for $\partial\rho/\partial\mathcal{B}$ of -1440 kg/m^3 used by Hines (1990) is on the low side for shelf sediments, but falls within the range derived from the aforementioned considerations. An assortment of divergent grain types as one would encounter in a geologically complex sedimentary regime (e.g. laminae composed of terrigenous turbidites, volcanic ash, biogenic carbonate and silica) is a rare consideration in surficial sediments pertinent to high-frequency acoustic scattering. Interaction between acoustic energy and sediment beds of diverse origin is more likely to occur in seismic studies, where low-frequency energy encounters numerous, thick strata at greater depths in the sediment.

Sediment sound velocity as a function of porosity, however, is not strictly linear (Bachman, 1985). Sediment compressional wave velocity decreases as porosity increases from 30 to just beyond 80 percent; as porosity continues to increase, sound velocity increases slightly because the amount of pore water has increased to the point where so few sediment particles are in contact with each other that the sound velocity is approaching the sound velocity through water alone. Because the relationship between sound velocity and sediment porosity describes a parabola, the slope of the curve described by $\partial V/\partial\mathcal{B}$ can vary from flat (0 m/s) in high porosity muds to very steep (negative slope) in low porosity sands. Indeed, the most rapid change in slope of the curve occurs within the porosity domain between the values of 60 and 80% where the porosity values of many surficial sediments are found. With such a wide latitude for possible values of $\partial V/\partial\mathcal{B}$, it is inaccurate to use an

average value for the dependence of sound velocity on sediment porosity. Moreover, the empirical relationship between sound velocity and sediment porosity is derived from a multitude of environments separated geographically and bathymetrically, including deep ocean basins and the continental slope (Hamilton and Bachman, 1982; Bachman, 1985). The diversity of environments from which the relationship is derived introduces variability not necessarily present at specific sites on the shelf. Sometimes sedimentary structures not encountered at the specific site are included in the database from which the regression is calculated. Therefore, a better estimate of $\partial V/\partial \beta$ in shallow-water environments would be derived from exclusively shallow-water velocity-porosity plots, and the best estimate would be generated from such data collected from the site of interest. This fidelity of the velocity-porosity model to data collected from specific sites is analogous to the fidelity of resistivity formation factor-porosity models to data from specific sediment types (Jackson *et al.*, 1978). Formation factor is determined from the ratio of the electrical resistivity of sediments to the electrical resistivity of the pore water and is used to assess sediment porosity. Factors such as packing and grain shape that affect the void spaces between grains are cited to explain the deviations from the formation factor-porosity model by data gathered from different environments. Packing and grain shape probably affect the velocity-porosity model in the same fashion.

Figure 24 is a plot of sediment compressional wave velocity as a function of sediment porosity for most of the shallow-water data presented in this paper. Values of sediment sound velocity are adjusted to conditions of 23 °C, 35‰, and 1 atm after

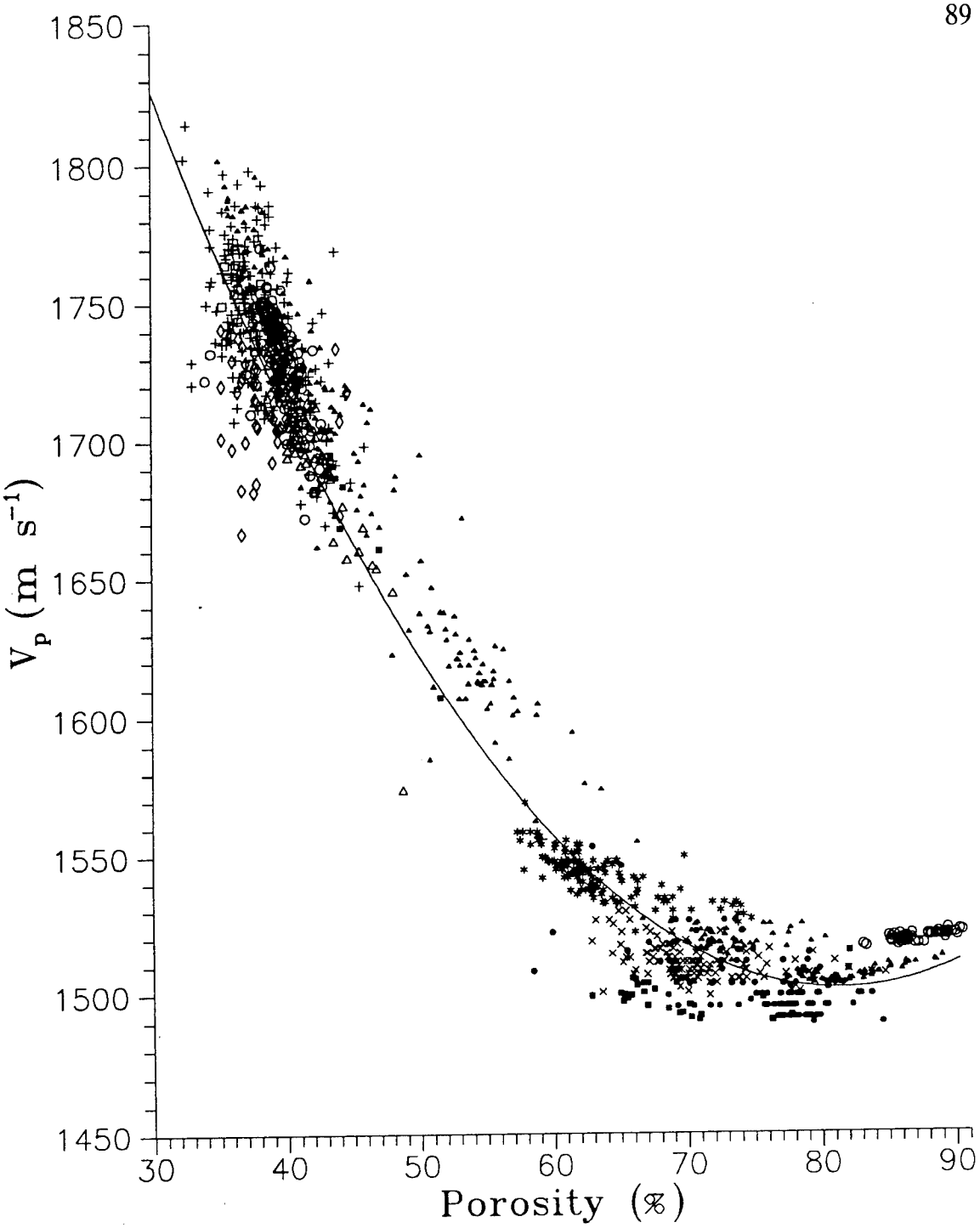

Figure 24. Plot of sediment compressional wave velocity (V_p, m/s) *vs.* sediment porosity (%) for various sites on continental shelves in this study. The symbols represent the following data sets: Arafura Sea (×), Charleston, SC (◇), Jacksonville, FL (+), Straits of Juan De Fuca (▲), La Spezia, Italy (▪), Long Island Sound (●), Montauk Point, NY (□), Panama City and St Andrew Bay, FL (○), Quinault Range, WA (△), and off the Russian River, CA (*). The regression line drawn through the points is described by the relation $V_p = 2315.6 - 20.02\beta + 0.12\beta^2$, where β is porosity in percent.

Hamilton (1971). The relationship between sediment velocity and porosity at 13 shallow-water sites is described by a second-order polynomial quite similar to that derived for continental terrace sediments by Hamilton and Bachman (1982). Differentiating this expression and solving with appropriate porosity values, results in values for $\partial V/\partial \beta$ of -1066 and -166 m/s for fine sand and mud, respectively (Table 5). Similar values of -1253 and -570 m/s are generated from the data presented by Hamilton and Bachman. There is the danger that variability in disparate sediment types geographically distant affect the curve of best fit and thus the slope at any one point on the curve. That is, local differences in sediment velocity due to local variations in porosity take precedence in establishing the relationship on which the acoustic model depends. A piecewise analysis of the sediment velocity-porosity curve in Fig. 24 divides the curve into site-specific regions. Table 5 presents a comparison of the results of piecewise analysis and evaluation of the NRL and Hamilton and Bachman (1982) sediment velocity-porosity regressions at various points of the curve according to a specific sediment type occurring at each site. Piecewise analysis of the data results in the steepest slope for fine sand off Panama City (-1302 m/s), but the least steep slopes for some other sites (-54 to -705 m/s). The regression of Hamilton and Bachman generates steeper slopes than the regression calculated from the NRL data. Slopes derived from data collected at muddy sites may be expected to vary greatly due to the inflection of the curve in the range of porosity values from 55 to 90%.

The value for $\partial V/\partial \beta$ of -570 m/s estimated from the regression of Hamilton and

Table 5. Slopes of V_p *vs.* porosity evaluated for different sediments.

Sediment Type	Porosity (%)	Slope (m/s)		
		a	*b*	*c*
coarse sand[d]	38.1	-247	-1088	-1278
medium sand[e]	37.9	-54	-1092	-1284
medium sand[f]	36.5	-705	-1126	-1323
fine sand[g]	39.0	-1302	-1066	-1253
fine sand[h]	44[i]	n.a.	-870	-1113
silty sand	53[j]	n.a.	-689	-861
mud[k] (clayey silt)	63.4	-166	-480	-570

[a]piecewise linear regression for specific NRL sites
[b]regression of NRL data (Fig. 24) evaluated at given porosity
[c]regression of Hamilton and Bachman (1982) data evaluated at given porosity
[d]Panama City (II), Florida
[e]Charleston, South Carolina
[f]Jacksonville (I), Florida
[g]Panama City (I), Florida
[h]Mission Bay, California
[i]estimated from grain size
[j]Jackson *et al.* (1986b)
[k]Russian River, California

Bachman by Hines (1990) is within the range of values applicable to sands and is located on the part of the regression which approaches linearity. Hines applies this value of dependence of velocity on porosity to three sites with either silty sand or fine sand. According to Table 5, silty sand with a porosity of 53% (Jackson *et al.*, 1986b) has a value for $\partial V/\partial \beta$ of -689 m/s and fine sand from Mission Bay, California (Richardson *et al.*, 1983a) has a value for $\partial V/\partial \beta$ of -870 m/s. Fine sands used in the laboratory experiment of Nolle *et al.* (1963) are similar in mean grain size (130 μm *vis-à-vis* 166 μm) to those investigated off Panama City, Florida which have porosity values of 39% and a corresponding $\partial V/\partial \beta$ value of -1066 m/s (Stanic *et al.*, 1988). Hines's model is in good agreement with the acoustic measurements from these three sediments despite a diversity of values for the $\partial V/\partial \beta$ parameter. Values of $\partial V/\partial \beta$ and $\partial \rho/\partial \beta$ are combined with the variance of porosity values in Hines's model to evaluate the expression for backscattering intensity. Thus, the variance of the porosity which is left as a free parameter by Hines becomes very important as a possible factor differentiating the level of backscatter from the three sediment types.

Correlation functions of porosity and velocity fluctuations

Frequency and grazing angle dependence in the volume scattering model of Hines are determined by the correlation function of acoustic impedance fluctuations in the sediment. Because impedance is the product of sediment density and sound velocity, measurements of both of these parameters can be used to calculate a

correlation function. Porosity is used in the calculations instead of density because of the dependence of density on porosity discussed in the previous section. The data presented here are restricted to vertical measurements of porosity and sound velocity. The correlation function and the correlation length associated with horizontal fluctuations in these properties could be different than those calculated from vertical fluctuations unless the inhomogeneities are isotropic.

The data in Figs. 7, 9, 11, 14 and 16 are a source of vertical measurements of sediment porosity and sound velocity from which autocorrelation functions may be derived. There are, however, several constraints to be considered in calculating the correlation length from these data. The length of the core and the number of measurements made from the cores should be large in order to derive the correlation length with facility. Constraints on making reliable measurements in surficial sediments, however, preclude collecting sufficient data for calculation of the autocorrelation function. For example, collection of long cores from sandy sediments requires greater physical force or agitation to drive the core deeper and this activity disturbs the sample sufficiently to question the results of measurements involving sediment structure. On the other hand, long cores are not necessary for this study of backscattering. Because of restricted acoustic penetration of high-frequency (20-180 kHz) sound, probably only the uppermost 20 to 30 cm of most shallow-water sediments are pertinent (although deeper penetration is expected for muds). Another constraint exists in the fact that sediment porosity is a bulk property and therefore has a lower limit on sample size for which the measurement remains

reliable and meaningful. Sample size is critical in finer-grained sediments also, where values of porosity display increasing variability with decreasing sample size. Values of porosity are a function of the collective size, shape, and orientation of the sediment particles and the resultant voids among them. For the measurement of porosity to be reliable, enough of the constituent particles and interstitial water has to be collected to represent the bulk property of the sediment. This constraint affects the thickness or the size of the increment at which porosity can be measured. In fact, there is a limit to the size of the sample from which measurement of porosity may be meaningful. As the sampling interval approaches the sediment grain size, values of porosity change erratically and the measurement becomes meaningless. Ultimately, fractional porosity is either zero or one depending on if the sample is a grain or a water-filled void, respectively. The increment over which porosity fluctuations affect high-frequency (20-180 kHz) acoustic transmission, however, is on the order of a wavelength (10-1 cm) and this increment is as large or larger than the lower measurement limit employed in this study (1 cm). Identical methodological and philosophical arguments can be made for an incremental size limit for measurements of compressional wave velocity in porous media.

A correlation length of 1 cm (or less) is used by Hines (1990) when evaluating his volume scattering model. This value of correlation length is chosen based on laboratory experiments and the fact that model predictions match measured data. Although the NRL data is measured at 1- or 2-cm intervals, the assumption that the fluctuations have a correlation length of 1 cm or less can be tested by the following

procedure. All core data are separated into groups corresponding to location and sediment type. A least-squares linear regression is performed on each core to remove any trend due to depth gradients of sediment porosity or sound velocity. The residuals from each core are examined to determine if the residuals could be considered as uncorrelated "white noise" as opposed to the alternative hypothesis, namely, that the residuals are generated by a positively correlated, first-order autoregressive process. If the residuals can be characterized as white noise, then Hines is probably correct in choosing 1 cm or less as the correlation length. The Durbin-Watson test at the $\alpha < 0.05$ level of significance is used to choose between the two hypotheses. For a given sample size (number of porosity or velocity measurements per core) the Durbin-Watson statistic must fall below the tabulated value D_U in order to reject the hypothesis of white-noise residuals. Conversely, if the calculated Durbin-Watson statistic is above D_U, then the residuals are white noise. In the cases where sample sizes are less than 15, a Monte-Carlo method (explained by Conover, 1971; p.304-305) is used to determine the D_U values for the Durbin-Watson statistic. Most data series prove to be positively correlated (Table 6). The majority of data series with uncorrelated, white noise for the least-square residuals are porosity measurements made at 2-cm intervals. Thus, many of the fluctuations of porosity may have correlation lengths less than 2 cm.

To avoid the problems involved in calculating the correlation function for essentially a truncated series of data, the first-order autoregressive model formulated by Diggle (1990) for analysis of a large number of relatively short series of data is

Table 6. Outcomes of the Durbin-Watson test for uncorrelated (white noise) residuals from regressions of porosity and velocity data measured at depth intervals of $\Delta z = 1$ or $\Delta z = 2$ cm.

	Positively Correlated	White Noise
Porosity		
$\Delta z = 1$	4	2
$\Delta z = 2$	62	45
Velocity		
$\Delta z = 1$	124	7

used. Because of the short spatial series, the autocorrelation coefficient is estimated by Burg's algorithm (Percival and Walden, 1993). The autocorrelation coefficients for the positively correlated data series are plotted as a function of sediment mean grain size in Fig. 25. Measurements having an autocorrelation coefficient (ϕ_1) near 0.9 indicate that the data have a repeatable pattern, and consequently porosity or velocity can be predicted with reasonable success using these data. Conversely, autocorrelation coefficients near 0.1 signify that the data tend toward randomness. The data in Fig. 25a reveal a great amount of variation in the autocorrelation coefficients for porosity measurements made in muds consisting of mixtures of sand, silt and clay (5 to 7 ϕ). This is not an unexpected result but indicates that stable predictions of density fluctuations in these type of sediments may be difficult to achieve with reasonable confidence. There is no discernible trend related to grain size in the autocorrelation coefficients for velocity measurements plotted in Fig. 25b, but values of correlation are higher than calculated for porosity measurements. Higher correlation values indicate that the velocity fluctuations occur in a more repeatable pattern than the porosity fluctuations. Autocorrelation functions of porosity and velocity fluctuations from each experiment site are displayed in Appendix B. Autocorrelation functions derived from the sediment porosity and velocity data exhibit an exponential decay.

Correlation length of a data sequence is calculated after Yaglom (1987) by

$$l = \left(\frac{1}{2} + \frac{\phi_1}{1 - \phi_1} \right) \Delta z,$$

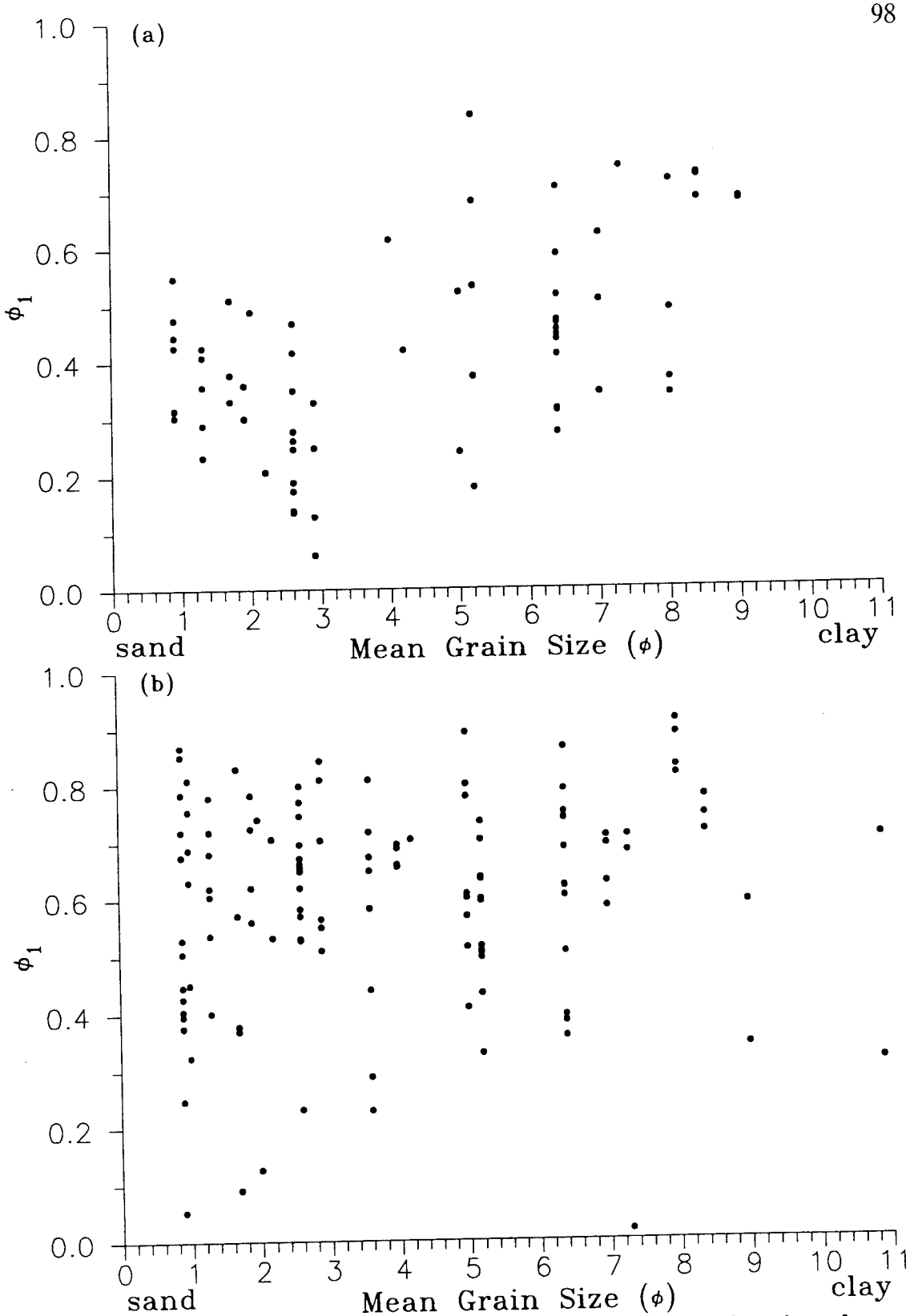

Figure 25. Plots of first-order autocorrelation coefficients (ϕ_1) as a function of mean grain size (ϕ) for all experiment sites. Coefficients estimated from (a) porosity fluctuations and (b) compressional wave velocity fluctuations.

where l is the correlation length, ϕ_1 is the autocorrelation coefficient at unit lag and Δz is the sampling interval. The data in Fig. 26a reveal more variation in the correlation lengths for porosity measurements made in fine-grained sediments (> 5 ϕ) than those made in sands. There is no discernible trend related to grain size in the correlation lengths calculated for velocity measurements depicted in Fig. 26b. Values of correlation lengths calculated from velocity fluctuations are smaller than those calculated from porosity measurements due chiefly to the smaller increment over which velocity is measured. The higher level of correlation in velocity measurements (Fig. 25b) may be explained by the ability of the autocorrelation function to resolve repeating patterns at correlation lengths less than 2 cm when the increment is only 1 cm.

Correlation length of porosity and velocity fluctuations is related to grain size in an indirect way, if not directly by grain diameter. Sediment porosity (and, hence, sediment compressional wave velocity) varies as a function of grain size. Hamilton and Bachman (1982) and Bachman (1985) have demonstrated the empirical relationship between porosity and grain size for a wide variety of surficial sediment types. Decreasing mean grain size results in an increase in porosity because of changes in the nature of void spaces between grains and, in the finest sediments, because of the adsorptive properties and cohesive nature of clays. Within sands, differences in porosity are attributable to changes in grain sorting. Figure 27 shows the relationship exhibited by the porosity and grain size data from 13 shallow-water sites (no porosity data are available from the Mission Bay study). The relationship between porosity

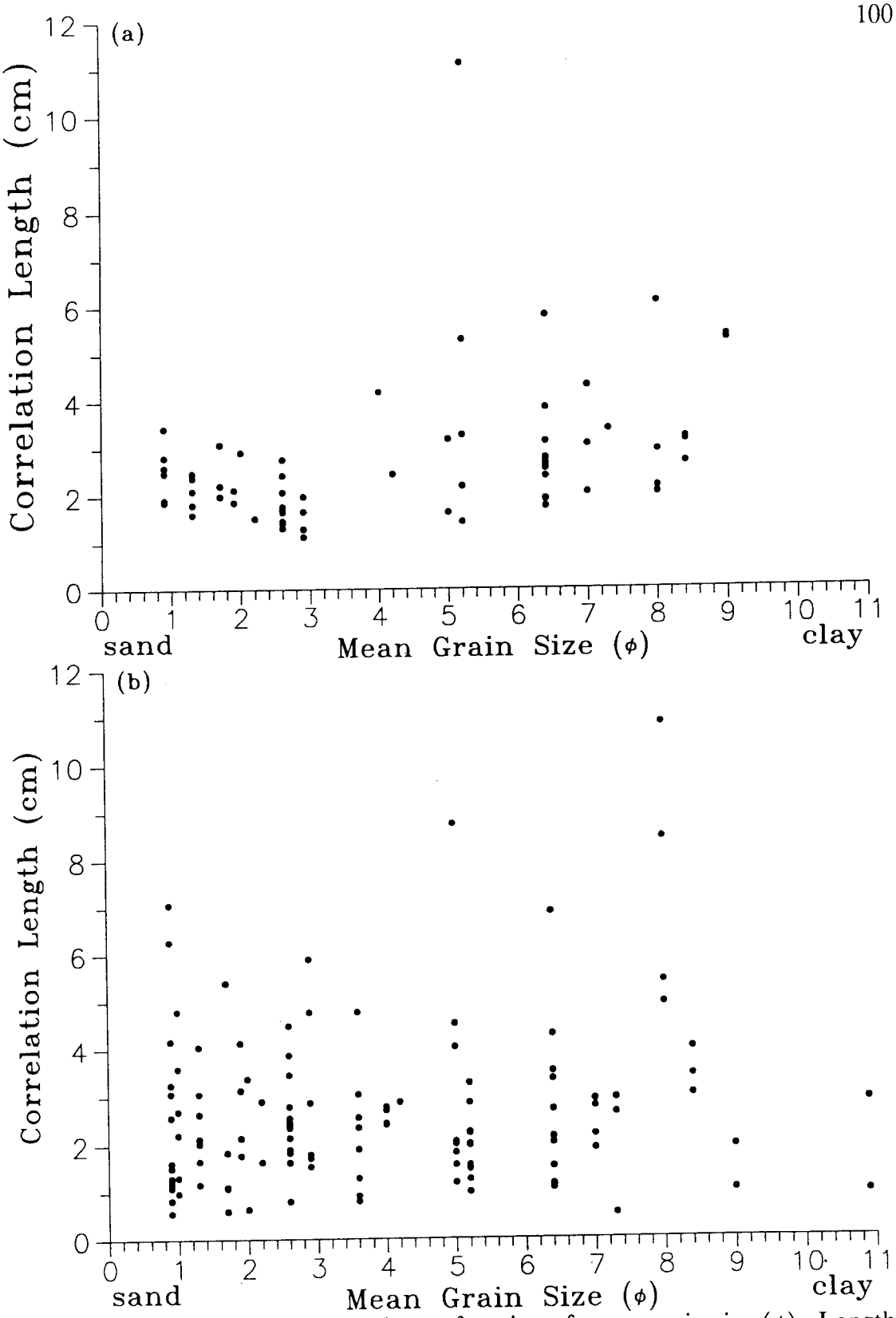

Figure 26. Plots of correlation length as a function of mean grain size (ϕ). Lengths calculated from (a) porosity fluctuations and (b) compressional wave velocity fluctuations.

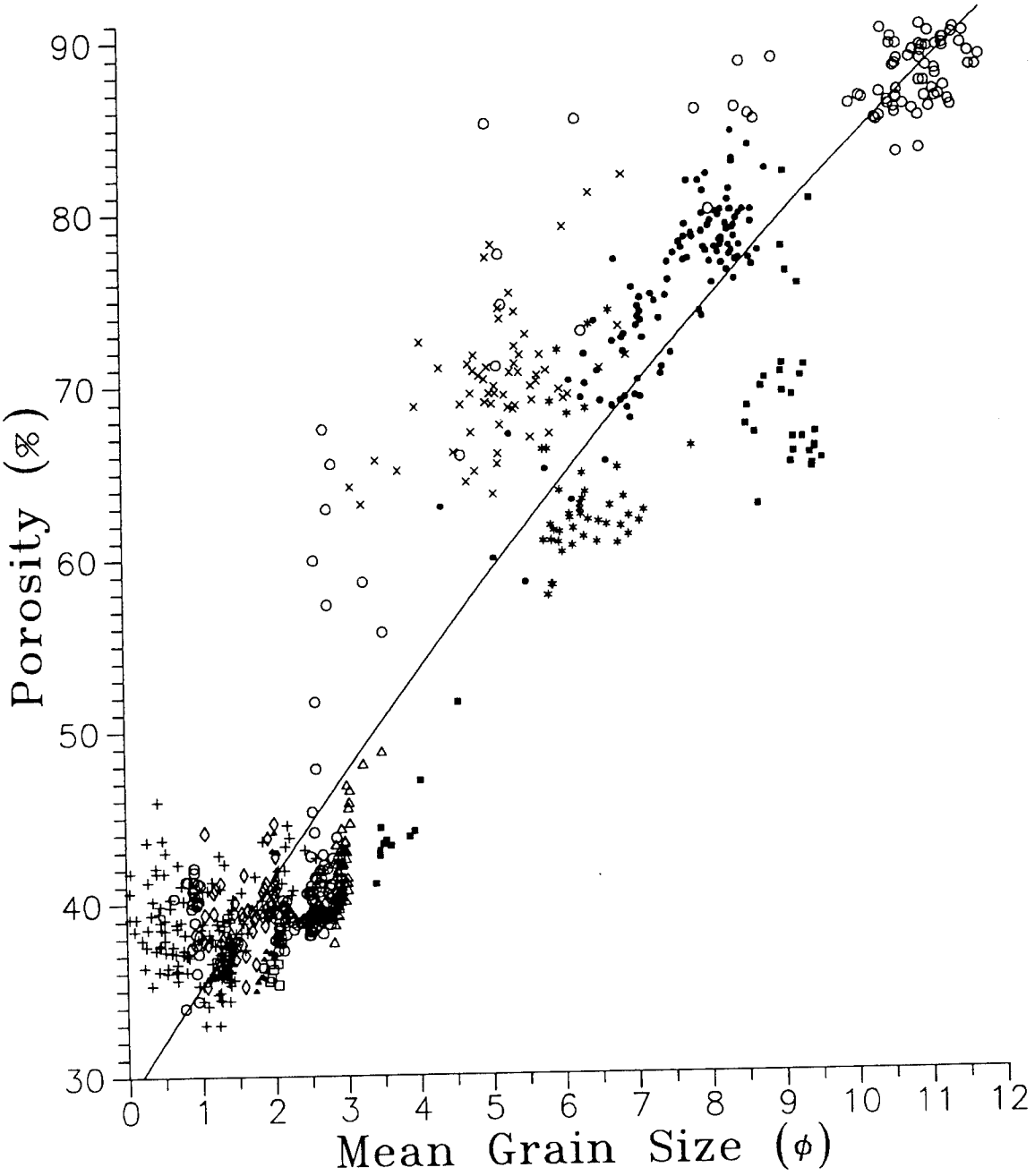

Figure 27. Plot of sediment porosity (%) *vs.* sediment mean grain size (ϕ) for various sites on continental shelves in this study. Symbols corresponding to each data set are the same as in Fig. 24. The regression line is described by the relation $\beta = 28.968 + 6.459\phi - 0.098\phi^2$, where β is porosity in percent and ϕ is mean grain size in phi units.

and mean grain size exhibits much scatter because of factors such as sorting, grain shape, packing of grains and grain mineralogy.

Grain sorting is a major factor in the appearance of scatter in the data occurring in the size range from 3 ϕ to 10 ϕ because many of the sites from which these data are collected have sediments with bimodal grain size distributions. In a bimodal distribution, fine particles associated with higher porosity fill the interstices between the large particles causing porosity to be greater than would be expected from the mean grain size (Hamilton and Bachman, 1982).

Scatter in the data among the sands (coarser than 4 ϕ) is partly due to methodological shortcomings in measurement of porosity in sands. Pure sands lack the cohesive properties of finer sediments that enable them to be collected without some draining of the pore water. Also, the slight disturbance of the grain structure that occurs when inserting a core changes the pore spaces and, hence, the porosity. This is especially true for medium and coarser sands (coarser than 2 ϕ).

Although alternate methods for determining sediment porosity have been proposed (*e.g.*, freeze-thaw, electrical resistivity), the conventional method employed in this study provides relative accuracy when performed with careful consistency. In order to confirm the relative accuracy of the conventional method, six cores were assayed for porosity *in toto* and seven cores were sectioned at 2-cm intervals before assaying for porosity. All cores were collected from coarse sand at the Panama City (II) site within a five-day period and randomly selected for either *in toto* or sectioned analyses. The mean porosity ($\pm$ 1 standard deviation) of the *in toto* cores was 41.3%

(± 0.8%) and the mean porosity (± 1 standard deviation) of the sectioned cores was 41.6% (± 1.2%). Thus, the average value for bulk porosity for a large sample is perceived as real.

Sediment porosity and velocity variances

The magnitude of the backscattering strength in the model of Hines is determined by the variance of the sediment density and sound velocity fluctuations. Table 7 displays the variance of sediment compressional wave velocity and porosity measurements made at the 14 sites. Variance is expressed as the mean of the individual variances from each core rather than a collective variance because the vertical variations of sediment velocity and porosity at any one point are of interest. Hines (1990) selects values for porosity variance that range from 0.001 to 0.006 in order to fit his model to measured data. These selected values of porosity variance are among the highest found in the experiment sites reported in Table 7. Moreover, there is little agreement between values of variance which Hines has chosen and sediment type corresponding to comparable NRL experimental data (Table 7). Hines assigns a variance value of 0.004 for silt: NRL data indicate silts vary between 0.0007 and 0.002. A porosity variance of 0.006 chosen for fine sand in Mission Bay, California by Hines is at odds with the range of 0.00005 to 0.0002 observed in NRL data. The laboratory experimental data from very fine sand used by Nolle *et al.* (1963) provide the closest agreement between selected (0.001) and measured (0.0007)

Table 7. Sediment type, number of sediment cores collected (n) and variances of compressional wave velocity (s_V^2) and porosity (s_β^2) at the 14 experiment sites.

Experimental Site	Sediment Type	n	s_V^2 †	s_β^2 §
Long Island Sound	silty clay	3	51.72	0.0008
	clayey silt	3	137.54	0.0020
Mission Bay, CA	fine sand	10	247.63	—
	coarse sand	7	789.60	—
Montauk Point, NY	fine sand	2	198.20	0.00004
Quinault Range, WA	fine sand	7	233.73	0.0003
Charleston, SC	med. sand	10	169.48	0.0003
La Spezia, ITALY	silty clay	2	14.94	0.0023
	v. fine sand	1	443.04	0.0007
Arafura Sea, AUSTRALIA	clayey sand	8	31.87	0.0016
Panama City, FL (I)	fine sand	13	226.77	0.0002
Panama City, FL (II)	coarse sand	4	192.89	0.0004
Jacksonville, FL (I)	med. sand	9	249.19	0.0001
Jacksonville, FL (II)	shelly sand	13	1180.57	0.0010
St. Andrew Bay, FL	clay	2	0.58	0.00003
	fine sand	2	19.29	0.00005
Straits of Juan de Fuca, WA	silty f. sand	4	144.12	0.0007
	med. sand	4	475.59	0.0004
	silty sand	8	1229.16	0.0026
	silty clay	4	5.33	0.0008
	clayey silt	4	8.24	0.0007
Russian River, CA	clayey silt	12	61.71	0.0015

† velocity variance is expressed as $(m\ s^{-1})^2$
§ porosity variance is expressed as the square of the fractional porosity

values of porosity variance. It is not surprising that such a discrepancy exists between values of variance that Hines selects and values measured at the experiment sites because the variance used in the model is fitted to the level of the acoustic data (*i.e.*, variance is a free parameter).

Variability of velocity within a particular site appears large when compared with the variability of porosity at the same site due to the larger magnitude of velocity values. When variability is expressed as a percentage of the mean value, however, the magnitude of variation is mitigated by a *de facto* normalization. Otherwise known as the coefficient of variation, this normalized value of variability may be more useful than the standard measure of variability for comparing parameters with mean values differing by an order magnitude or more. The coefficient of variation of sediment velocity is in fact less than the coefficient of variability in sediment porosity at the same site (Richardson, 1986).

Parameter Variance and Sediment Type

The variances of sediment porosity and sound velocity define the nature of the impedance fluctuations in the sediment and these impedance fluctuations are responsible for the scattering of the sound from the sediment volume. Furthermore, values for sediment sound velocity and porosity variances are somewhat inter-dependent and are indicative of particular sediment types. Values given in Table 7 are plotted in two-dimensional variance space in Fig. 28. Some experimental sites exhibit high values for porosity variance, but low values for velocity variance. Other

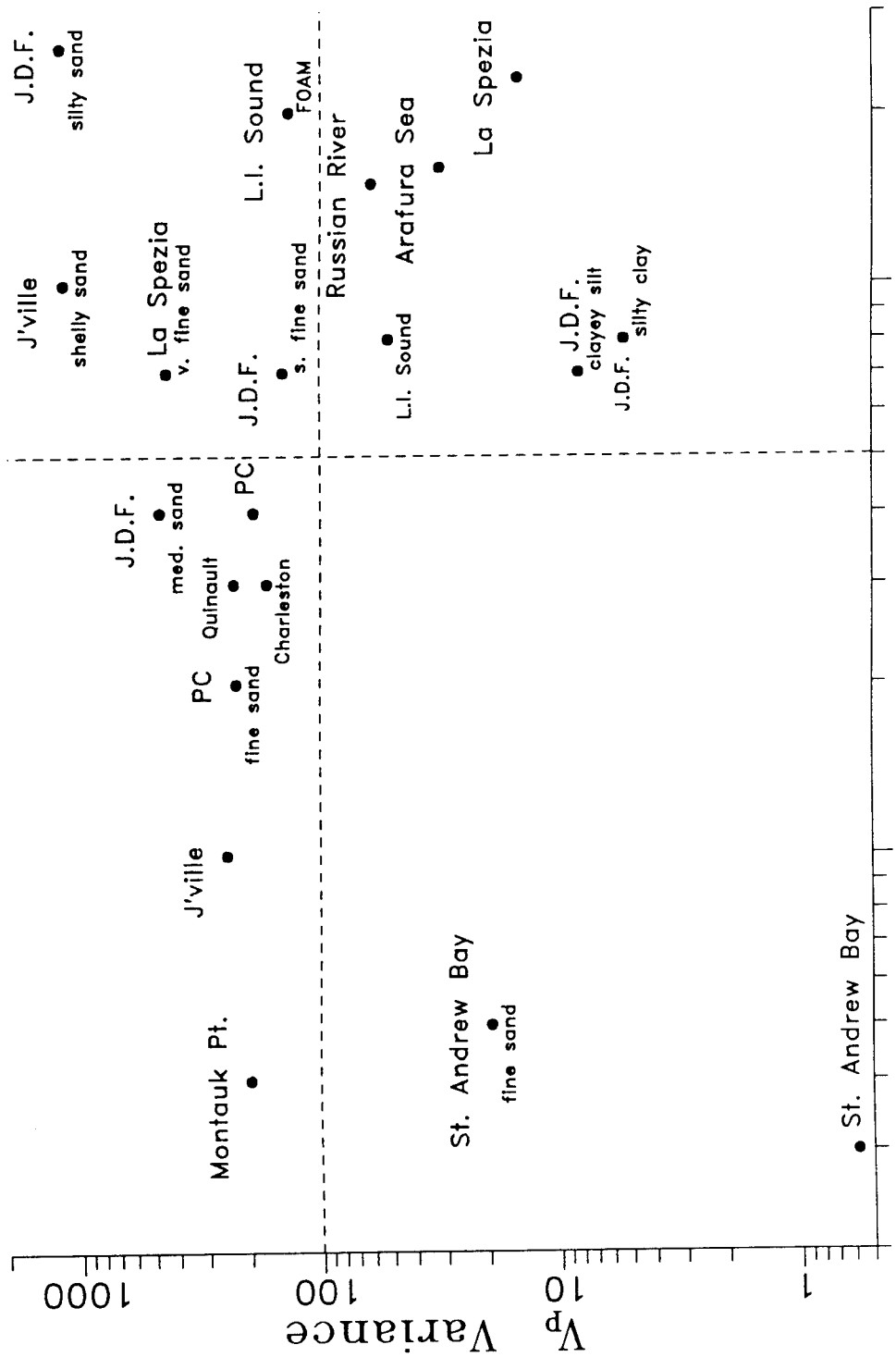

Figure 28. Plot of sediment compressional wave velocity variance *vs.* sediment porosity variance for various experiment sites investigated.

sites exhibit low values for porosity variance, but high values for velocity variance. The former sites are usually muds and the latter sites are generally sands. The dashed lines demarcating the four regions in Fig. 28 are arbitrarily drawn, but effectively illustrate the pattern created by the distributions of the two variances. The relationship between sediment compressional wave velocity and porosity in Fig. 24 explains some of the pattern of high variance from one parameter paired with low variance from the other parameter: low porosity variance and high velocity variance is typical of the vertical segment of the regression, high porosity variance and low velocity variance is typical of the flattened segment of the regression.

Those sediments having low variances in both velocity and porosity are unlikely to exhibit significant volume scattering. The two sites exhibiting low values for variance in sound velocity and sediment porosity are from St. Andrew Bay in Panama City, Florida. One sediment is a well-sorted fine sand which is relatively homogeneous and loosely packed since it is under the influence of strong oscillatory tidal currents. The other sediment is a lagoonal mud of low rigidity and high organic content. This latter sediment lacks heterogeneities due to the hydrodynamically quiescent environment inside the lagoon and the resultant anoxic conditions which abate biological disturbances of the sediment fabric. Sediments having high variances in both parameters, however, are very likely to exhibit volume scattering. Sites located in the upper right quadrant of Fig. 28 are either sands with shell hash mixed in the sediment matrix or mixtures of silt and sand or silt and clay. Backscattering levels measured from Jacksonville and approaches to the Strait of Juan de Fuca in

this quadrant of Fig. 28 are quite high (Stanic *et al.*, 1989; unpublished data of D.R. Jackson).

Those sites exhibiting high variance in sediment porosity but low variance in sediment sound velocity (lower right of Fig. 28) are muds with inhomogeneities such as shell hash (Richardson *et al.*, 1983a; Briggs *et al.*, 1989a) or animal burrows (Jackson and Briggs, 1992). Backscattering levels measured from the Arafura Sea, the California coast off the Russian River, and approaches to the Strait of Juan de Fuca are all anomalously high for muds (Jackson and Briggs, 1992; D.R. Jackson, unpubl.). The sands in the upper left quadrant of Fig. 28 are mixed with larger fragments of shells or other carbonate debris. Some of the elevation in sound velocity variance values in these sediments may be due to measurement error caused by scattering of the high-frequency sound by shell fragments (Briggs *et al.*, 1986; Richardson, 1986; Richardson *et al.*, 1986). Nevertheless, scattering of sound from the sediment volume is characteristic of sediments in this region of the plot.

Processes active on the continental shelf which tend to increase the variance of the sediment porosity are primarily biological and sedimentological. Burrowing organisms such as polychaete worms and thalassinoid shrimps increase sediment porosity by building and maintaining irrigated tunnels within the sediment fabric. Sea cucumbers and heart urchins create a high-porosity, open sediment fabric by their ingestion and defecation of sediment as they burrow (Rhoads, 1974). The presence of coarse shell hash layers within the sediment fabric decreases sediment porosity. Incorporation of mollusk shells in sediment fabric occurs during burial of

coarse lag deposits by sedimentary events. Burial may occur through gradual or catastrophic settling of suspended material or migration of sand ripples over accumulations of coarser shells or shell fragments. The presence of burrows, reworked sediments and shells within the sediment fabric increases variance in porosity.

Variance of sediment sound velocity increases primarily as a result of hydrodynamic processes. Increasing fluid stress on the bottom caused by either oscillatory or unidirectional currents winnows the finer sediments and leaves coarser sediment behind. The episodic nature of hydrodynamic stress events, varying from regular tidal periods to occasional storms, creates layers of coarser sediments with higher values of sound velocity. The presence of coarse layers within the sediment fabric increases variance in sound velocity. Sites associated with higher values of velocity variance near the upper quadrants of Fig. 28 are characteristic of higher stress regimes than sites associated with lower values of velocity variance. Hydrodynamic conditions vary from a quiescent lagoon in St. Andrew Bay at the lower left quadrant of Fig. 28 to continental shelf sediments subjected to stress from winter storms at the Russian River, Charleston, Quinault, and Jacksonville sites at the upper portion of the figure.

Conclusions

Backscattering data from Arafura Sea and Russian River sites demonstrate that seafloor microroughness is of little importance compared with the scattering

contribution from the sediment volume at these three sites. A lack of seafloor roughness and the presence of large quantities of buried scatterers in the Arafura Sea explain the relatively high backscattering strengths measured from a mud bottom. Backscattering intensities before and after winter storms off the Russian River are not significantly different, indicating that some phenomenon other than seafloor roughness is responsible for the scattering measured at this silty site. The Russian River site is an area characterized by bioturbation by sub-surface heart urchins.

In the coarser sediments of Panama City and Jacksonville, the bottom roughness contribution to scattering is sufficient to account for most of the measured backscattering intensity. The coarse shell hash off Jacksonville creates a featureless sea floor on a larger scale but with a very rough surface on a smaller scale. This feature presents a unique situation which the composite roughness model handles incompletely. Artificial inflation of the volume scattering component raises the model prediction to the level of the measured backscattering intensity, but is not supported by physical measurements from the sediment.

There were no significant differences in measured or predicted backscattering intensity between the two orthogonal orientations in the Quinault Range despite prominent sand ripples indicated in photographs and characterized by roughness spectra. The Quinault Range site was a transitional case where contributions to backscattering from interface and sediment volume scattering were nearly commensurate.

The sediment volume scattering component of the composite roughness model

is not supported rigorously by physical measurements, whereas the bottom roughness scattering component is supported by roughness spectra. Clearly, mathematical description of sediment inhomogeneity is necessary for the parameterization of sediment volume scattering.

Sediment inhomogeneities are identified through visual observation and analysis of physical and acoustic properties. The physical structure of the sediment fabric is evident from observations of cores collected carefully so as to not disturb the sample. Burrows, laminae, and buried shells and mud lenses can be correlated with physical measurements in cores. The processes generating such inhomogeneities, while operating during the experiment, did not make observable changes during the time of the data collection (7-12 days).

Sediment inhomogeneities are quantified by measurement of physical and acoustic properties from cores. Empirical relationships between sediment physical properties and acoustic properties have been developed by Hamilton (1974), Hamilton and Bachman (1982), Keller (1974), Bachman (1985) and Briggs *et al.* (1985), but never before in specific sites where acoustic backscattering experiments were conducted. Measurement of these physical properties such as sediment porosity and density at small intervals downcore identifies inhomogeneities potentially creating sediment volume scattering. Fluctuations in sediment density and sediment compressional wave velocity are the most effective indicators of sediment fabric inhomogeneity because fluctuations in these two properties define sediment impedance differences.

The variance of sediment porosity and sediment sound velocity is an easily attainable parameter determining volume scattering intensity. Correlation functions derived from vertical gradients of sediment porosity and sound velocity are parameters determining the frequency and grazing angle dependence of sediment volume scattering in the model by Hines. The composite roughness model of Jackson *et al.* (1986a), however, requires modification to incorporate the use of these parameters.

Variance and correlation length of physical parameters depend on sediment type and the processes (deposition, transport, bioturbation) in effect at the particular location. The more uniform the sediment size (the better the sorting) the lower the variance of the sediment sound velocity. Sediments with uniform sediment size tend to exhibit stable estimates for correlation length. Conversely, sediments with a wider range of grain sizes or bimodal grain-size distributions exhibit higher variance of the sediment sound velocity and diverse estimates for correlation length.

Although values for sediment sound velocity and porosity variances are somewhat interdependent, their relationship to each other provides information on sediment type and processes acting upon the sediments. Sediments having low variances in both velocity and porosity are unlikely to exhibit significant volume scattering. Sediments having high variances in both parameters are very likely to exhibit volume scattering. Sediments exhibiting contrasting magnitudes in variances of porosity and sound velocity are sediments with inhomogeneities and sediments exhibiting bimodal size distributions. Although biological, sedimentological and hydrodynamic processes

do not act exclusively from one another, certain generalizations are apparent in the data from the continental shelf: biological and sedimentological processes increase the porosity variance, whereas hydrodynamic processes increase the sound velocity variance.

REFERENCES

Bachman, R.T., 1985. Acoustic and physical property relationships in marine sediment. *J. Acoust. Soc. Am.*, 78: 616-621.

Barnes, C.A., A.C. Duxbury and B.A. Morse, 1972. Circulation and selected properties of the Columbia River effluent at sea. In: A.T Pruter and D.L. Alverson (Eds.), *The Columbia River Estuary and Adjacent Ocean Waters, Bioenvironmental Studies*. University of Washington Press, Seattle, WA, pp. 41-80.

Bell, T.H., 1975. Statistical features of sea-floor topography. *Deep-Sea Res.*, 22: 883-892.

Bloomfield, P., 1976. *Fourier Analysis of Time Series: An Introduction.* John Wiley & Sons, New York, 258p.

Boehme, H., N.P. Chotiros, L.D. Rolleigh, S.P. Pitt, A.L. Garcia, T.G. Goldsberry and R.A. Lamb, 1985. Acoustic backscattering at low grazing angles from the ocean bottom. Part I. Bottom backscattering strength. *J. Acoust. Soc. Am.*, 77: 962-974.

Boehme, H. and N.P. Chotiros, 1988. Acoustic backscattering at low grazing angles from the ocean bottom. *J. Acoust. Soc. Am.*, 84: 1018-1029.

Briggs, K.B., 1989. Microtopographical roughness of shallow-water continental shelves. *IEEE J. Ocean. Eng.*, 14: 360-367.

Briggs, K.B., 1991. Comparison of measured compressional and shear wave velocity values with predictions from Biot theory. In: J.M. Hovem, M.D. Richardson and R.D. Stoll (Eds.), *Shear Waves in Marine Sediments*. Kluwer Academic Publishers, Boston, MA, pp. 121-130.

Briggs, K.B., M.D. Richardson and D.K. Young, 1985. Variability in geoacoustic and related properties of surface sediments from the Venezuela Basin, Caribbean Sea. *Mar. Geol.*, 68: 73-106.

Briggs, K.B., P. Fleischer, R.I. Ray, W.B. Sawyer, D.K. Young, M.D. Richardson and S. Stanic, 1986. *Environmental support for a high-frequency acoustic backscatter experiment off Charleston, South Carolina, 17-28 June 1983.* NORDA Report No. 130, Naval Research Laboratory, Stennis Space Center, MS, 90p.

Briggs, K.B., P. Fleischer, W.H. Jahn, R.I. Ray, W.B. Sawyer and M.D. Richardson, 1989a. *Investigation of high-frequency acoustic backscattering model parameters: Environmental data from the Arafura Sea.* NORDA Report No. 197, Naval Research Laboratory, Stennis Space Center, MS, 94p.

Briggs, K.B., P. Fleischer, W. B. Sawyer, R. I. Ray, and S. Stanic, 1989b. *High-frequency acoustic bottom scattering experiments Part II: Environmental characterization data.* NORDA Tech. Note No. 376, Naval Research Laboratory, Stennis Space Center, MS, 635p.

Briggs, K.B., P. Fleischer, D. N. Lambert, R. I. Ray, and W. B. Sawyer, 1989c. *Environmental support for high-frequency acoustic experiments conducted aboard the USNS Bartlett 2 August to 3 September 1985.* NORDA Tech Note No. 458, Naval Research Laboratory, Stennis Space Center, MS, 241p.

Bunchuk, A.V. and Yu. Yu. Zhitkovskii, 1980. Sound scattering by the ocean bottom in shallow-water regions (review). *Sov. Phys. Acoust.*, 26: 363-370.

Cacchione, D.A., D.E. Drake, W.D. Grant, A.J. Williams and G.B. Tate, 1983. *Variability of sea-floor roughness within the Coastal Ocean Dynamics Experiment (CODE) region.* Woods Hole Oceanographic Institution Tech. Rep. 16, Woods Hole, MA, 50p.

Chesher, R.H., 1969. Contributions to the biology of *Mcoma ventricosa* (Echinoidea: Spatangoidea). *Bull. mar. Sci. Gulf Caribb.*, 19: 72-110.

Clay, C.S. and H. Medwin, 1977. *Acoustical Oceanography: Principles and Applications.* Wiley-Interscience, New York, 544p.

Conover, W.J., 1971. *Practical Nonparametric Statistics.* Wiley & Sons, New York, 462p.

Crowther, P.A., 1983. Some statistics of the sea-bed and scattering therefrom. In: N.G. Pace (Ed.), *Acoustics and the Sea-Bed.* Bath University Press, Bath, pp. 147-155.

Diggle, P.J., 1990. *Times Series, A Biostatistical Introduction.* Clarendon Press, Oxford, 257p.

Doyle, L.J. and T.N. Sparks, 1980. Sediments of the Mississippi, Alabama, and Florida (MAFLA) continental shelf. *J. Sediment. Petrol.*, 50: 905-916.

Drake, D.E. and D.A. Cacchione, 1985. Seasonal variation in sediment transport on the Russian River shelf, California. *Contin. Shelf Res.*, 4: 495-514.

Duane, D.B., M.E. Field, E.P. Meisburger, D.J.P. Swift and S.J. Williams, 1972. Linear shoals on the Atlantic inner continental shelf, Florida to Long Island. In: D.J.P. Swift, D.B. Duane and O.H. Pilkey (Eds.), *Shelf Sediment Transport: Process and Pattern*. Dowden, Hutchinson & Ross, Stroudsburg, PA, 447-498.

Field, M.E., J.H. Barber, Jr., D.A. Cacchione, D.E. Drake and F.L. Wong, 1992. *Holocene sediment map of the central California continental shelf*. USGS Open-File Rep. 92-338, U.S. Geological Survey, Denver, CO.

Folk, R.L., 1965. *Petrology of Sedimentary Rocks*. Hemphill's Publ., Austin, TX, 159p.

Folk, R.L. and W.C. Ward, 1957. Brazos River bar, a study in the significance of grain size parameters. *J. Sediment. Petrol.*, 27: 3-26.

Fox, C.G. and D.E. Hayes, 1985. Quantitative methods for analyzing the roughness of the seafloor. *Rev. Geophys.*, 23: 1-48.

Garcia de Figueiredo, A., Jr. 1984. Submarine sand ridges: geology and development, New Jersey, U.S.A. Ph.D. dissertation, Univ. of Miami, Coral Gables, 408p.

Gardner, J.V., M.E. Field, H. Lee and B.E. Edwards, 1991. Ground-truthing 6.5-kHz side scan sonographs: What are we really imaging? *J. Geophys. Res.*, 96: 5955-5974.

Goldhaber, M.B., R.C. Aller, J.K. Cochran, J.K Rosenfeld, C.S. Martens and R.A. Berner, 1977. Sulfate reduction, diffusion and bioturbation in Long Island Sound sediments: Report of the FOAM group. *Am. J. Sci.*, 277: 193-237.

Gross, T.F., A.E. Isley and C.R. Sherwood, 1992. Estimation of stress and bed roughness during storms on the Northern California Shelf. *Contin. Shelf Res.*, 12: 389-413.

Hamilton, E.L., 1971. Prediction of in-situ acoustic and elastic properties of marine sediments. *Geophysics*, 36: 266-284.

Hamilton, E.L., 1972. Compressional wave attenuation in marine sediments. *Geophysics*, 37: 620-646.

Hamilton, E.L., 1974. Prediction of deep-sea sediment properties: State-of-the-art. In: A.L. Inderbitzen (Ed.), *Deep-Sea Sediments, Physical and Mechanical Properties*. Plenum Press, New York, pp. 1-43.

Hamilton, E.L. and R. T. Bachman, 1982. Sound velocity and related properties of marine sediments. *J. Acoust. Soc. Am.*, 72: 1891-1904.

Harms, J.C., J.B. Southard, D.R. Spearing and R.G. Walker, 1975. *Depositional environments as interpreted from primary sedimentary structures and stratification sequences.* SEPM Short Course 2, 161p.

Herzer, R.H. and B.D. Bornhold, 1982. Glaciation and post-glacial history of the continental shelf off southwestern Vancouver Island, British Columbia. *Mar. Geol.*, 48: 285-319.

Hines, P.C., 1990. *Theoretical model of acoustic backscatter from a smooth seabed. J. Acoust. Soc. Amer.*, 88: 324-334.

Howard, J.D., H.-E. Reineck and S. Rietschel, 1974. Biogenic sedimentary structures formed by heart urchins. *Senckenbergiana marit.*, 6: 185-201.

Ivakin, A.N. and Yu.P. Lysanov, 1981. Underwater sound scattering by volume inhomogeneities of a bottom medium bounded by a rough surface. *Sov. Phys. Acoust.*, 27: 212-215.

Jackson, D.R., D.P. Winebrenner and A. Ishimaru, 1986a. Application of the composite roughness model to high-frequency bottom backscattering. *J. Acoust. Soc. Am.*, 79: 1410-1422.

Jackson, D.R., A.M. Baird, J.J. Crisp and P.A.G. Thomson, 1986b. High-frequency bottom backscattering measurements in shallow water. *J. Acoust. Soc. Am.*, 80: 1188-1199.

Jackson, D.R. and K.B. Briggs, 1992. High-frequency bottom backscattering: roughness vs. sediment volume scattering. *J. Acoust. Soc. Am.*, 92: 962-977.

Jackson, P.D., D. Taylor Smith and P.N. Stanford, 1978. Resistivity-porosity-particle shape relationships for marine sands. *Geophysics*, 43: 1250-1268.

Jackson, P.D. and the shipboard scientific party of Leg 133 of ODP, 1991. Electrical resistivity core scanning: a new aid to the evaluation of fine scale structure in sedimentary cores. *Scien. Drill.*, 2: 41-54.

Jongsma, D., 1974. *Marine geology of the Arafura Sea.* Geol. Geophys. Bull. 157, Department of Minerals and Energy, Bureau of Mineral Resources, Australian Govt. Publ. Serv., Canberra, Australia, 76p.

Keller, G.H., 1974. Marine geotechnical properties: Interrelationships and relationships to depth of burial. In: A.L. Inderbitzen (Ed.), *Deep-Sea Sediments, Physical and Mechanical Properties.* Plenum Press, New York, pp. 77-100.

Komar, P.D., R.H. Neudeck and L.D. Kulm, 1972. Observations and significance of deep-water oscillatory ripple marks on the oregon continental shelf. In: D.J.P. Swift, D.B. Duane and O.H. Pilkey (Eds.), *Shelf Sediment Transport: Process and Pattern.* Dowden, Hutchinson and Ross, Stroudsburg, PA, pp. 601-619.

Krell, R.M., 1980. *Shallow water range region bottom sediment characteristics: summarization of investigations and facts obtained to date.* Applied Research Division Memo. 19-80, Naval Undersea Warfare Engineering Station, Keyport, WA, 114p.

Kulm, L.D., R.C. Roush, J.C. Harlett, R.H. Neudeck, D.M. Chambers and E.J. Runge, 1975. Oregon continental shelf sedimentation: interrelations of facies distribution and sedimentary process. *J. Geology*, 83: 145-175.

Kuo, E.Y., 1964. Wave scattering and transmission at irregular surfaces. *J. Acoust. Soc. Am.*, 36: 2135-2142.

Lambert, D.N. and R.H. Bennett, 1972. *Tables for determining porosity of deep-sea sediments from water content and average grain density measurements.* NOAA Tech. Memo. ERL/AOML-17, National Oceanic and Atmospheric Administration, Miami, FL, 57p.

Lie, U. and D.S. Kisker, 1970. Species composition and structure of benthic infauna communities off the coast of Washington. *J. Fisheries Res. Bd. Canada*, 27: 2273-2285.

Lyons, A.P., 1991. *Modeling acoustic backscatter from the seafloor by long-range side-scan sonar.* M.S. Thesis, Texas A&M Univ., College Station, TX, 76p.

McKinney, C.M. and C.D. Anderson, 1964. Measurements of backscattering of sound from the ocean bottom. *J. Acoust. Soc. Am.*, 36: 158-163.

McMaster, R.L. and L.E. Garrison, 1967. A submerged Holocene shoreline near Block Island, Rhode Island. *Mar. Geol.*, 75: 335-340.

Neurauter, T.W., 1979. *Bed forms on the West Florida Shelf as detected with side scan sonar.* M.S. Thesis, Univ. of So. Florida, St. Petersburg, FL, 125p.

Nichols, F.H., D.A. Cacchione, D.E. Drake and J.K. Thompson, 1989. Emergence of burrowing urchins from California continental shelf sediments--a response to alongshore current reversals? *Estuar. Coast. Shelf Sci.*, 29: 171-182.

Nolle, A.W., W.A. Hoyer, J.F. Mifsud, W.R. Runyan, and M.B. Ward, 1963. Acoustic properties of water-filled sands. *J. Acoust. Soc. Am.*, 35: 1394-1408.

Percival, D.B. and A. T. Walden, 1993. *Spectral Analysis for Physical Applications.* Cambridge University, 580p.

Phipps, C.V.G., 1967. The character and evolution of the Australian continental shelf. *Aust. Pet. Explor. Assoc. J.*, 7: 44-49.

Pyle, T.E., V.J. Henry, J.C. McCarthy, R.T. Giles and T.W. Neurauter, 1977. *Geophysical investigations for biolithologic mapping of the MAFLS-OCS lease area, v. 5, Geophysical investigation.* State University System of Florida, Institute of Oceanography, St. Petersburg, Florida, Report for BLM Contr. No. 08550-CT-30, 258p.

Reineck, H.-E. and I.B. Singh, 1980. *Depositional Sedimentary Environments.* Springer-Verlag, New York, 549p.

Rhoads, D.C., 1974. Organism-sediment relations on the muddy sea floor. *Oceanogr. Mar. Biol. Ann. Rev.*, 12: 263-300.

Rhoads, D.C., J.Y. Yingst and W.J. Ullman, 1978. Seafloor stability in Central Long Island Sound. Part I: temporal changes in erodibility of fine-grained sediment. In: M.L. Wiley (Ed.), *Estuarine Interactions*, Academic Press, New York, NY, pp. 221-244.

Richardson, M.D., 1986. Spatial variability of surficial shallow water geoacoustic properties. In: T. Akal and J. M. Berkson, (Eds.), *Ocean Seismo-Acoustics,* Plenum Press, New York, pp. 527-536.

Richardson, M.D. and D.K. Young, 1980. Geoacoustic models and bioturbation. *Mar. Geol.*, 38: 205-218.

Richardson, M.D., D.K. Young and K.B. Briggs, 1983a. Effects of hydrodynamic and biological processes on sediment geoacoustic properties in Long Island Sound, USA. *Mar. Geol.*, 52: 201-226.

Richardson, M.D., D.K. Young, and R.I. Ray, 1983b. *Environmental support for high frequency acoustic measurements a NOSC oceanographic tower, 26 April-7 May 1982; Part I: Sediment geoacoustic properties.* NORDA Tech. Note No. 219, Naval Research Laboratory, Stennis Space Center, MS, 68p.

Richardson, M.D., J.H. Tietjen, and R.I. Ray, 1983c. *Environmental support for Project WEAP east of Montauk Point, New York 7-28 May 1982.* NORDA Rep. No. 40, Naval Research Laboratory, Stennis Space Center, MS, 52p.

Richardson, M.D., K.B. Briggs, R.I. Ray and W.H. Jahn, 1986. *Environmental support for high-frequency acoustic experiments conducted at the Quinault Range, April-May 1983.* NORDA Report No. 132, Naval Research Laboratory, Stennis Space Center, MS, 76p.

Schnable, J.E. and H.G. Goodell, 1968. Pleistocene-Recent stratigraphy, evolution and development of the Apalachicola coast, Florida. *Geol. Soc. Am., Spec. Publ. 112*, 72p.

Sokal, R.R. and F.J. Rohlf, 1969. *Biometry.* W.H. Freeman, San Francisco, 776p.

Southard, J.B., J.M. Lambie, D.C. Federico, H.T. Pile and C.R. Weidman, 1990. Experiments on bed configurations in fine sands under bidirectional purely oscillatory flow, and the origin of hummocky cross-stratification. *J. Sediment. Petrol.*, 60: 1-17.

Stanic, S., K.B. Briggs, P. Fleischer, R.I. Ray and W.B. Sawyer, 1988. Shallow-water high-frequency bottom scattering off Panama City, Florida. *J. Acoust. Soc. Am.*, 83: 2134-2144.

Stanic, S., K.B. Briggs, P. Fleischer, W.B. Sawyer and R.I. Ray, 1989. High-frequency acoustic backscattering from a coarse shell ocean bottom. *J. Acoust. Soc. Am.*, 85: 125-136.

Stanton, T.K., 1984. Sonar estimates of seafloor microroughness. *J. Acoust. Soc. Am.*, 75: 809-818.

Stewart, R., 1980. *Mineralogy of NUWES cores from the Washington and continental shelf.* Applied Research Division Memo. 19-80, Encl. 4, Naval Undersea Warfare Engineering Station, Keyport, WA, 4p.

Stewart, R.A. and N.P. Chotiros, 1992. Estimation of sediment volume scattering cross section and absorption loss coefficient. *J. Acoust. Soc. Am.*, 91: 3242-3247.

Stockhausen, J.H., 1963. *Scattering from the volume of an inhomogeneous half-space.* Naval Research Establishment, Canada, NRE Rep. 63/9, 9p.

Stoll, R.D., 1974. Acoustic waves in saturated sediments. In: L. Hampton (Ed.), *Physics of Sound in Marine Sediments,* Plenum Press, New York, pp. 19-39.

Swift, D.J.P., D.J. Stanley and J.R. Curray, 1971. Relict sediments on continental shelves: a reconsideration. *J. Geol.*, 79: 322-346.

Urick, R.J., 1983. *Principles of Underwater Sound*. McGraw-Hill, New York, 423p.

Wong, H.K. and W.D. Chesterman, 1968. Bottom backscattering near grazing incidence in shallow water. *J. Acoust. Soc. Am.*, 44: 1713-1718.

Yaglom, A.M., 1987. *Correlation Theory of Stationary and Related Random Functions, Volume I: Basic Results.* Springer-Verlag, New York, 526p.

APPENDIX A

The Composite Roughness Model

The composite-roughness model divides bottom-scattered energy into two parts: one part due to interface roughness and the other part due to sediment inhomogeneity. Roughness scattering is estimated by two separate approximations. The composite roughness approximation is used for small-to-moderate grazing angles (0-80°) and the Kirchhoff approximation is used near vertical incidence (80-90°). Scattering from sediment volume inhomogeneities is estimated by a modified version of the volume scattering model of Stockhausen (1963).

The model uses the parameters defined in Table 8. All parameters but the spectral strength are dimensionless and all can be considered independent of acoustic frequency. Values of sound velocity ratio are depicted as a function of sediment depth in Figs. 7, 9, 11, 14 and 16. The density ratio is calculated from the sediment bulk density and the seawater density. The sediment bulk density is a function of porosity, sediment grain density and seawater density (*see calculation of density under the heading in the Discussion section,* Prediction of Sediment Volume Scattering). The loss parameter δ is defined as the ratio of the imaginary and real components of the wavenumber in the sediment and can be expressed as

$$\delta = \frac{\alpha v V_p \ln(10)}{40\pi f},$$

where α is the absorption coefficient in dB m^{-1} and is identical to the compressional

Table 8. Definitions of input parameters for the composite roughness model.

Symbol	Nomenclature	Definition
ρ	Density ratio	Ratio of sediment bulk density to water density
v	Sound velocity ratio	Ratio of sediment sound velocity to water sound velocity
δ	Loss parameter	Ratio of imaginary wave number to real wave number for the sediment
σ_2	Volume scattering parameter	Ratio of sediment volume scattering cross section to sediment absorption coefficient
γ	Spectral exponent	Exponent of bottom roughness spectrum
w_2	Spectral strength	Strength of bottom roughness spectrum (cm^3) at wave number $2\pi/\lambda = 1\ cm^{-1}$

wave attenuation described in the Methods section, v is the sound velocity ratio, V_p is the sound velocity of the seawater overlying the bottom, and f is the acoustic frequency, in kHz, at which the attenuation was measured. In order to maintain consistency in units, V_p must be expressed as m ms^{-1}. Because attenuation is proportional to frequency (Hamilton, 1972), δ is virtually independent of frequency.

The volume scattering parameter σ_2 is defined by Jackson *et al.* (1986a) as

$$\sigma_2 = \frac{\sigma_V}{\alpha},$$

where σ_V is the sediment volume backscattering cross section and α is the absorption coefficient, or compressional wave attenuation in dB m^{-1}. The volume scattering parameter can be described as a surface backscattering cross section, although the cross section used in the model involves a product of σ_2 and angle-dependent factors. Depth of penetration of acoustic energy into the bottom is dependent on the grazing angle. The fate of acoustic energy directed into the bottom is determined according to the critical angle. The critical angle is defined as the angle below which the acoustic energy is completely reflected back into the water from the bottom. For grazing angles less than the critical angle, penetration is affected by a variety of physical factors. For angles steeper than the critical angle, depth of penetration is inversely proportional to α. Consequently, σ_2 is essentially the product of the volume scattering strength and the thickness of the volume scattering region in the sediment. If v is the compressional wave velocity ratio (defined as the ratio of the sound velocity through sediment to the sound velocity through the overlying water, the

critical angle θ_c is calculated as

$$\theta_c = \cos^{-1}\left(\frac{1}{v}\right).$$

If the sound velocity ratio is greater than a value of one, as is the case in most silty, sandy and gravelly sediments, the acoustic energy will be refracted out of the bottom at subcritical grazing angles. If the sound velocity is less than one, as in the case of muddy sediments, there is no critical angle (Urick, 1983).

The volume scattering parameter is dimensionless because the volume backscattering cross section in the numerator has dimensions of length^2 length^{-3} solid angle^{-1} and the absorption coefficient in the denominator has dimensions of dB length^{-1}. Hence, σ_2 is independent of the units used in the calculation if consistency is maintained. Furthermore, σ_2 tends to be independent of acoustic frequency over the range from 10 to 100 kHz. Values of σ_2, ranging from 0.0001 to 0.005, have been obtained by fitting backscattering data to the model predictions (Jackson *et al.*, 1986a; 1986b). Stewart and Chotiros (1992) derive values of σ_2 that range from 0.009 to 0.1. Values of σ_2 less than 0.0001 are required to fit the data of McKinney and Anderson (1964) to the model predictions.

Characterization of the bottom roughness by use of a power spectrum assumes a Gaussian distribution of bottom relief measurements. Use of a simple power-law relationship in the composite roughness model is predicated on the assumptions that the roughness is a fractal random process possessing features of all length scales and the bottom can be characterized by an isotropic spectrum. A variety of regions of

the sea floor have been characterized with roughness power spectra over various length scales (Fox and Hayes, 1985; Briggs, 1989). The model uses parameters appropriate to the isotropic two-dimensional spectrum, whereas the measured parameters of the roughness power spectra in Table 3 are one-dimensional. The spectral exponent γ of the two-dimensional roughness spectrum described in Table 8 is obtained by changing the sign of the one-dimensional spectral slope given in Table 3 and adding a value of one. The isotropic two-dimensional spectral strength w_2 is derived from the one-dimensional spectral intercept w_1 in Table 3 by the following expression:

$$w_2 = w_1 (2\pi)^{\gamma-2} h_0 \frac{\Gamma\left(\frac{\gamma}{2}\right)}{\pi^{1/2}\,\Gamma\left(\frac{\gamma-1}{2}\right)}.$$

In this expression, γ is the two-dimensional spectral slope, h_0 is a dimensional constant equal to 1 cm required to reconcile the difference in units between the one-dimensional spectrum (cm^3) and the two-dimensional spectrum (cm^4), and Γ represents the gamma function.

Because the two-dimensional spectral parameters are derived for an isotropic spectrum, a justification is required for application of the isotropic model to anisotropic data. The one-dimensional spectral parameters for the two orthogonal directions are used separately as model inputs under the assumption that above expression is valid. If the two model predictions are essentially identical, the prediction of the isotropic model is not expected to differ significantly from that

which a more complicated anisotropic model would generate. Conversely, if the two model predictions differ significantly, the isotropic model must be deemed inadequate.

APPENDIX B

Correlation Functions Estimated from Porosity and Velocity Fluctuations

Exponential correlation functions are calculated from the core data collected at each of the 14 experimental sites using Burg's algorithm (see Discussion: Correlation functions of porosity and velocity fluctuations). Estimates are made for sediment porosity and sound velocity fluctuations and are presented in Figs. 29-42. Correlation functions having autocorrelation coefficients which did not pass the Durbin-Watson test for white noise residuals are not plotted in these figures. The exponential autocorrelation function $R(\tau)$ can be calculated as

$$R(\tau)=\phi_1^{\tau},$$

where τ is the lag value in cm. The first-order autocorrelation coefficient ϕ_1 is evident in the figures as the value of the autocorrelation function at lag 1 cm. First-order autocorrelation coefficients are plotted as a function of mean grain size of the experiment site in Fig. 25 in the Discussion. The correlation lengths corresponding to each autocorrelation coefficient are plotted as a function of mean grain size in Fig. 26 in the Discussion. Values of the autocovariance function $C(\tau)$ may be similarly calculated as

$$C(\tau)=\sigma^2\cdot\phi_1^{\tau},$$

where σ^2 is the residual variance and τ is the lag value in cm. The autocovariance

function at lag 0 cm is equal to the residual variance. Therefore, the autocovariance function has the equivalent information of the autocorrelation function, but has the addition of the variance of the process. Although the covariance function provides an indication of a possible relationship between the dispersion and the correlation length of sediment porosity and velocity fluctuations, the autocorrelation function is presented in this appendix for ease of comparison within and among experiment sites.

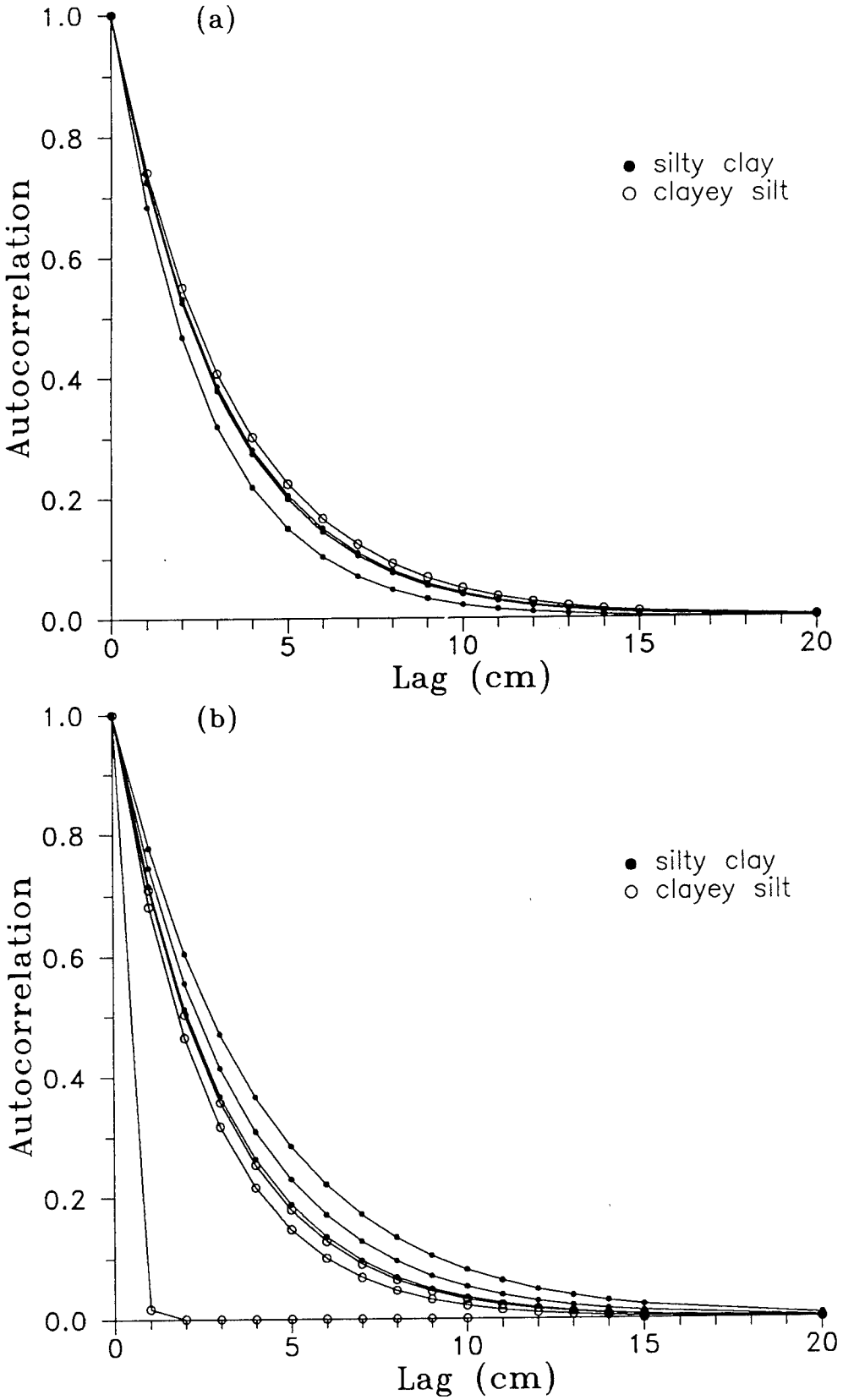

Figure 29. Autocorrelation functions estimated from fluctuations in (a) sediment porosity and (b) sediment velocity for cores collected in Long Island Sound.

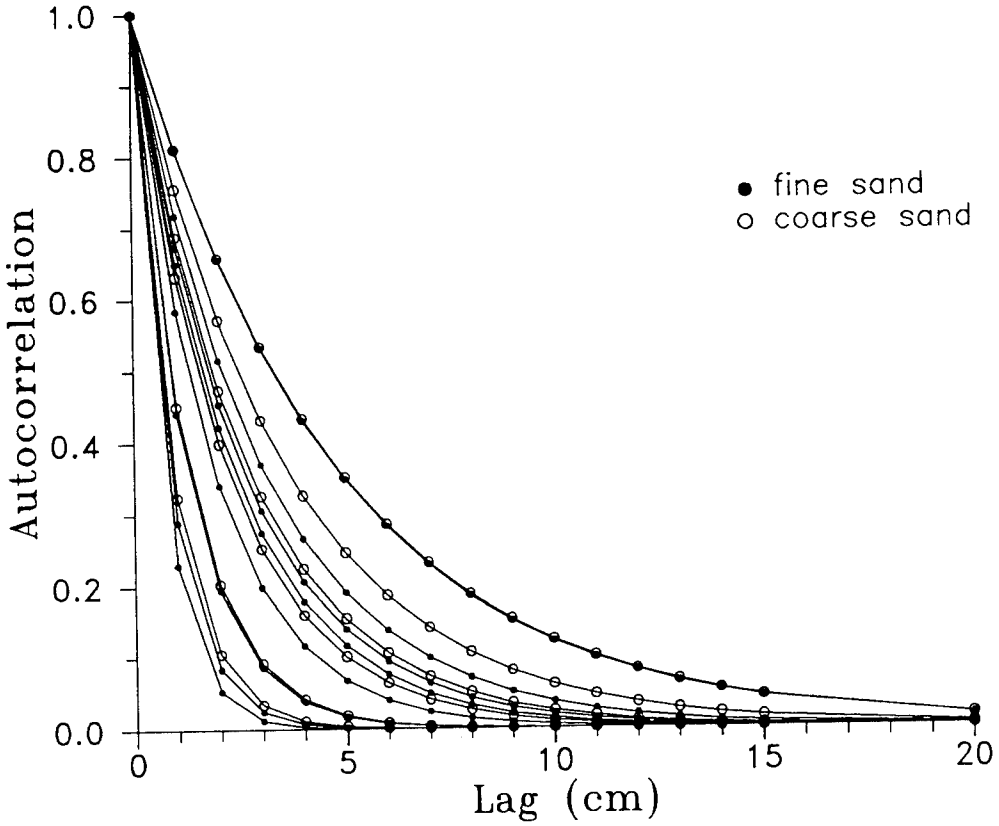

Figure 30. Autocorrelation functions estimated from fluctuations in sediment velocity for cores collected in Mission Bay, CA.

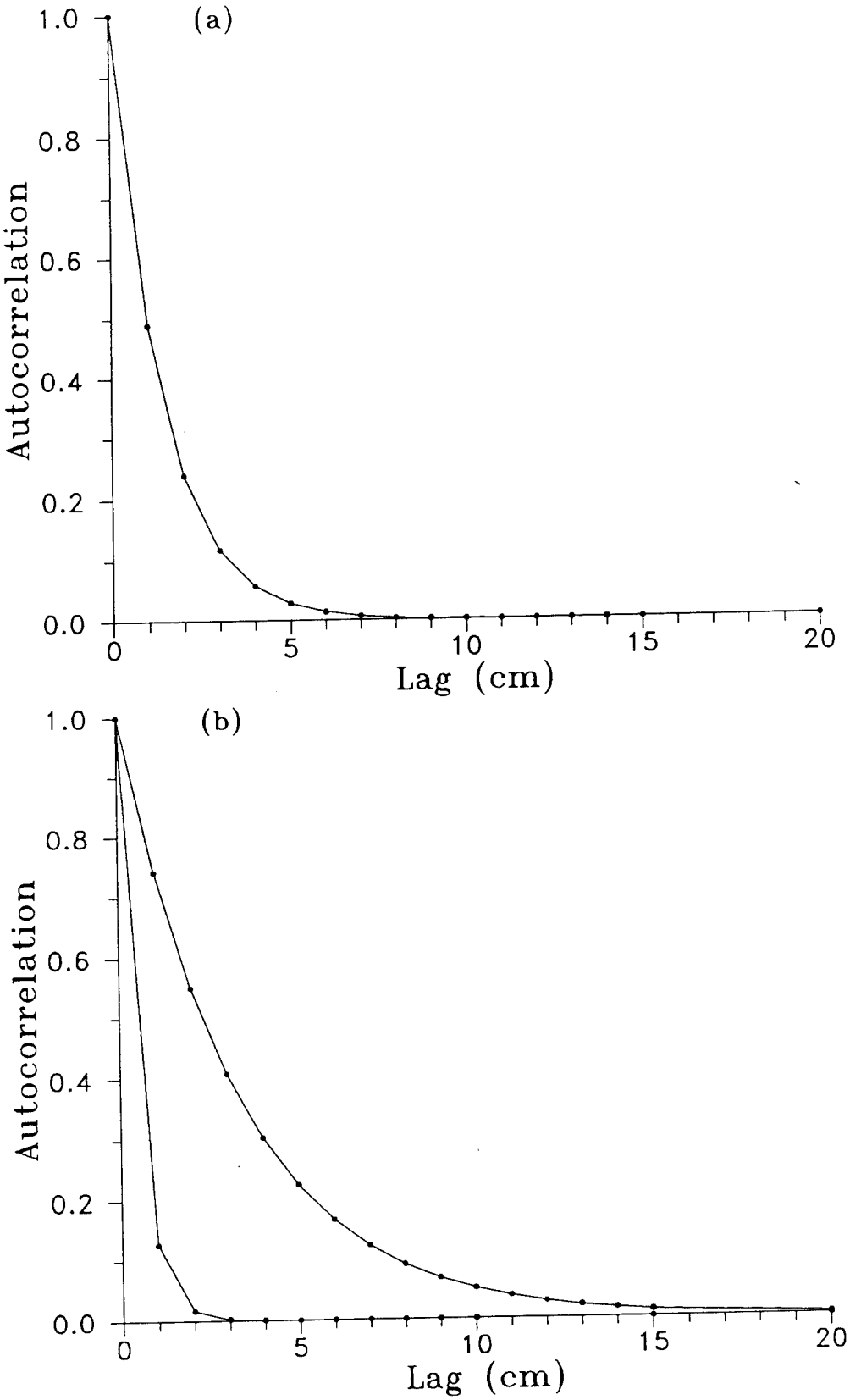

Figure 31. Autocorrelation functions estimated from fluctuations in (a) sediment porosity and (b) sediment velocity for cores collected off Montauk Point, NY.

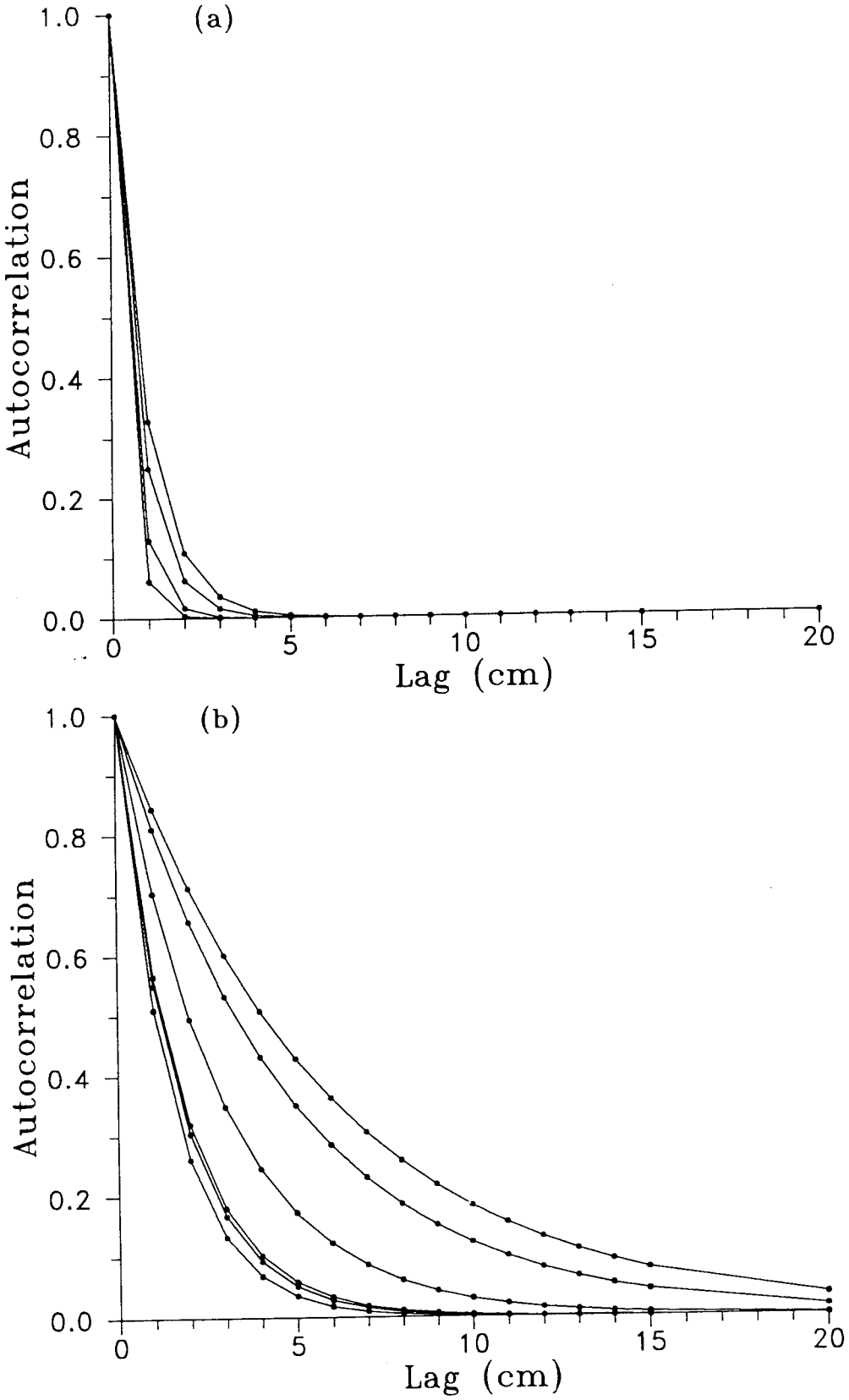

Figure 32. Autocorrelation functions estimated from fluctuations in (a) sediment porosity and (b) sediment velocity for cores collected in the Quinault Range, WA.

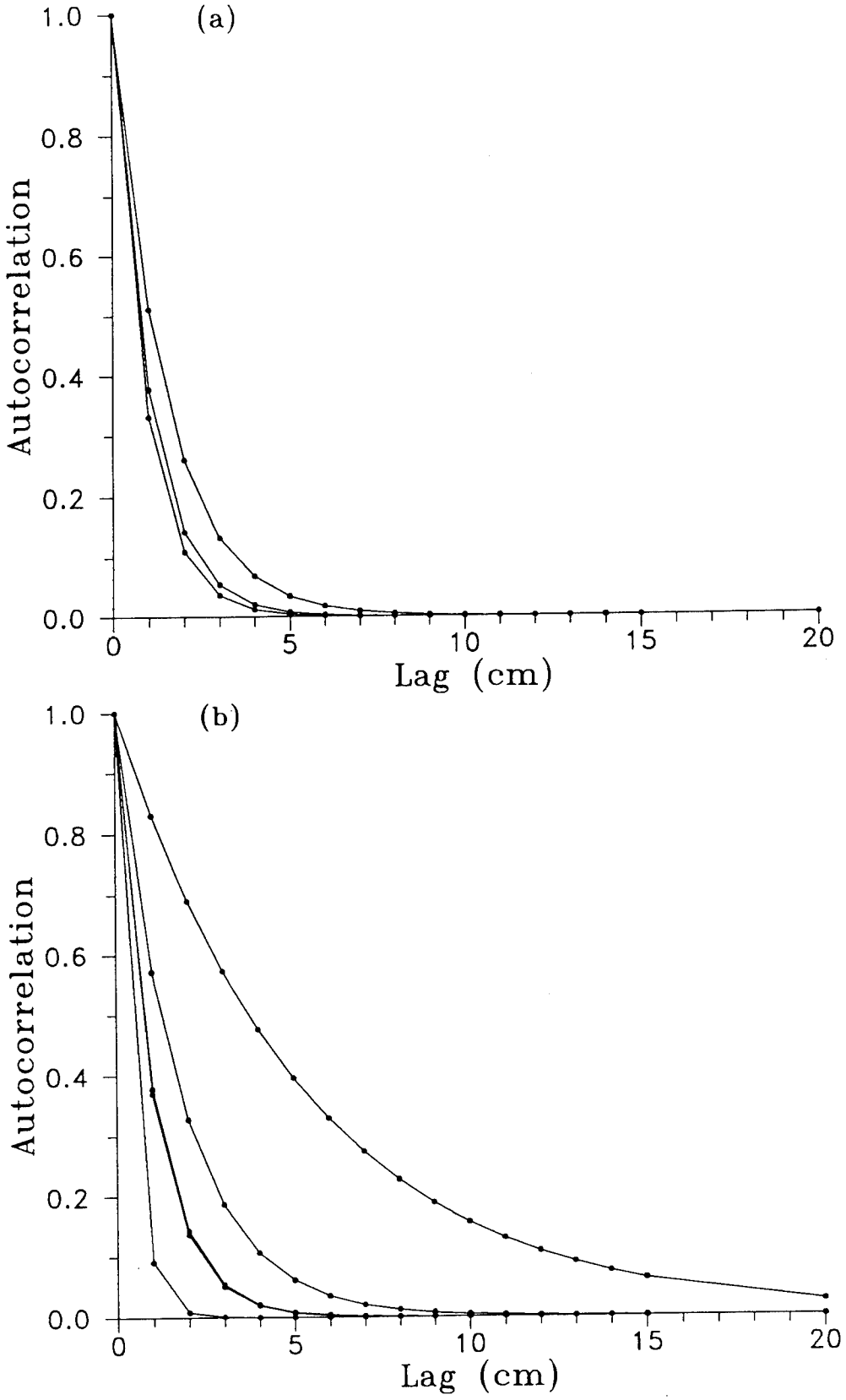

Figure 33. Autocorrelation functions estimated from fluctuations in (a) sediment porosity and (b) sediment velocity for cores collected off Charleston, SC.

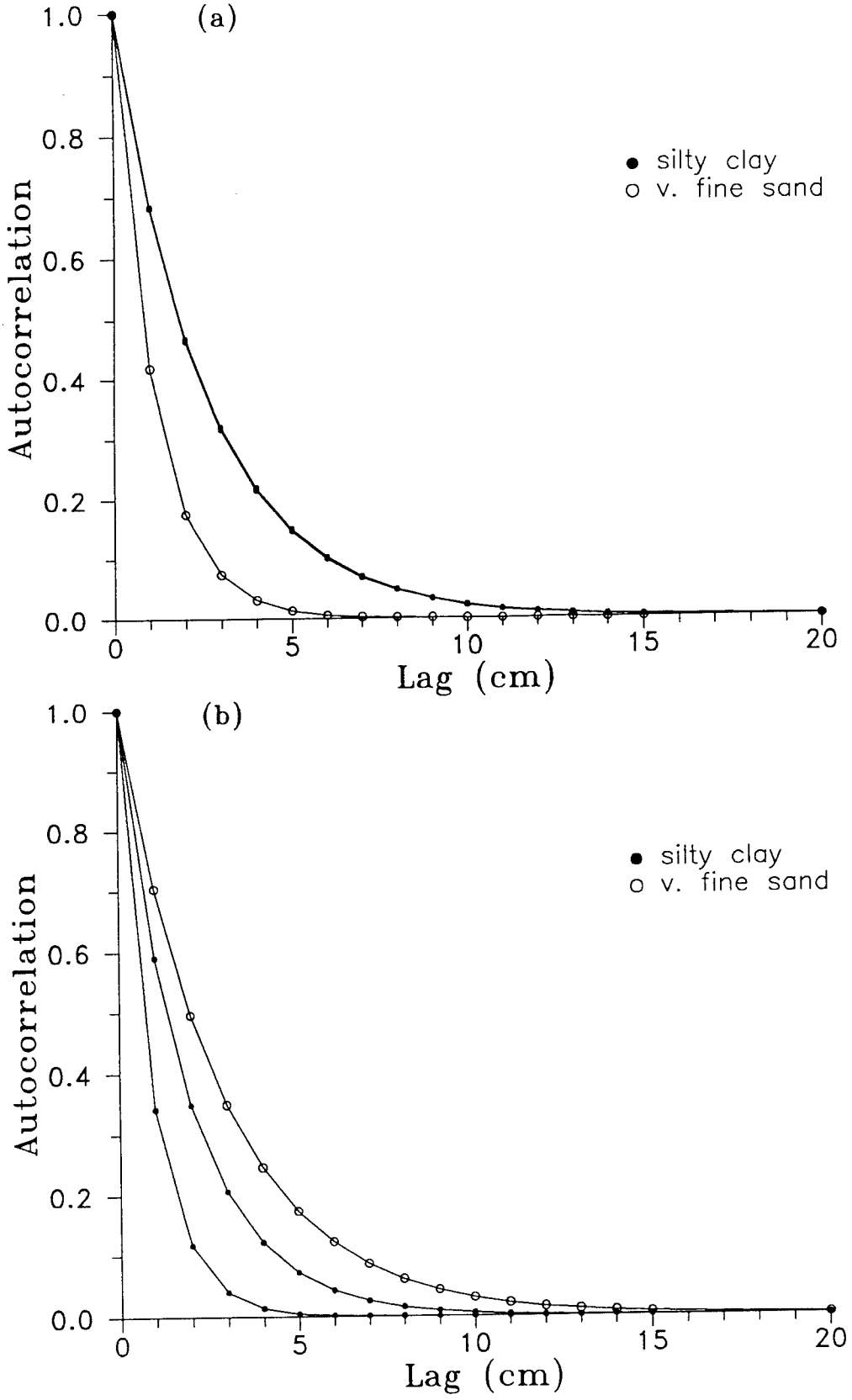

Figure 34. Autocorrelation functions estimated from fluctuations in (a) sediment porosity and (b) sediment velocity for cores collected off La Spezia, Italy.

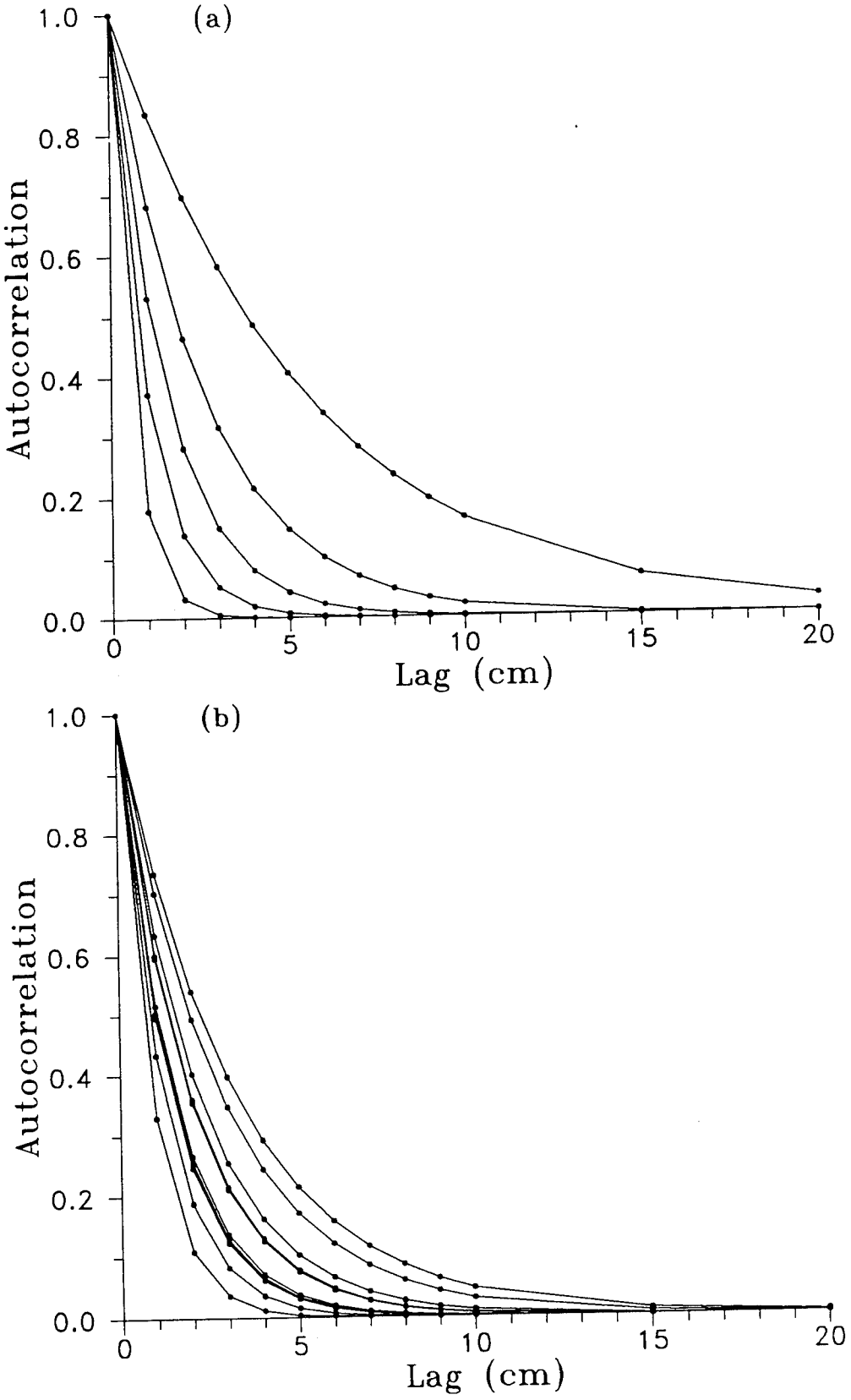

Figure 35. Autocorrelation functions estimated from fluctuations in (a) sediment porosity and (b) sediment velocity for cores collected in the Arafura Sea.

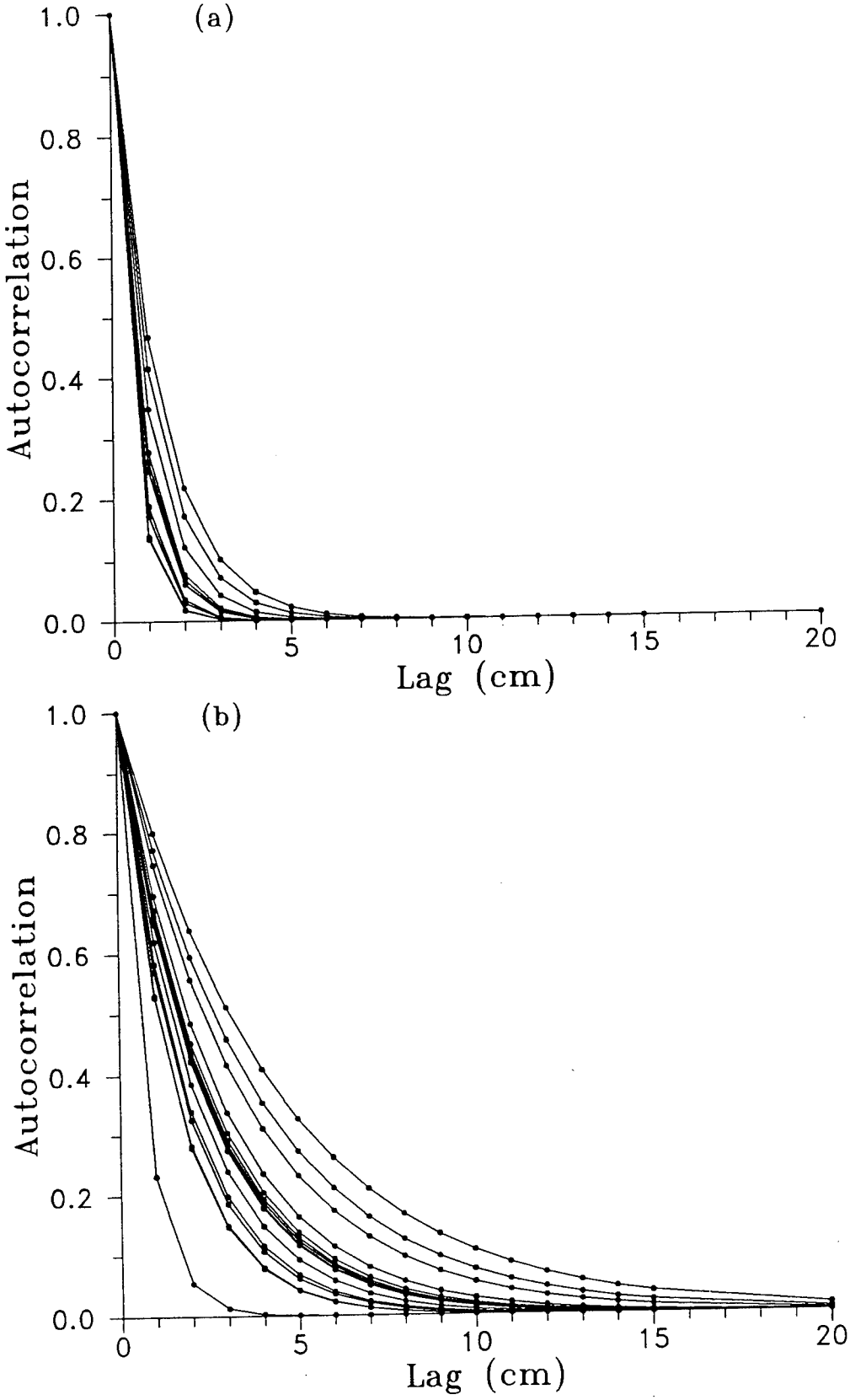

Figure 36. Autocorrelation functions estimated from fluctuations in (a) sediment porosity and (b) sediment velocity for cores collected at the Panama City, FL (I) site.

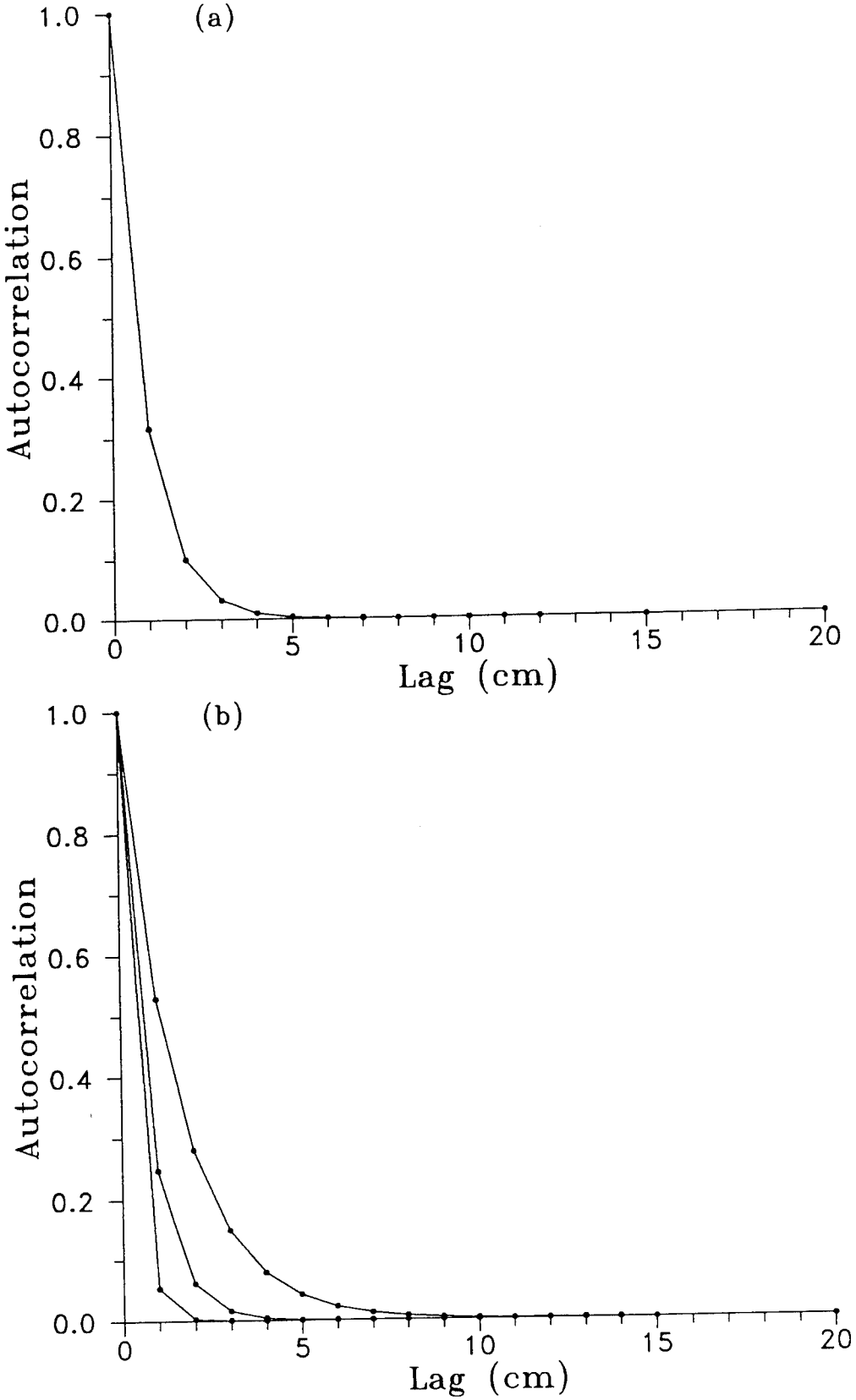

Figure 37. Autocorrelation functions estimated from fluctuations in (a) sediment porosity and (b) sediment velocity for cores collected at Panama City, FL (II) site.

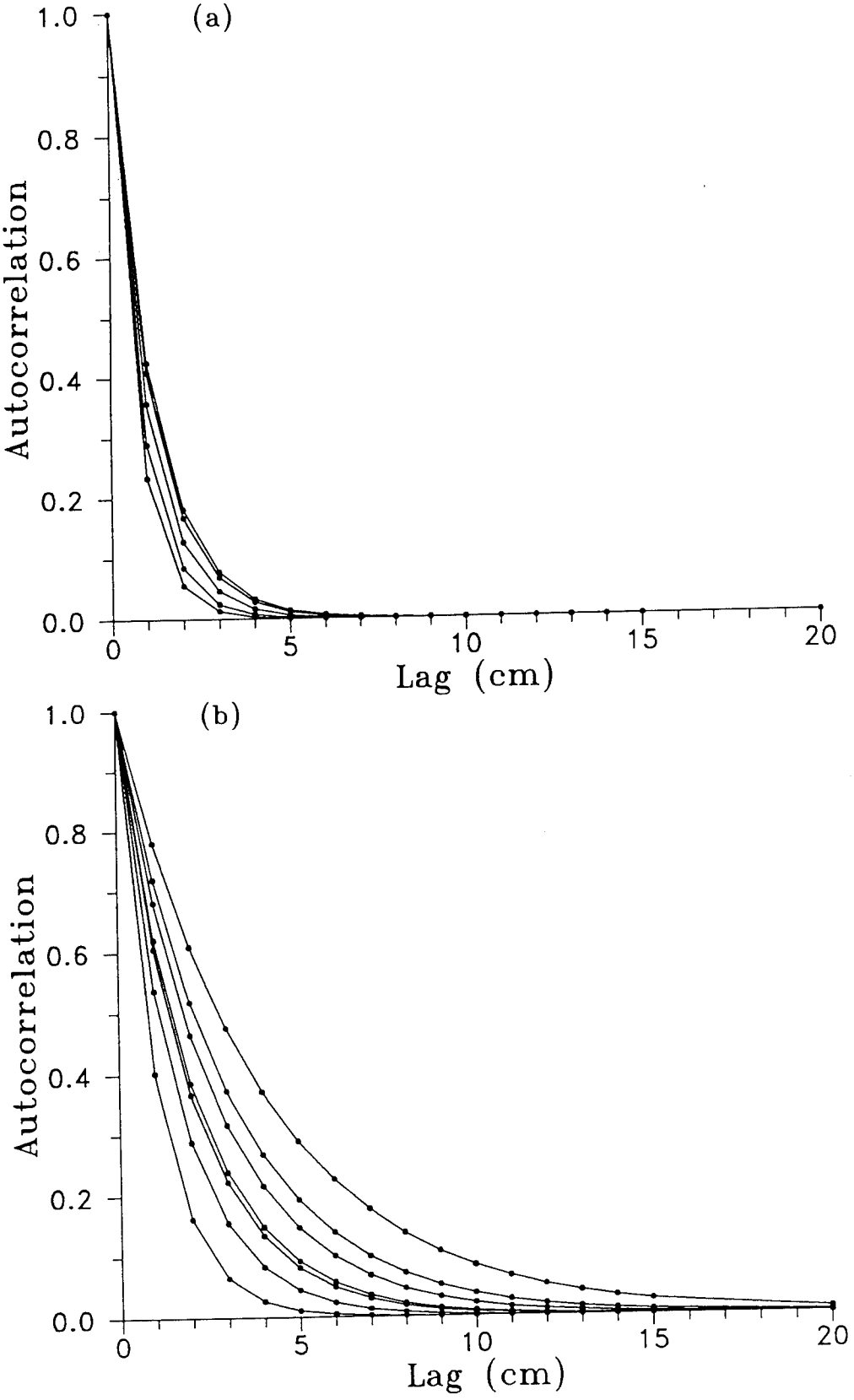

Figure 38. Autocorrelation functions estimated from fluctuations in (a) sediment porosity and (b) sediment velocity for cores collected at Jacksonville, FL (I) site.

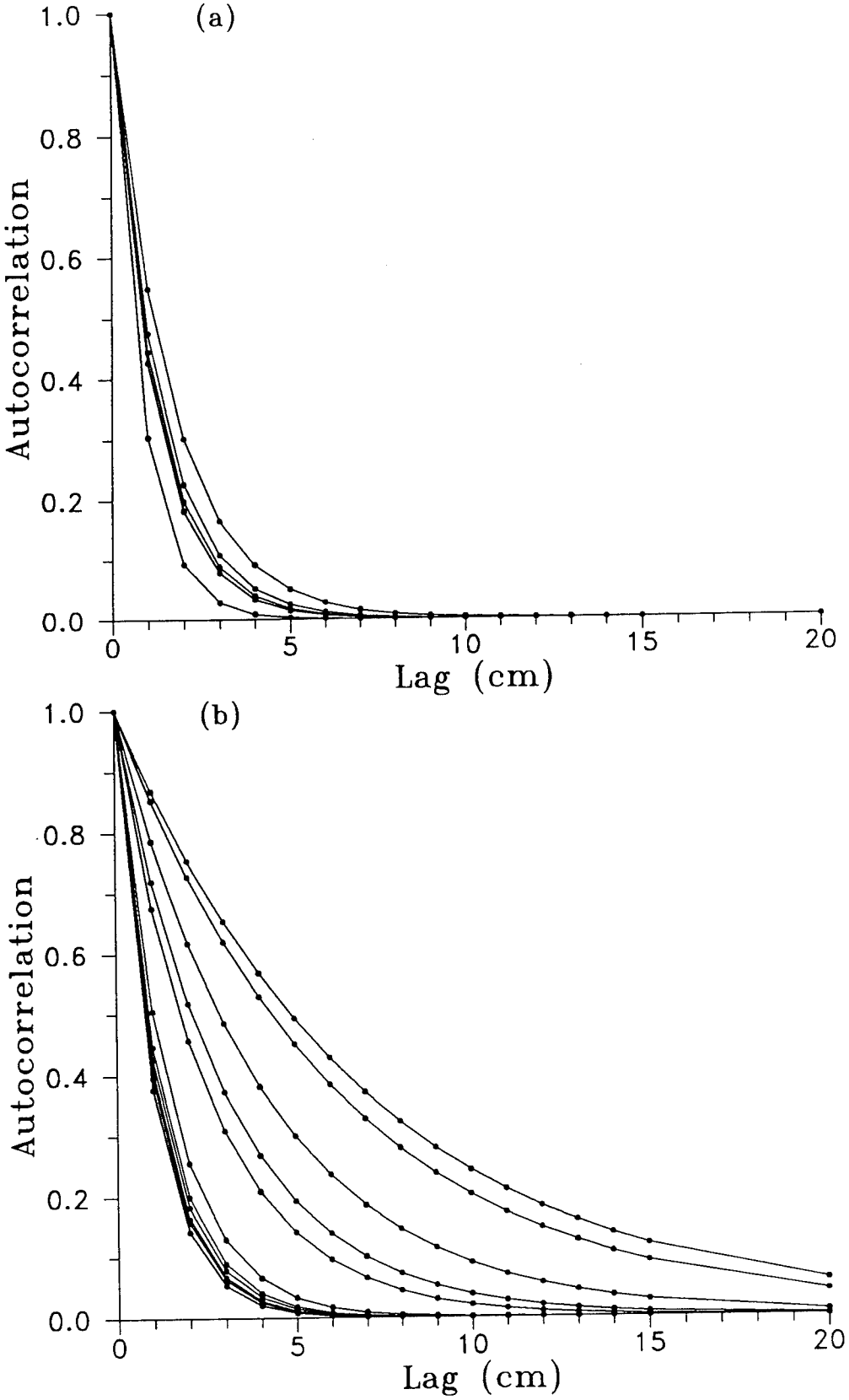

Figure 39. Autocorrelation functions estimated from fluctuations in (a) sediment porosity and (b) sediment velocity for cores collected at Jacksonville, FL (II) site.

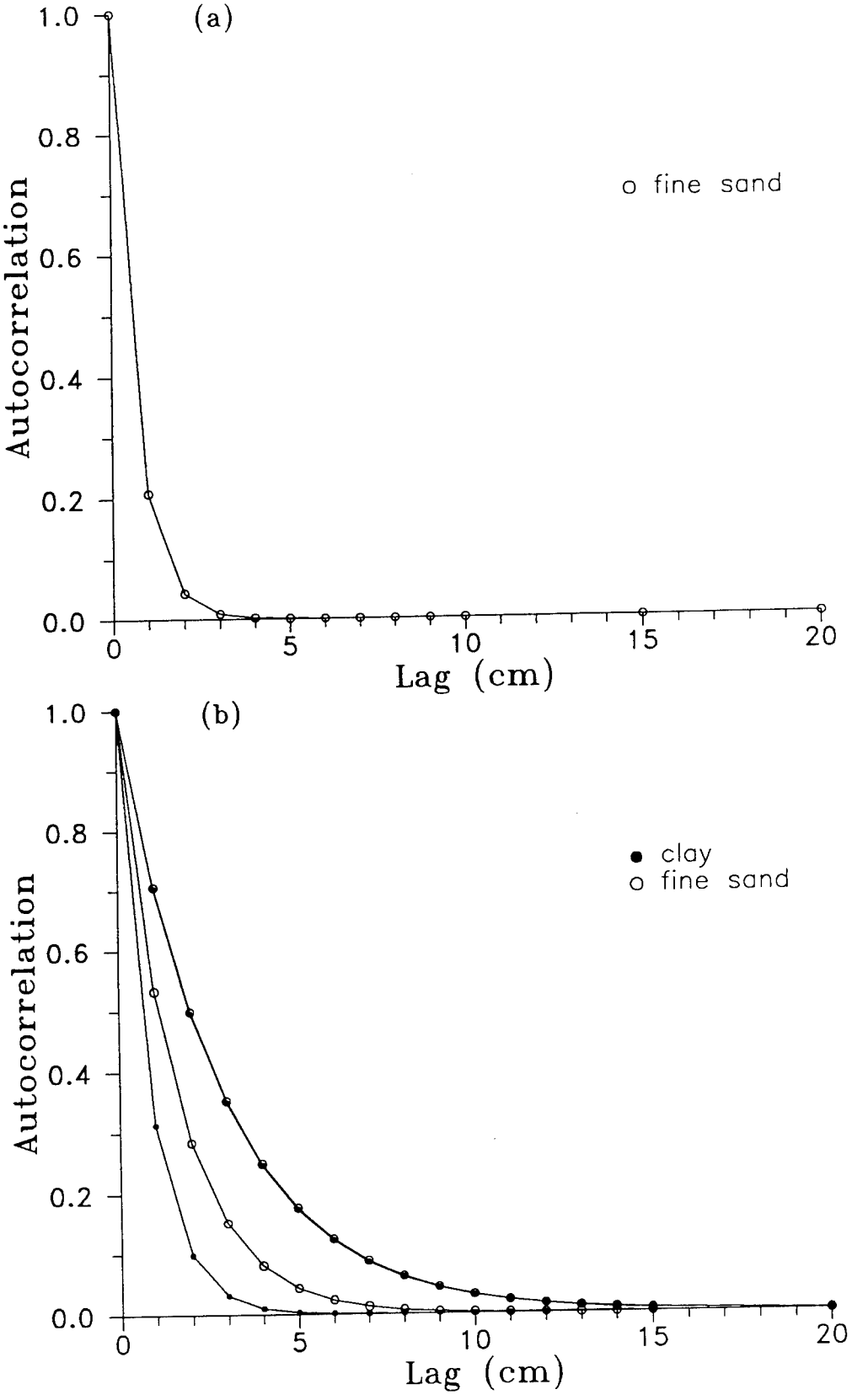

Figure 40. Autocorrelation functions estimated from fluctuations in (a) sediment porosity and (b) sediment velocity for cores collected in St. Andrew Bay, FL.

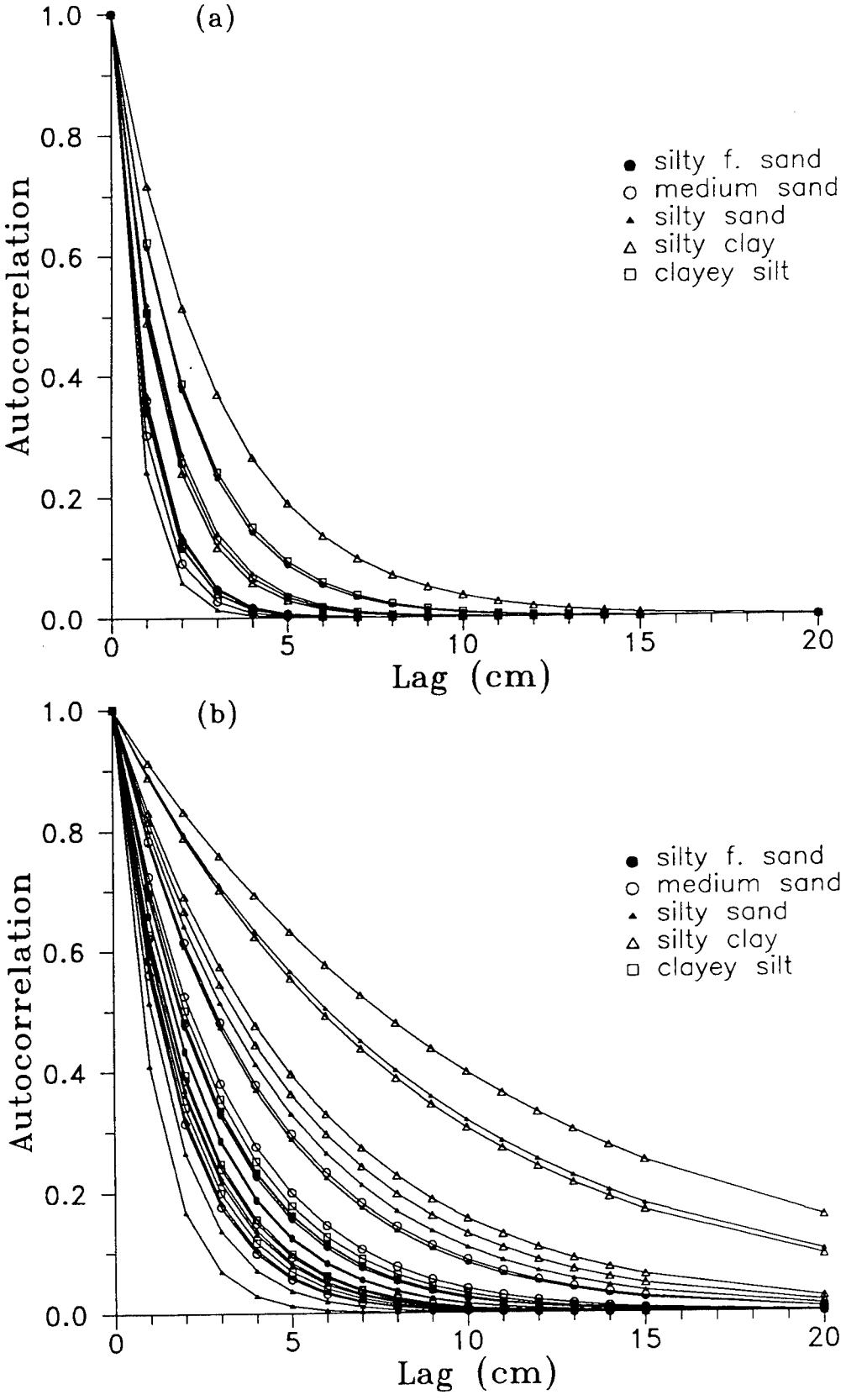

Figure 41. Autocorrelation functions estimated from fluctuations in (a) sediment porosity and (b) sediment velocity for cores collected off the Straits of Juan de Fuca.

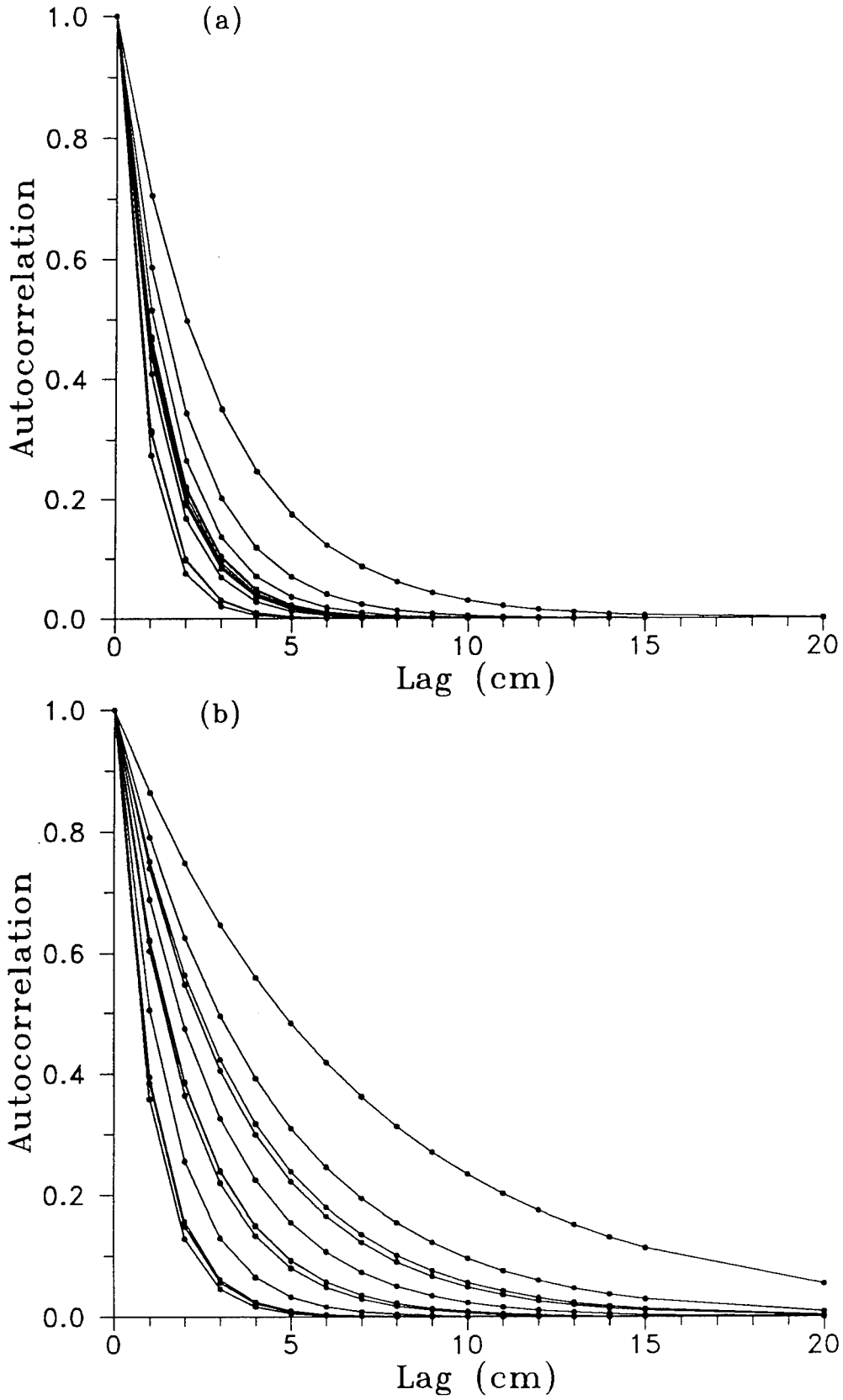

Figure 42. Autocorrelation functions estimated from fluctuations in (a) sediment porosity and (b) sediment velocity for cores collected off the Russian River, CA.

VITA

Kevin Bradford Briggs was born in Montgomery, Alabama on December 20, 1954. His parents are Ann King Briggs and the late John Alden Briggs. In September 1972 he entered the College of Arts and Sciences of Florida Atlantic University from which he was graduated with the B.S. degree in Biology in June 1975. In August 1975 he entered the graduate school in the College of Arts and Sciences of the University of Georgia. After completing his thesis research at Skidaway Institute of Oceanography in Savannah, Georgia he was granted the M.S. degree in Zoology in June 1978. His thesis was entitled "An investigation of the role of microfauna in detrital utilization by the polychaete, *Nereis succinea* (Frey and Leuckart)". In February 1979 he began employment at the Naval Ocean Research and Development Activity which later became the Naval Research Laboratory, Stennis Space Center in Mississippi.

In August 1989 he was admitted to the Graduate School of the University of Miami at the Rosenstiel School of Marine and Atmospheric Science. He was granted the degree Doctor of Philosophy in May, 1994.

Permanent Address: 109 Palm Avenue, Pass Christian, Mississippi 39571